[redacted]

ABSTRACT

The performance characteristics have been determined for two types of general purpose diodes, and for five types of microwave diodes, in radiation environments equivalent to at least 1000 hours' exposure to 10^{10} neutron/cm^2-sec and 2×10^5 Rad/hour.

None of the units studied showed satisfactory performance characteristics after this exposure, although the germanium 1N263 point-contact diode was degraded less than others investigated, and still exhibited measurable properties following the exposure.

Results, although not conclusive, seem to indicate that energizing the microwave mixers at x-band (9375 Mc) during radiation is helpful in prolonging the life of the units.

PUBLICATION REVIEW

The publication of this report does not constitute approval of the Air Force of the findings or conclusions contained therein. It is published only for the exchange and stimulation of ideas.

FOR THE COMMANDER:

George A. Kirsch

GEORGE A. KIRSCH
Colonel, USAF
Ass't Deputy Commander/Test and Support

Concurred in: Robert G. Merkle
ROBERT G. MERKLE
Project Engineer

Concurred in: for Carl A. Reichert
LOUIS SCHAFFER
Colonel, USAF
Director of Engineering Test
Deputy Commander/Test & Support

Concurred in: Hugh S. Lippman
HUGH S. LIPPMAN
Technical Director
Deputy Commander/Test & Support

Approved by: George A. Kirsch
GEORGE A. KIRSCH
Colonel, USAF
Ass't Deputy Commander/Test and Support

TABLE OF CONTENTS

LIST OF ILLUSTRATIONS

LIST OF ILLUSTRATIONS

LIST OF TABLES

SEMICONDUCTOR DIODE PERFORMANCE IN NUCLEAR RADIATION ENVIRONMENTS

I. INTRODUCTION

The increasing use of nuclear energy as a power source, along with the discovery of a belt of radiation outside the earth's atmosphere, require the determination of the degree of function loss to be experienced by components operating in these environments. This program was concerned specifically with the performance characteristics of certain semiconductor diodes being considered for use in nuclear systems. The effects of steady state nuclear radiation on the noise figure and conversion loss of five types of microwave diodes, and on the rectification characteristics of two types of general purpose diodes, have been determined.

Two separate, long-term reactor exposures were scheduled, each to consist of at least 1000 hours of exposure at a fast neutron flux level of 10^{10} neutron/cm^2-sec, or until a significant portion of the specimen diodes had failed.

Preliminary experiments were conducted prior to the long-term exposures, using the central exposure port of the reactor. This port allows access to fast neutron flux levels of 10^{12} neutron/cm^2-sec and gamma flux levels up to 10^7 Rad/hour, and was used to determine, in a relatively short time, the behavior to be expected from the specimens, instrumentation, cabling and shielding during the longer exposures at the lower flux levels.

The long-term reactor investigations were conducted in the reactor thermal column, which has a fast neutron flux level of approximately 10^{10} neutrons/cm^2-sec and gamma flux of up to 2×10^5 Rad/hour. Integrated flux measurements were made on each individual diode specimen under investigation.

This report presents the results and discussion of the preliminary and full-scale investigations of diode performance. Details regarding the design and construction of instrumentation, reactor shielding problems, and dosimetry are appended.

Manuscript released by the authors 21 February 1962 for publication as an ASD Technical Documentary Report.

II. GENERAL PURPOSE DIODES

A. Sample Selection and Handling

Two types of general purpose diodes were included in this investigation. These are the 1N464 (Silicon junction) and the 1N127 (Germanium point-contact). A total of forty diodes constituted the sample taken for the general purpose diodes in the full-scale reactor run. Each type was obtained from two manufacturers. The 1N127 diodes were obtained from Mfg. A and Mfg. B, while the 1N464 diodes were supplied by Mfg. B and Mfg. C. These diodes were further subdivided into equal groups of dynamic and static specimens.

The dynamic specimens were operated continuously under an electrical load during irradiation. Rated voltage for the 1N127 was used for both types, but each type was made to pass its own rated forward current. The dynamic diodes were monitored periodically, with measurements of forward voltage drop and reverse current taken at selected intervals. The dynamic voltampere characteristics were displayed and photographed at less frequent intervals, as determined by changes in forward and reverse characteristics. The static group was energized only during measurements. Temperatures were monitored periodically by thermocouples placed in selected locations.

In establishing load conditions for the general purpose diodes, there were two general approaches which could have been taken. One approach would have been to establish the correct value of forward current in the diode initially, and then periodically monitor forward current and adjust the load resistor to compensate for changes occurring in the diode. The other approach would have been to establish the correct value of forward current with an initial adjustment of the load resistor, with this value of load resistance remaining fixed throughout the test. The concept of a fixed value of load resistance throughout the test simulates actual operation of the diode in a typical circuit more accurately, and allows greatly reduced monitoring, adjusting and switching operations. For these reasons, this latter approach is more suitable and is the one which was taken in the full-scale investigations on this program. However, during actual measurement of forward and reverse characteristics, rated forward current was maintained in the diodes to establish a firm basis for comparison of properties.

B. Preliminary Experiments

The forward voltage drop and reverse current were measured for five specimens of each of the two types of general purpose diodes under consideration (1N464 Silicon and 1N127 Germanium). These specimens were then subjected to combined fast neutron and gamma radiation which was approximately equivalent to a 1500 hour exposure at 10^{10} neutron/cm^2-sec. The length of this exposure was inadvertent, but the forward and reverse characteristics were again determined following the radiation exposure. All of the germanium specimens (1N127) were destroyed with respect to their characteristics as rectifiers. The silicon specimens (1N464) continued to show different forward and reverse characteristics;

however, the forward resistance increased three orders of magnitude and the reverse resistance decreased one to two orders of magnitude. These changes were quite uniform for all five specimens of each type. Table 1 summarizes data from these diodes.

Because the data obtained from this first preliminary experiment was somewhat inconclusive, another experiment was conducted in the central exposure port with four specimens of each of the two types of general purpose diodes. Specimen diodes from three manufacturers were used. Four of these diodes were energized with rated forward current during radiation exposure, while the remaining four were energized only during measurements. Allocation and identification were as shown in Table 2. Measurements were made of the average forward voltage drop and the average reverse current. In addition, cable insulation resistance and ambient temperature were monitored during exposure, and measurements were made to determine whether these parameters were affecting measurements. Cable insulation resistance was stable at 3000 megohms during reactor operation, and the temperature at no time exceeded the ambient operating temperature for either of these diode types. Results of the measurements of diode parameters are listed in Tables 3 and 4.

Some observations are possible on the basis of these preliminary measurements. For instance, all of the 1N127 germanium diodes failed when total exposure was less than 2×10^{12} nvt; failure was evidenced by the diodes' exhibiting the same values for forward and reverse current. Relatively little change was shown in the forward voltage drop for these diodes. The silicon diodes also showed deterioration in the reverse characteristic; however, failure occurred for those diodes from only one manufacturer (Mfg. B) at the end of a total exposure of 3.6×10^{14} nvt. Those silicon diodes from the second manufacturer (Mfg. C) had not failed completely at the end of a total exposure of 1.4×10^{15} nvt. However, the reverse current had increased by three orders of magnitude. In all instances for the silicon diodes, the forward voltage drop had increased from four to eight times the initial values. These findings are in general agreement with the results reported in the literature. (References 4, 9, and 21) However, one point should be emphasized here. The values for nvt in this report are based upon the measurements of flux above the level of 1.8 Mev. Dosimetry has shown that the assumption of a fission spectrum is not valid (Appendix C) and that calculation of nvt above 0.5 Mev involves a multiplier which can vary from 5.3, based on the data in Figure C-5, to a value of 7.2, if the provisional data on "damaging flux" is considered. For this reason, data is reported as "nvt for $\emptyset > 1.8$ Mev," with the value above 0.5 Mev calculable with an appropriate multiplier.

Again, with regard to the diodes, there was some evidence of partial recovery in the reverse characteristics when measured one hour after removal from the high flux area for the dynamic 1N464 from Mfg. C. Reverse current decreased from 900 microamperes to 350 microamperes in one hour. However, the reverse current increased with one-hour cooling of the static Mfg. C 1N464, but decreased after 20 hours of cooling following subsequent exposures. Although based on results of only two diodes, this tends to support the idea that diodes which are energized during irradiation will have a longer operating life.

Table 1

PRELIMINARY EXPERIMENTS

Effects of Radiation on General Purpose Diodes

1N 464 (Silicon)(70 Volts Applied)						1N 127 (Germanium)(70 Volts Applied)					
Before Irradiation			After Irradiation			Before Irradiation			After Irradiation		
$I_{F(A)}$	$V_{F(V)}$	$I_{R(\mu A)}$	$I_{F(A)}$	$V_{F(V)}$	$I_{R(\mu A)}$	$I_{F(A)}$	$V_{F(V)}$	$I_{R(\mu A)}$	$I_{F(A)}$	$V_{F(V)}$	$I_{R(A)}$
.04	0.44	0.11	$.05 \times 10^{-3}$	31.0	3.0	.03	1.68	162	.03	2.00	.03
.04	0.49	0.095	$.05 \times 10^{-3}$	31.0	7.7	.03	1.72	250	.03	2.15	.03
.04	0.44	0.092	$.045 \times 10^{-3}$	30.5	5.2	.03	1.69	127	.03	1.90	.03
.04	0.47	0.090	.045x10-3	30.5	4.0	.03	1.80	120	.03	2.25	.03
.04	0.42	0.082	$.060 \times 10^{-3}$	31.0	7.9	.03	1.64	166	.03	2.35	.03

Table 2

General Purpose Diode Identification

Dynamic Diodes

1	Mfg. A	1N127
2	Mfg. B	1N127
3	Mfg. C	1N464
4	Mfg. B	1N464

Static Diodes

5	Mfg. A	1N127
6	Mfg. B	1N127
7	Mfg. C	1N464
8	Mfg. B	1N464

Dynamic diodes are continuously energized during radiation exposure. Rated forward current is set in each diode. (30MA-1N127, 40 MA-1N464). Static diodes are energized only during measurement.

Table 3

PRELIMINARY EXPERIMENTS - GENERAL PURPOSE DIODES

Reverse Current, Milliamperes, rms

Nvt* > 1.8 Mev

Diode No.	0	$1x10^{11}$	$1x10^{12}$	$7x10^{13}$	$1.8x10^{14}$	$3.6x10^{14}$	After cooling 1 hour	$5.5x10^{14}$	$7x10^{14}$	After cooling 20 hours
1	.134	.230	30	30	30	30	30	30	30	30
2	.074	.215	30	30	30	30	30	30	30	30
3	.0024	.0038	.062	.130	.260	.900	.350	1.00	3.5	.600
4	.0023	.0042	.47	2.5	30	35	35	35	35	40
5	.192	1.50	30	30	30	30	30	30	30	30
6	.058	.085	30	30	30	30	30	30	30	30
7	.0028	.0035	.400	.425	.450	.550	2.5	35	35	2.5
8	.0023	.0040	3	30	30	0	0	0	0	0

* These specimens also received a total gamma dosage of approximately 10^7 rad.

Table 4

PRELIMINARY EXPERIMENTS - GENERAL PURPOSE DIODES

Average Forward Voltage Drop, Volts

Diode No.	Nvt* > 1.8 Mev									
	0	$1x10^{11}$	$1x10^{12}$	$7x10^{13}$	$1.8x10^{14}$	$3.6x10^{14}$	After Cooling 1 hour	$5.5x10^{14}$	$7x10^{14}$	After Cooling 20 hours
1	1.54	1.60	1.62	1.90	1.90	1.90	1.90	1.90	1.90	2.4
2	1.22	1.34	1.90	1.90	1.90	1.90	1.90	1.90	1.90	2.4
3	0.52	0.74	1.61	1.59	1.80	1.98	2.0	2.0	2.4	2.5
4	0.57	1.61	3.7	3.4	3.7	4.0	4.1	4.1	4.1	4.5
5	1.69	1.80	2.2	2.4	2.4	2.5	2.5	2.5	2.5	2.8
6	1.26	1.82	2.5	2.6	2.8	2.8	3.0	3.0	3.0	3.1
7	0.66	0.80	2.1	2.8	2.9	3.2	3.3	3.2	3.2	3.6
8	0.75	2.1	4.5	4.5	4.7	Open Ckt	Open	Open	Open	Open

* These specimens also received a total gamma dosage of approximately 10^7 rad.

Measurements made in the central exposure port, while informative, do not accurately establish failure times for the diodes to be operated in the thermal column. The gamma dose rate is two orders of magnitude higher in the central exposure port, and may have been an important factor in degrading some of the general purpose diodes to failure in a rather short time. However, these measurements did result in relative information which was useful in establishing ranges of parameter changes and the manner in which deterioration occurs.

C. Thermal Column Experiments

The grouping of diodes shown in Table 2 was retained for the first scheduled full-scale reactor run. However, the number of diodes in each group was increased to five. Measurements of forward voltage drop, reverse current, and dynamic display characteristics were made initially and at subsequent selected intervals during reactor exposure. Figures 1 and 2 show characteristics of the 1N127 germanium point-contact diodes plotted versus integrated flux. Each point represents an average of measured values obtained for the five static or five dynamic specimens, as the case may be. Obviously, failure in the reverse characteristic was quite rapid for these specimens. The temperature was monitored at five different points on the diode mounting assembly. At no time did the temperature exceed 45° C, even for those thermocouples in direct contact with the diode case.

Figures 3 and 4 show similar data accumulated for the 1N464 silicon junction diodes. Figure 3 shows the increases occurring in forward voltage drop, but the changes in reverse current shown in Figure 4 illustrate more strikingly the differences in performance. As may be seen, those diodes which were energized during exposure did not deteriorate as rapidly as those which were not energized. In addition, the diodes of Mfg. C were superior in performance to others investigated. But even these had drastically reduced rectification ratios following radiation exposures.

These results follow quite closely the pattern of results reported in the literature. Behrens and Shaull, (Ref. 4), although investigating only statically irradiated specimens, report failure in germanium point-contact diodes in the reverse characteristic to occur at about 10^{12} nvt. Silicon junction diodes failed next at about 5×10^{12} nvt. Their results show, as do the results obtained in this investigation, that the integrated dose is of more significance than the dose rate, and that neutron-inflicted damage is quite permanent.

Figures 5 and 6 illustrate the initial dynamic characteristics of the general purpose diodes. Since both the 1N127 and 1N464 characteristics were photographed using identical gain settings, the superiority in characteristic of the 1N464 is evident. Figures 7 and 8 show the same diodes after being irradiated. However, it was necessary to use reduced gain settings to contain the pattern on the oscilloscope screen. The greater magnitude of failure in the reverse direction is evident, together with the overall loss in rectification properties.

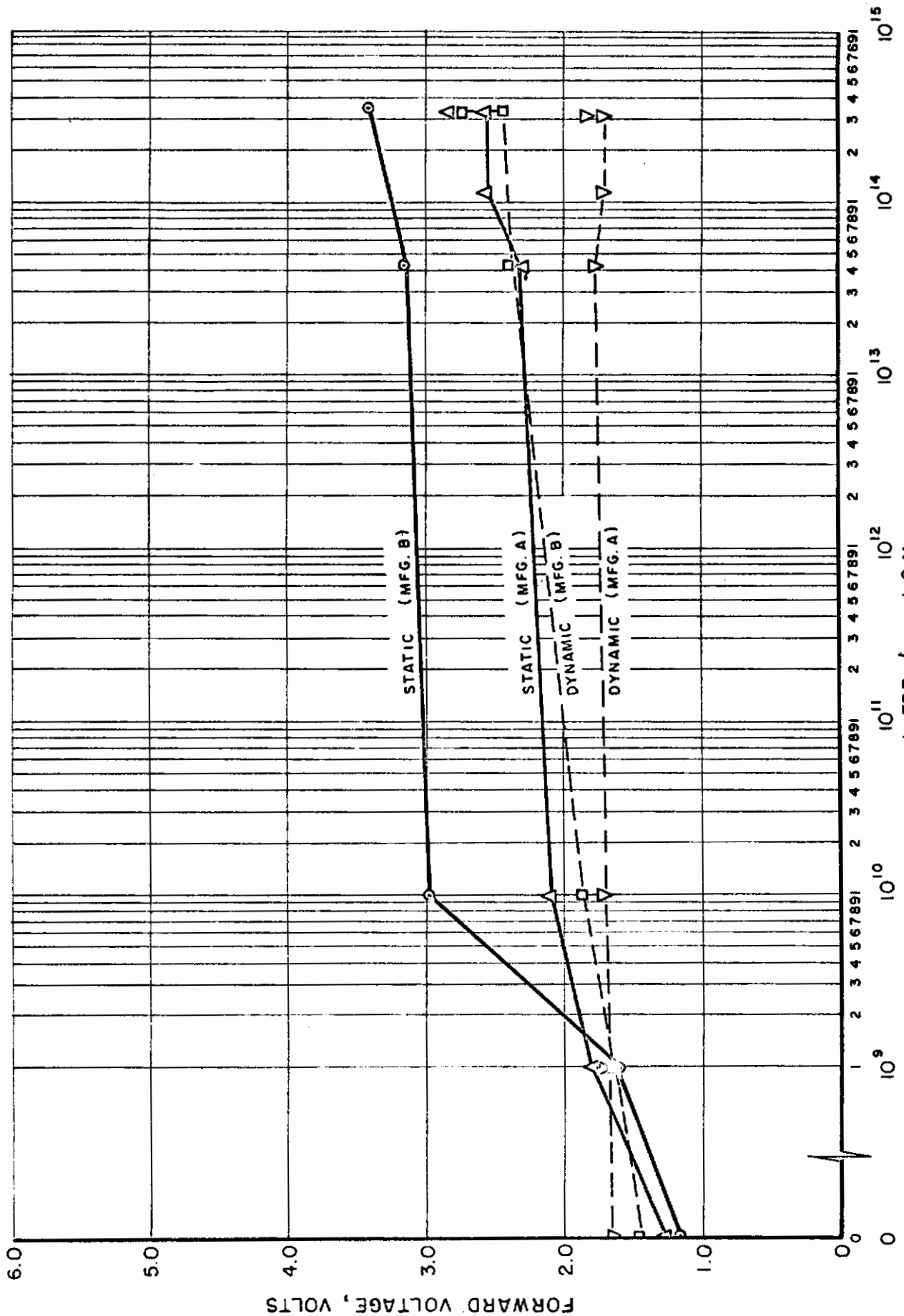

FIG. 1 FORWARD VOLTAGE DROP — IN127 GERMANIUM DIODES

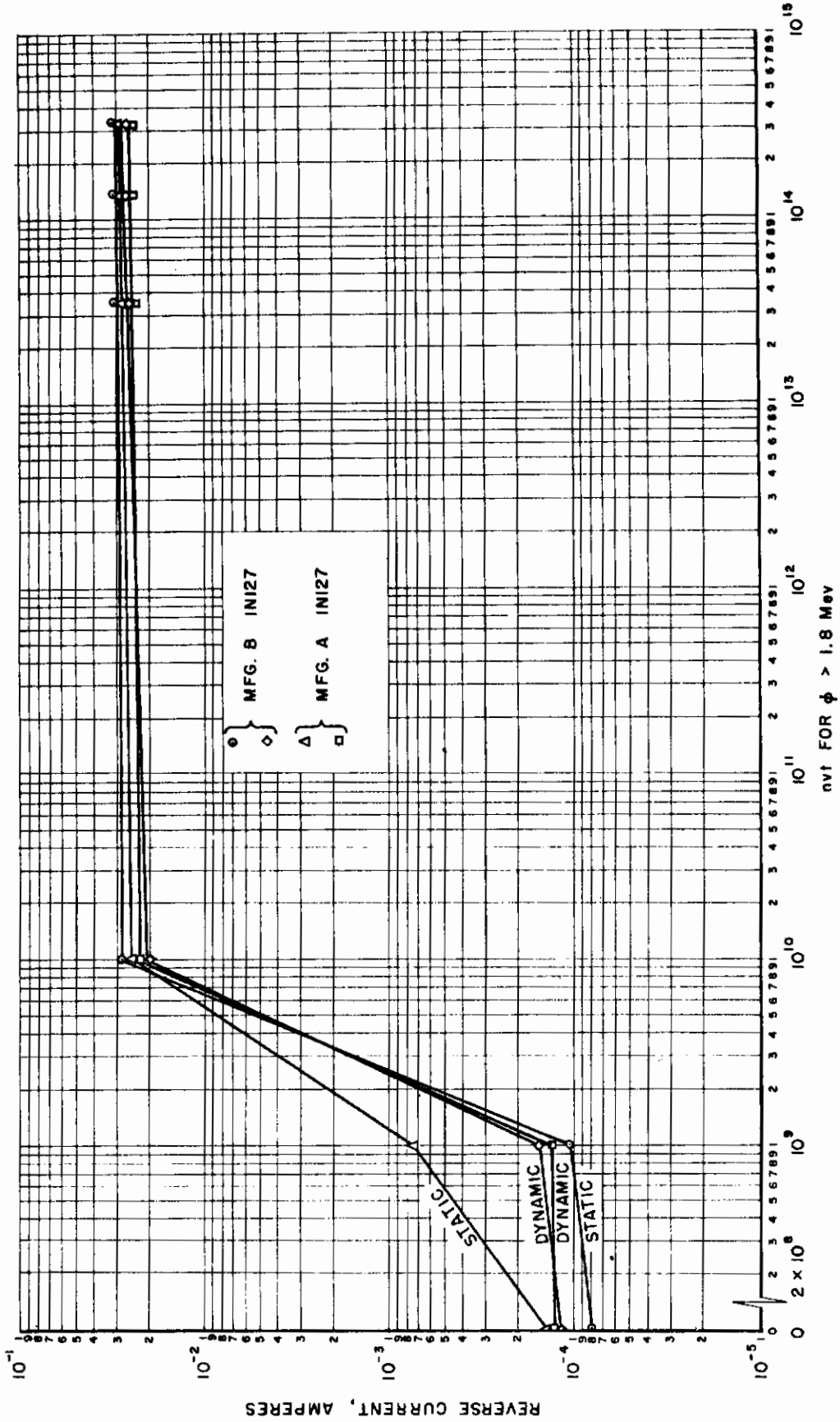

FIG. 2 REVERSE CURRENT — IN127 GERMANIUM DIODES

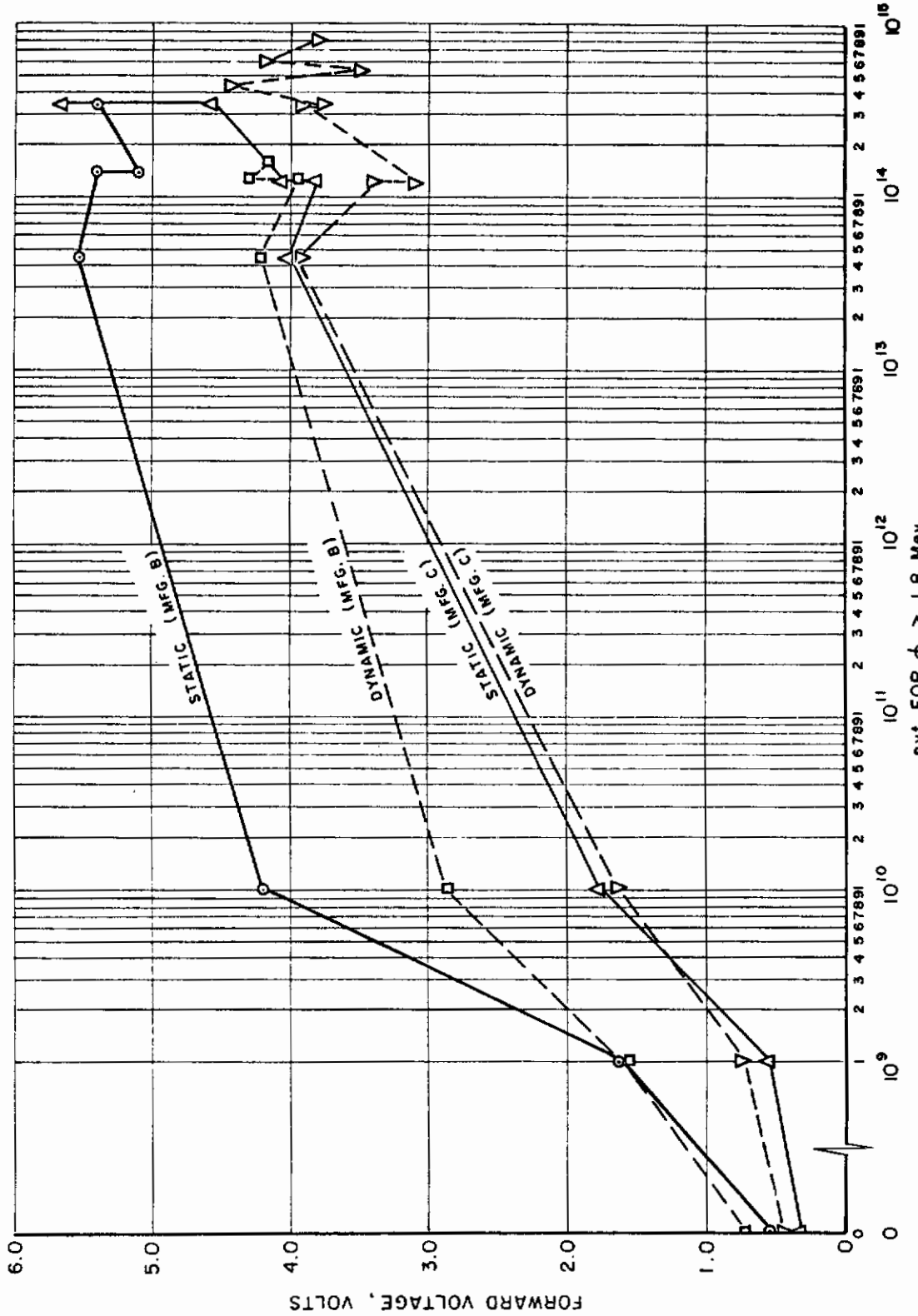

FIG. 3 FORWARD VOLTAGE DROP — IN464 SILICON DIODES

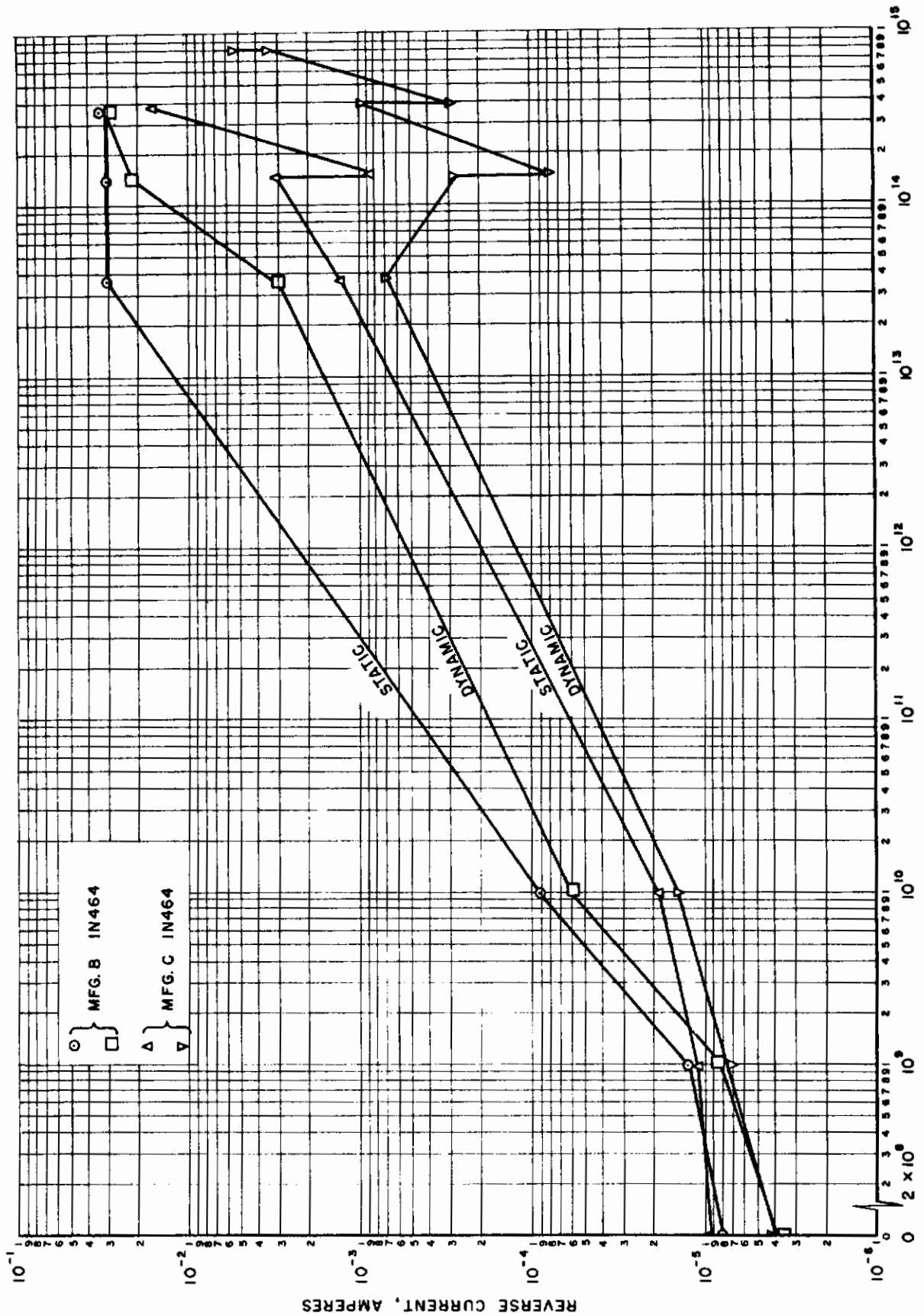

FIG. 4 REVERSE CURRENT — IN464 SILICON DIODES

FIG. 5 DYNAMIC CHARACTERISTICS
IN127 DIODES
STATIC AND DYNAMIC GROUPS
INITIAL MEASUREMENTS

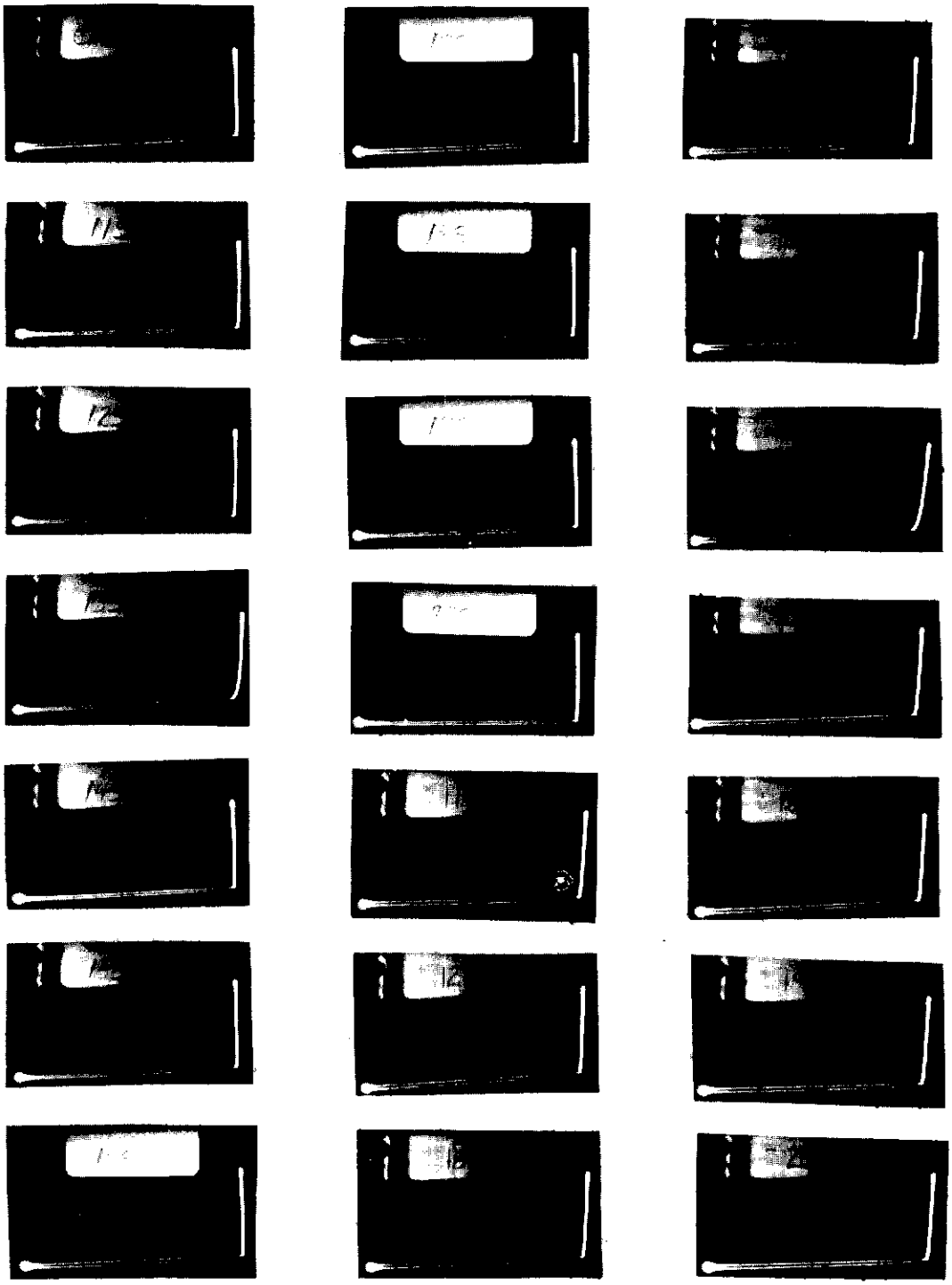

FIG. 6 DYNAMIC CHARACTERISTICS
IN464 DIODES
STATIC AND DYNAMIC GROUPS
INITIAL MEASUREMENTS

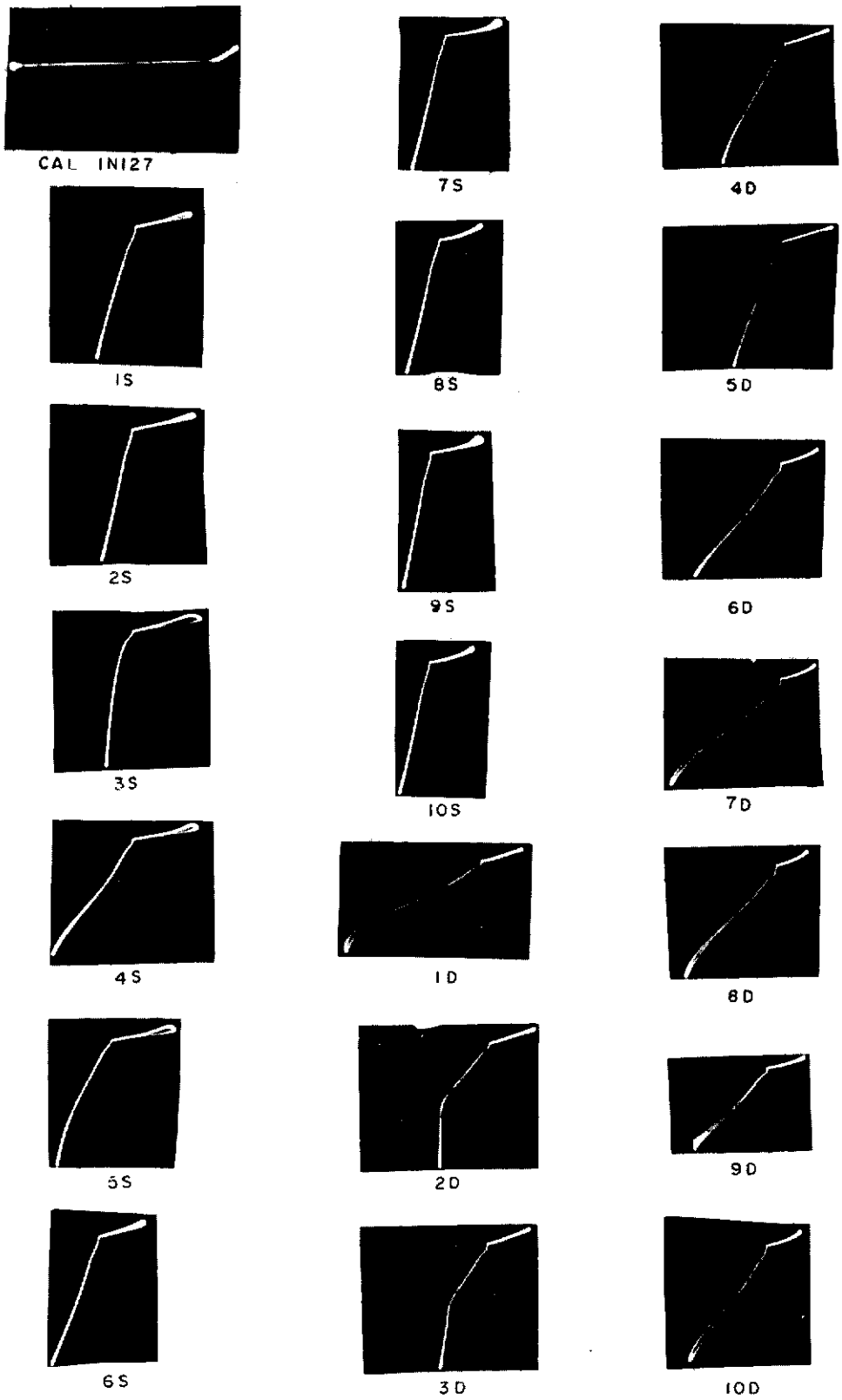

FIG. 7 DYNAMIC CHARACTERISTICS
IN127 DIODES
STATIC AND DYNAMIC GROUPS
AT nvt FOR ϕ > 1.8 Mev = 3.6×10^{13}

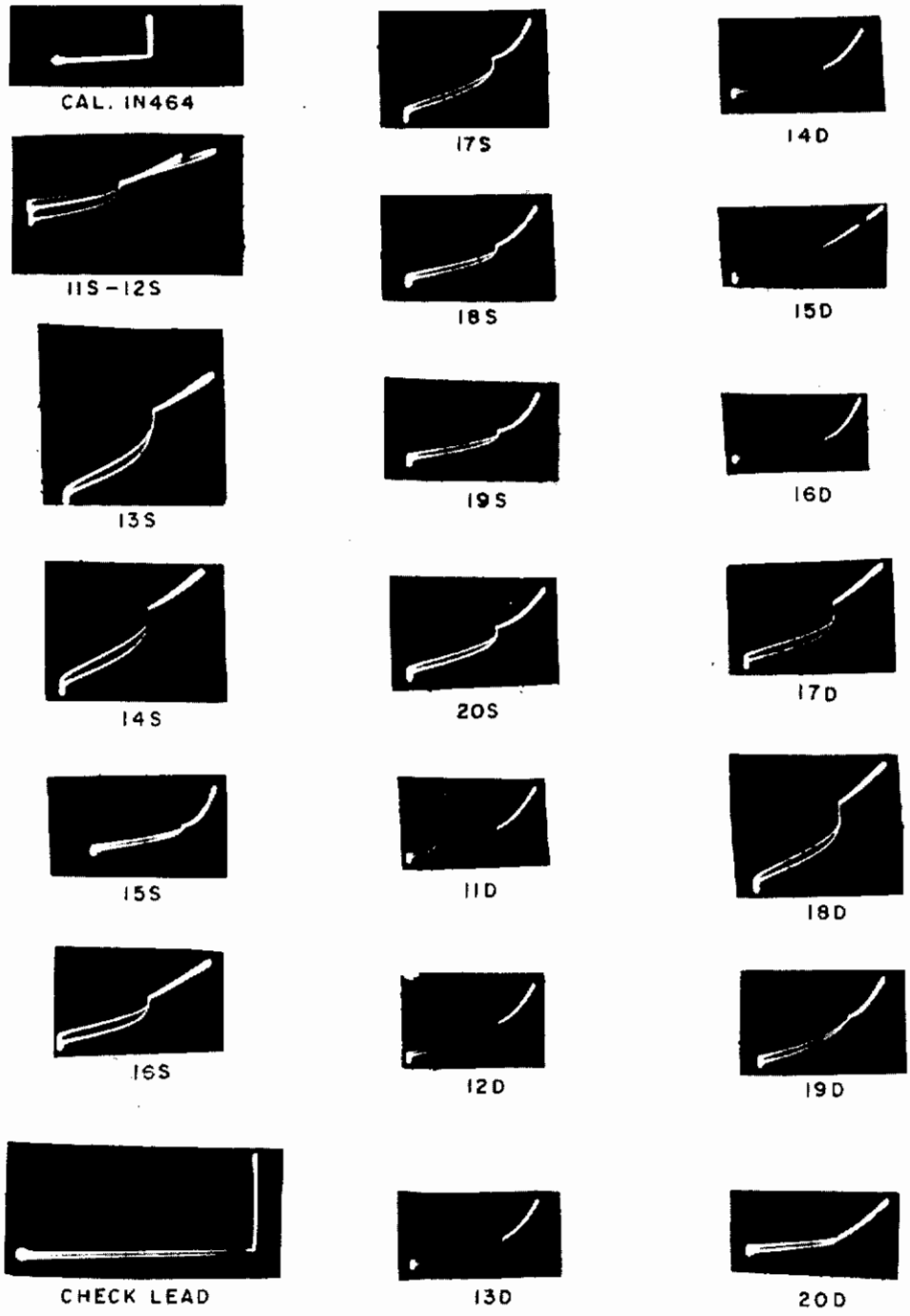

(VERTICAL AND HORIZONTAL GAIN SETTINGS ARE 0.4 OF THAT USED FOR INITIAL MEASUREMENTS. ONLY CHECK LEAD SETTING = 1)

FIG. 8 DYNAMIC CHARACTERISTICS
IN464 DIODES
STATIC AND DYNAMIC GROUPS
AT nvt FOR ϕ > 1.8 Mev = 3.6×10^{13}

III. MICROWAVE DIODES

A. Sample Selection and Handling

Six types of microwave diodes were designated for investigation, with these particular diode types available from three manufacturers. However, the number of types was reduced to five in Supplemental Agreement No. 1 (61-2019). With this as a guide, sample procurement was allotted in the following manner:

1N25 and 1N23B	Mfg. D
1N21WE and 1N23WE	Mfg. E
1N263	Mfg. F

Two separate reactor runs were scheduled into the program. There were totals of forty microwave diodes in the first reactor run and twenty-four microwave diodes in the second run. Those used in the first run were divided into equal groups of dynamic and static diodes. The second run was made up of six dynamic and eighteen static diodes. For the first run, there were four diodes in each group, designed to operate at 1 kmc (1N25); four were those designed for 3 kmc (1N21WE); and twelve were those designed for 10 kmc (1N23B, 1N23WE, and 1N263).

Of the dynamic specimens, six of the 10 kmc diodes (two each of 1N23B, 1N23WE and 1N263) were supplied with r.f. energy during radiation exposure on both of the reactor runs. The remaining fourteen dynamic diodes in the first run were energized with 60 cps current during radiation. All of the microwave diodes were measured initially for noise figure and conversion loss, using r.f. techniques. In addition, those energized by 60 cps current, and the static group, were measured initially (noise figure and conversion loss) using a d-c crystal test set. To minimize handling problems, the static group and those energized by 60 cps current were monitored using the d-c crystal test set without removing the diodes from the reactor. The r.f. powered diodes were measured using r.f. techniques only, while the 60 cps diodes were measured initially and finally using r.f. techniques and monitored with d-c. The static diodes were measured initially with r.f. and d-c and monitored with d-c.

This program had available to it a total of only ten gallium arsenide diodes (1N3096R). Initially, each of the two full-scale reactor runs was to make use of eight diodes of each type, so it was obvious that the gallium arsenide diodes could be tested only in one run. Therefore it was planned to defer investigation of the gallium arsenide diodes until the second reactor run, in order to take advantage of results derived from the first run and any subsequent preliminary experiments. However, in attempting to measure the gallium arsenide samples, it was found that degradation had taken place during normal storage, so it was not possible to include these samples in the reactor schedule. These were subsequently removed from consideration in the Supplemental Agreement.

B. Preliminary Experiments

Prior to the first full-scale reactor run, preliminary experiments were also conducted in the central exposure port with two specimens of each of three types of microwave diodes: the 1N23B, 1N25, and 1N263. Measurements were made using a d-c incremental test set, as well as measurements

of forward and reverse resistance. Standard 300 ohm, polyethylene-insulated twin-lead was used to obtain connection to the diodes. In addition, an unconnected line was inserted in the reactor with the diodes, and its insulation resistance was monitored to determine whether degradation affected measurements.

Noise figure and conversion loss were obtained using the measured values and calibration curves supplied with the d-c test set. These data are shown in Table 5. Data obtained from measurements of forward and reverse resistance are shown in Table 6. It was also found that the decrease in insulation resistance of the twin lead was insignificant compared to diode deterioration.

The data in Table 5 and 6 formed the basis for an assumption that it was possible for at least some of the diodes to survive a 1000-hour exposure at a flux level of 10^{10} n/cm^2-sec, although all had exceeded specification requirements after the tabluated exposure. Remeasurement after approximately 28 days with no subsequent exposure did not indicate substantial improvement in these characteristics.

C. Thermal Column Experiments

Microwave diodes which were exposed to radiation during the first full scale reactor run were mounted as indicated in Figure C-8, Appendix C. The twenty diodes represented in the side view of the side panel are the static microwave diodes. Diode numbers 8 through 20 located above the mixer mounts were the dynamic microwave diodes energized with 60 cps current.

The static and 60 cps dynamic diodes failed quite rapidly and, in many instances, suddenly, during exposure in the first reactor run. Also it was found that the changes were of such magnitude that they could not be monitored with the d-c incremental test set during radiation. For these reasons, further reactor exposure was halted, pending redirection of effort, and measurements were made of those diodes still exhibiting measurable properties. These measurements were made external to the reactor, using L-Band, S-Band, and X-Band power to energize the appropriate diodes. The following is a summary of diode condition following an exposure of approximately 10^{14} nvt for $\phi > 1.8$ Mev:

1. All 1N25 (L-Band) diodes seriously degraded. Overall noise figures were greater than 19 db and could not be measured accurately. Conversion losses ranged up to 25 db, with no observable difference in static and dynamic units.

2. All 1N21 WE (S-Band) diodes also seriously degraded. Overall noise figures ranged from 11 to 24 db, with conversion losses ranging from 11 to 12 db.

3. The 1N23B and 1N23WE (X-Band) units were less affected in the conversion loss characteristic than were the L and S-Band units. Conversion loss in these diodes ranged from 7-12 db. Overall noise figures ranged from 16.4 to 25 db.

Table 5

Preliminary Experiments - Microwave Diodes - DC Measurements Only

Noise Figure (F) and Conversion Loss (L)-db

Nvtx10^{15} for $\phi > 1.8$ Mev

Diode Type		0	1.8	3.6	4.3	5.8	6.5	7.2	9.0	10.8	After Cooling 28 days
1N25-F		9.3	14.2	17.2	>20	>20	>20	open	open	open	open
	L	6.4	7.7	8.6	>14	>14	>14				
1N25-F		6.2	9.3	10.2	9.3	9.8	11.2	11.2	-	17.2	15.2
	L	5.6	6.4	6.6	6.4	6.5	6.9	6.9	-	8.6	8.0
1N23B-F		7.0	9.1	8.5	8.5	8.5	9.8	9.8	9.8	14.	16.7
	L	5.3	6.0	5.8	5.8	5.8	6.2	6.2	6.2	7.4	8.3
1N23B-F		9.3	9.1	9.1	>20	9.8	11.2	11.2	>20	>20	>20
	L	6.4	6.0	6.0	>14	6.2	6.9	6.9	10.8	10.7	>14
1N263-F		14.0	14.9	14.9	9.1	8.5	9.8	9.8	9.8	14.9	16.7
		7.4	7.7	7.7	6.0	5.8	6.2	6.2	6.2	7.7	8.3
1N263-F		19.4	17.5	15.7	15.7	15.7	19.4	17.0	14.9	18.4	19.2
	L	9.3	8.7	8.0	8.0	8.0	9.3	8.5	7.7	9.0	9.3

Table 6

Preliminary Experiments - Microwave Diodes - Forward and Reverse Resistances

$Nvtx10^{15}$ for $\phi > 1.8$ Mev

Diode Type	0	4.3	5.8	6.5	7.2	9.0	10.8	After cooling 28 days
1N25 R_f	19.	800.	1.5K	1.3K	2.1K	-	-	20K
R_r	28K.	210K	170K	130K	150K	-	-	500K
1N25 R_f	19	160	250	250	320	-	600	550
R_r	28K	15K	21K	50K	18K	-	48K	45K
1N23B R_f	22	350	400	410	430	500	780	440
R_r	21K	55K	55K	50K	60K	80K	80K	15K
1N23B R_f	22	320	400	440	500	800	1.2K	430
R_r	21K	1.1K	1.7K	1.5K	1.9K	2.1K	2.5K	43K
1N263 R_f	15	30	370	340	360	410	460	540
R_r	19K	10K	14K	14K	14K	22K	14K	90K
1N263 R_f	15	380	390	400	400	420	700	1.2K
R_r	19K	5K	5K	4.6K	5.5	14K	38K	20K

4. The 1N263 (X-Band) units showed considerably less change due to radiation than any of the other diodes. Conversion loss ranged from 5 to 11 db, while overall noise figures ranged from 7.9 to 15 db.

5. The diodes being energized with X-Band power during radiation showed less degradation in general. For example, the 1N263 units showed a conversion loss of less than 6.db; 1N23WE, a conversion loss of about 4 db; 1N23B, a conversion loss of 4.8 to 5.4 db. Noise figures were also similarly reduced.

The foregoing information prompted a redirection of effort which was agreed upon in consultation with the program monitor. No further consideration was to be given to the general purpose, the L and S-Band, nor to the static or 60 cps dynamic 1N23B or 1N23WE diodes that had already been exposed. The diodes being operated in the X-Band holders and energized during radiation would be continued in the second reactor run, together with the other six 1N263 units from the first run. Six new units each of 1N23B and 1N23WE diodes would also be included in the second run. Thus, the second reactor run was to be comprised of six diodes energized during irradiation in the X-Band holders, and 18 diodes statically irradiated. The mountings were essentially the same as for the first run. (See Figure C-8).

Radiation exposures were scheduled for short intervals at the start of the schedule, with intervals to increase if little change in characteristics was observed. The static diodes were removed after every interval and measured, using X-Band power in a waveguide holder external to the reactor.

The following sections, then, will be concerned with the results and discussion of microwave diodes studied during the second reactor run.

1. Conversion Loss (Static Diodes)

The data shown in Figures 9, 10, and 11 represents results of measurements made on diodes after they had been subjected to successive periods of radiation exposure at a flux level of approximately 10^{10} neutrons/cm^2-sec. It is apparent, in comparing the results of the 1N23B (Figure 9) with those of the 1N23WE (Figure 10), that the 1N23WE units were more stable in operation during radiation exposure. Four of the six 1N23WE did not fail catastrophically until after an exposure of 10^{15} nvt, while the 1N23B units all exhibited erratic behavior. In further comparison with the 1N263 units (Figure 11), it may be seen that none of the 1N263 units failed catastrophically due to radiation. The two units which did fail did so due to mechanical breakage during handling after exposure. Apparently, the glass envelope is embrittled during radiation exposure, and the exposed units must be handled with extreme care.

At this point, it is perhaps opportune to examine some of the basic properties of the semiconductor which contribute directly to conversion loss. The microwave diodes being considered are all point-contact diodes, so each may be represented by a simple equivalent circuit,

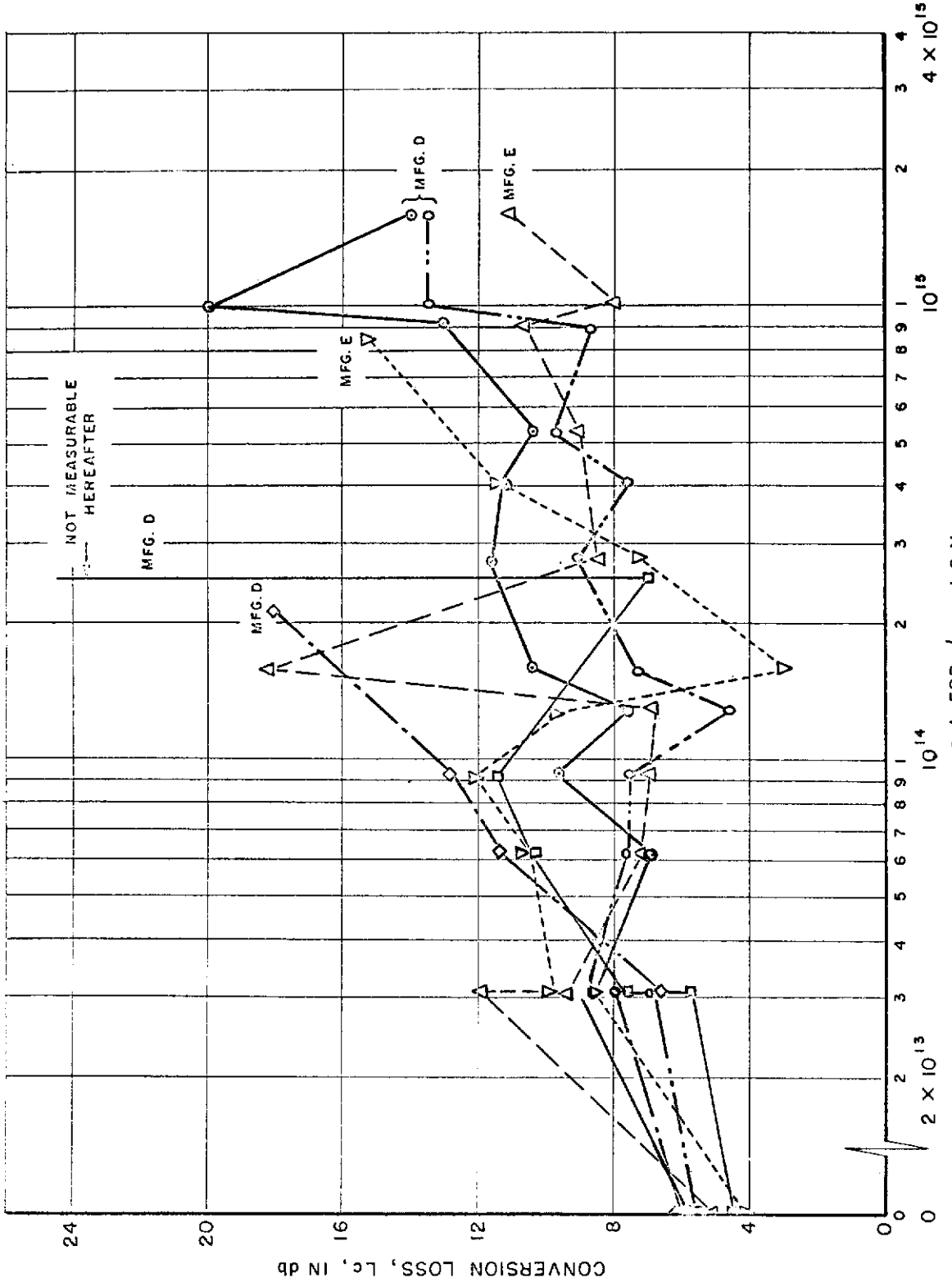

FIG. 9 CONVERSION LOSS — IN23B SILICON DIODES (STATIC)

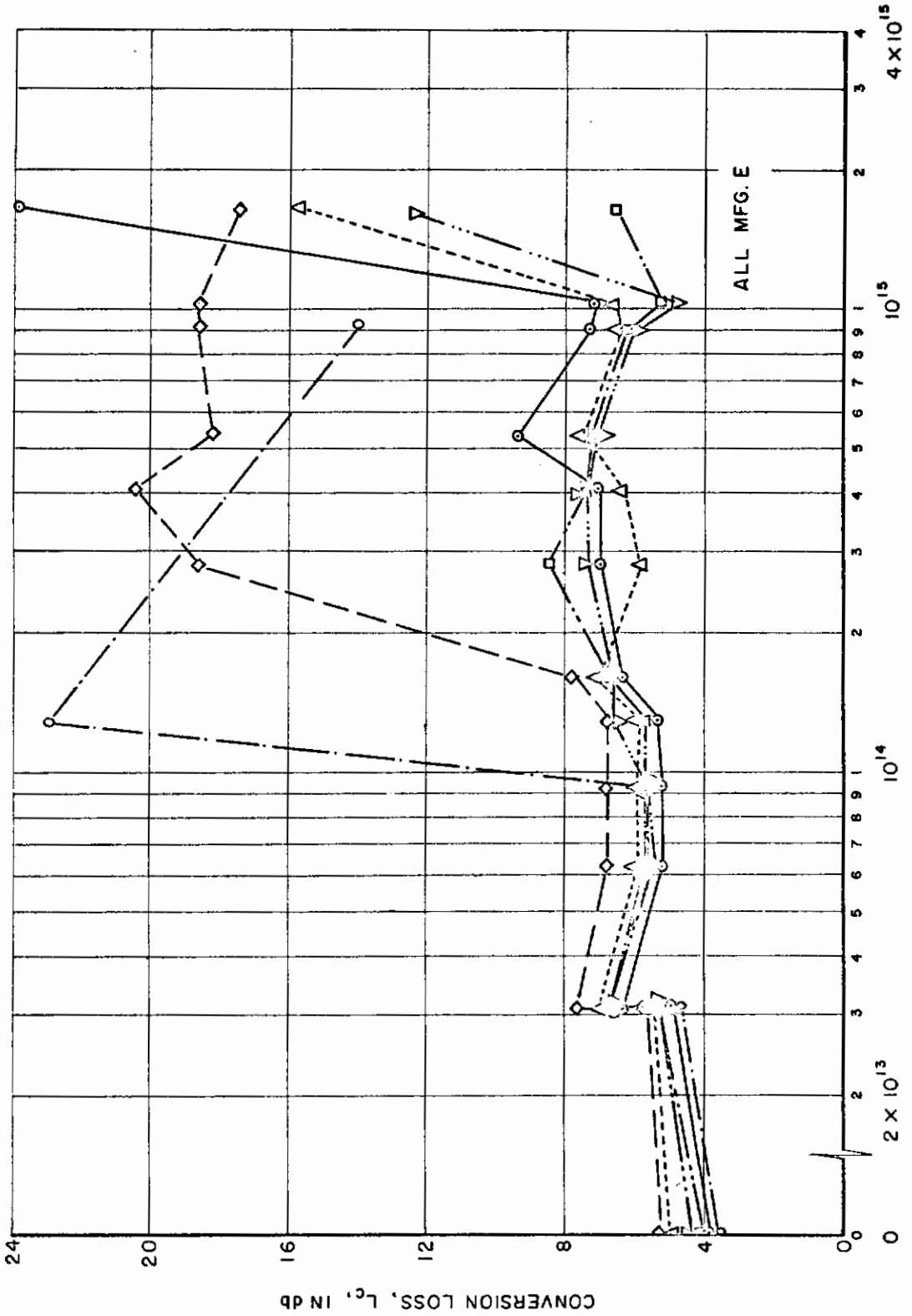

FIG. 10 CONVERSION LOSS—IN23WE SILICON DIODES (STATIC)

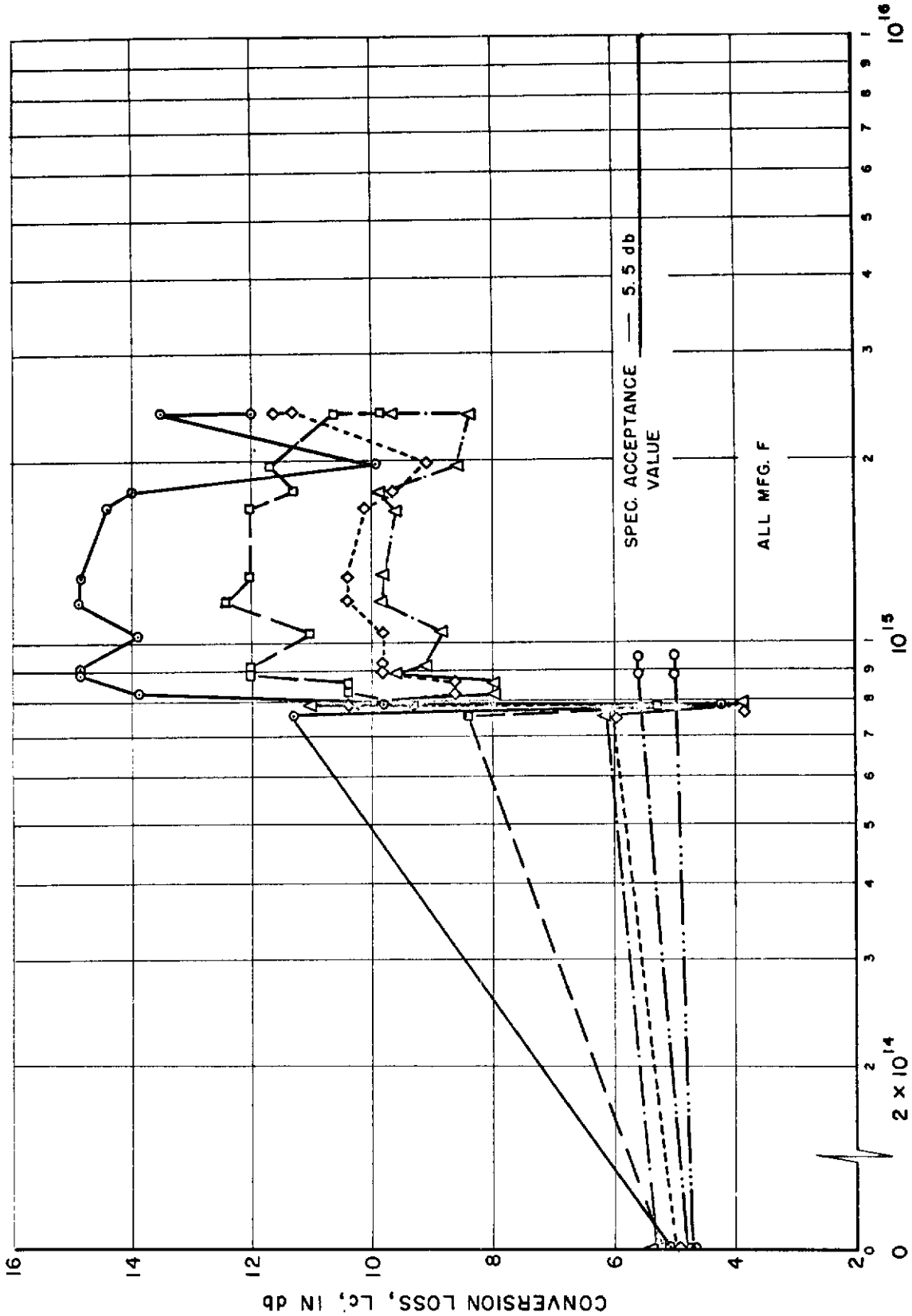

FIG. 11 CONVERSION LOSS — IN263 GERMANIUM DIODES (STATIC)

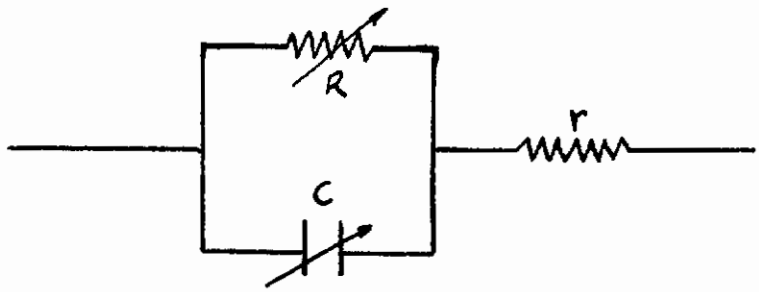

where: R = barrier resistance

C = barrier capacitance

r = spreading resistance

It has been shown (Ref. 11) that the barrier resistance limits the lowest conversion loss, and that the spreading resistance and barrier capacitance increase the conversion loss above that caused by the barrier resistance alone. The barrier resistance is a non-linear function of applied voltage; the spreading resistance is essentially constant (if conductivity modulation in the forward direction is neglected); and the barrier capacitance varies approximately as the square root of the applied voltage. This investigation is further limited to a mixer application at X-Band, so that $\frac{1}{\omega C} \ll R$ in the reverse direction, and the spreading resistance, r, dominates R in the forward direction. In the design of diodes for mixer applications, the voltage dependence of C is generally neglected, and a dimensionless figure of merit, $M = 1/\omega rC$, is evolved. Conversion loss then reaches its minimum at an optimum figure of merit, determined effectively by

$$r = \frac{1}{4a\sigma} \tag{1}$$

for a circular contact of radius, a, where σ is defined as the conductivity. The spreading resistance may further be expressed by

$$r = \frac{1}{4aen\mu} \tag{2}$$

where n is the number of charge carriers, e is the electronic charge, and μ is the charge carrier mobility. Thus, the majority carrier concentration n is the only independent variable adjustable at will. Optimum majority carrier concentrations of about $10^{18}/cm^3$, in germanium, and of about $5 \times 10^{18}/cm^3$, in silicon, have been determined and are in common usage. Further, a standard radius "a", equal to about 4×10^{-4} cm, has been determined as the best compromise for mechanical stability, burnout, and an improved noise figure at X-Band. This radius produces spreading resistances of from 3 to 20 ohms for germanium, and of from 15 to 75 ohms for silicon. In general, the lower conversion losses in germanium devices are due to the lower spreading resistance. Mixer crystals are also highly doped, so that the spreading resistance is essentially constant over the range of from -0.5 to +0.5 volts. This heavy doping retards conversion of n-type germanium to p-type (Ref. 1), and may be another reason for the general superiority

of germanium mixer diodes, since silicon does not experience this preferential conversion.

It has further been found (Ref. 15), that structures which minimize minority carrier storage give minimum conversion loss under matched conditions in converting a high frequency to a low frequency (mixer action). This storage is minimized by a "variable resistor" action which is favored by recombination. However, sufficient amounts of injected carriers can swamp the recombination centers so that recombination fails when most needed. The "variable-resistor" action may be approached in point-contact designs by making the point small enough that minority carriers which have been stored for an appreciable time, compared to the frequency involved, have little chance of diffusing back to the contact. The "variable-resistor" action at X-Band requires a contact whose radius is approximately 2×10^{-5} cm. Thus the typical contact radius is too large to achieve the variable resistor action. However, the reduced mechanical strength may have to be accepted to achieve increased radiation resistance.

2. Overall Noise Figure (Static Diodes)

In general, a very low resistivity is needed in both germanium and silicon to achieve low noise-figure diodes. Although both the spreading resistance and the barrier resistance generate noise, it has been found that the reverse resistance, and hence the barrier resistance, correlates with noise figure. (Ref. 2) Evidence of this is also found in examining the data shown in Figures 12 and 13. In all of the 1N23 series units, failure was evidenced first by an excessive noise figure. This is followed by a sharp decrease in rectified output current. Each diode was calibrated before radiation by recording the rectified output current for one milliwatt of input power. When these characteristic sharp decreases took place, the rectified output current was reduced to about twenty-five percent of its initial value. No reduction in current was apparent until this point. Following this decrease in output current, the conversion loss usually, but not always, increased greatly. Thus in most instances the total failure point is well defined. However, gradual degradations occurring before this total failure made several of the units only marginally useful. It is significant that again the 1N23WE units showed quite stable operation up to the total failure point, while the 1N23 B units were erratic in noise figure as well as in conversion loss. Gradual degradation was more apparent in the noise figure for the 1N23WE than in the conversion loss.

As was the case in the conversion loss characteristic, all of the 1N263 units exhibited measurable noise figure characteristics (Figure 14) throughout their radiation exposure, even though all had considerably exceeded the military specification acceptance levels for post environmental exposure. All changes in static diode properties were irreversible with respect to a twenty day-period of room-temperature annealing.

3. Dynamic Diode Performance

The data presented in Figures 15 through 20 is the result of measurements of six diodes which were energized continuously with X-Band power (9375 MC) during their exposure to radiation. These diodes remained in the crystal holders in the reactor throughout their entire exposure. It may be seen that these units followed the general pattern of behavior of the

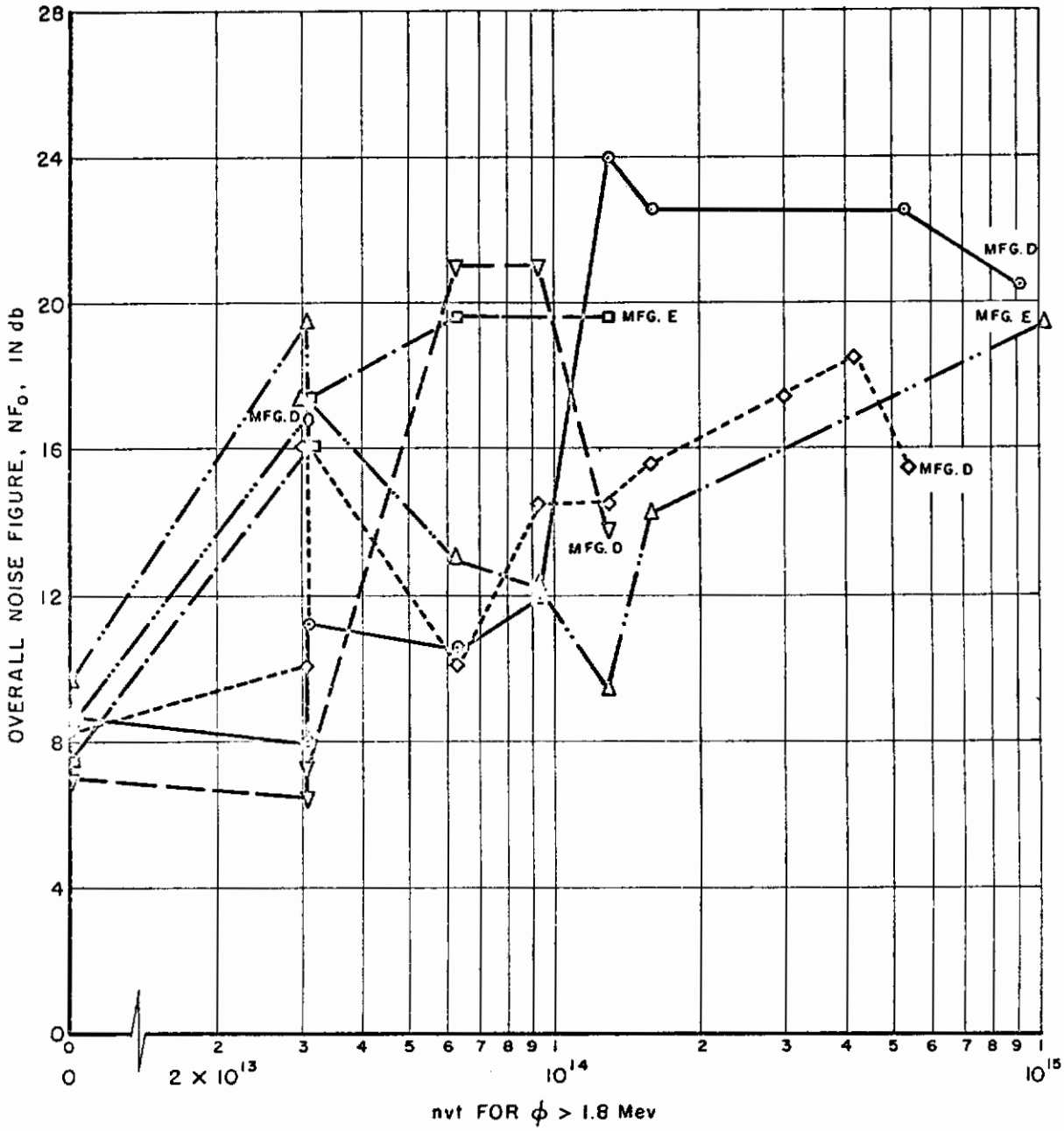

FIG. 12 NOISE FIGURE — IN23B SILICON DIODES (STATIC)

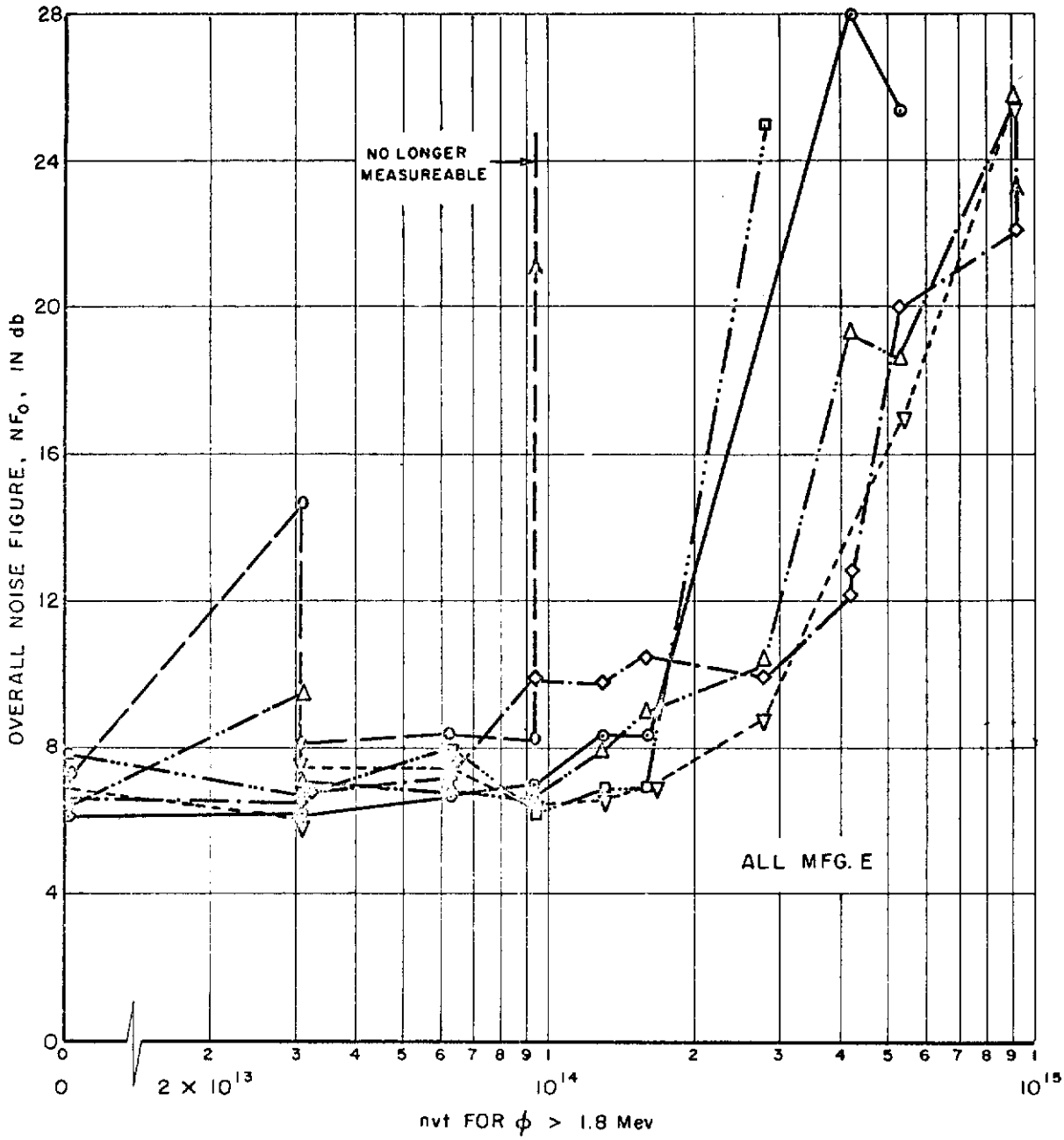

FIG. 13 NOISE FIGURE — IN23WE SILICON DIODES (STATIC)

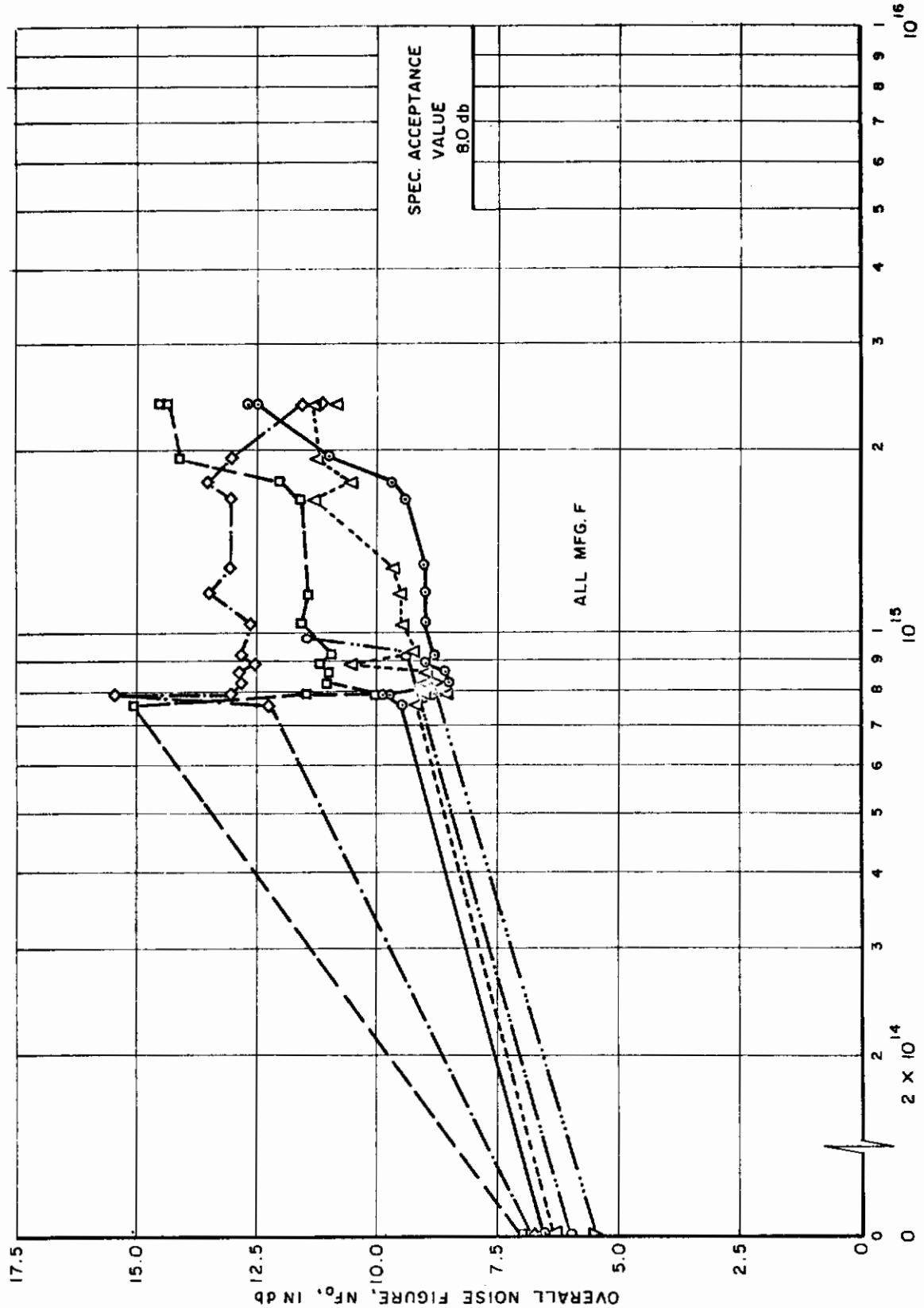

FIG. 14 NOISE FIGURE — IN263 GERMANIUM DIODES (STATIC)

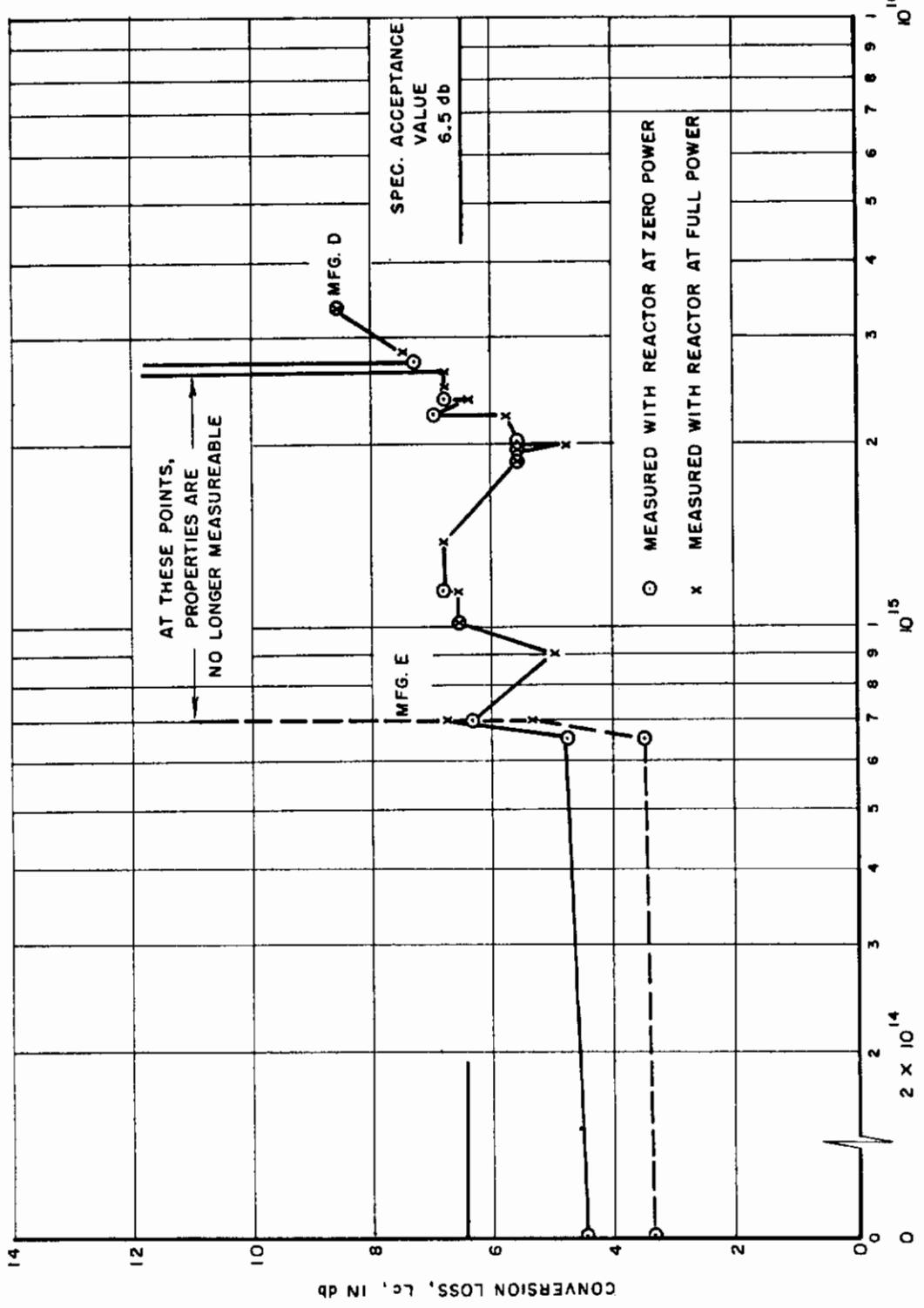

FIG. 15 CONVERSION LOSS — IN23B SILICON DIODES (ENERGIZED WITH X-BAND POWER DURING IRRADIATION)

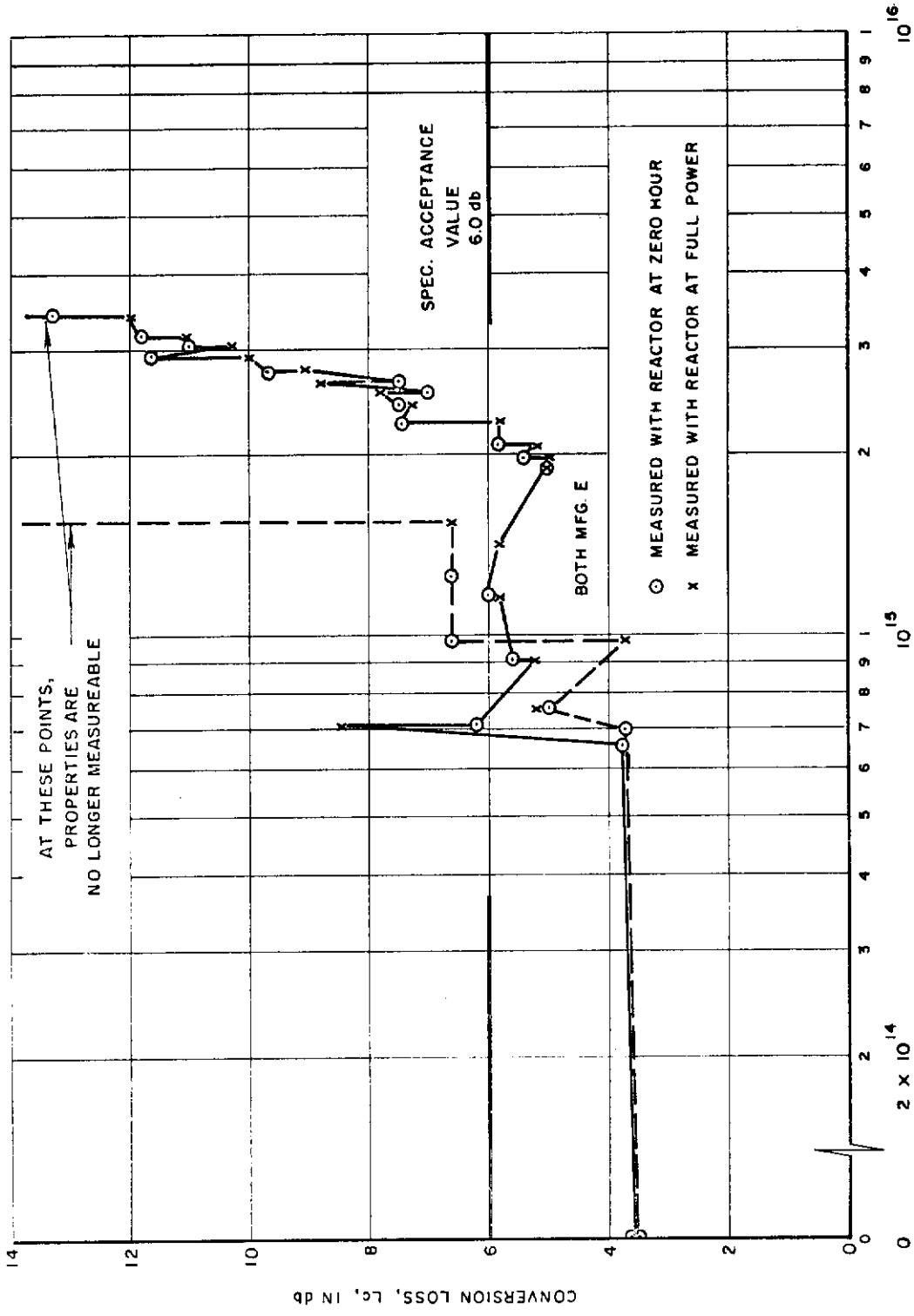

FIG. 16 CONVERSION LOSS — IN23WE SILICON DIODES (ENERGIZED WITH X-BAND POWER DURING IRRADIATION)

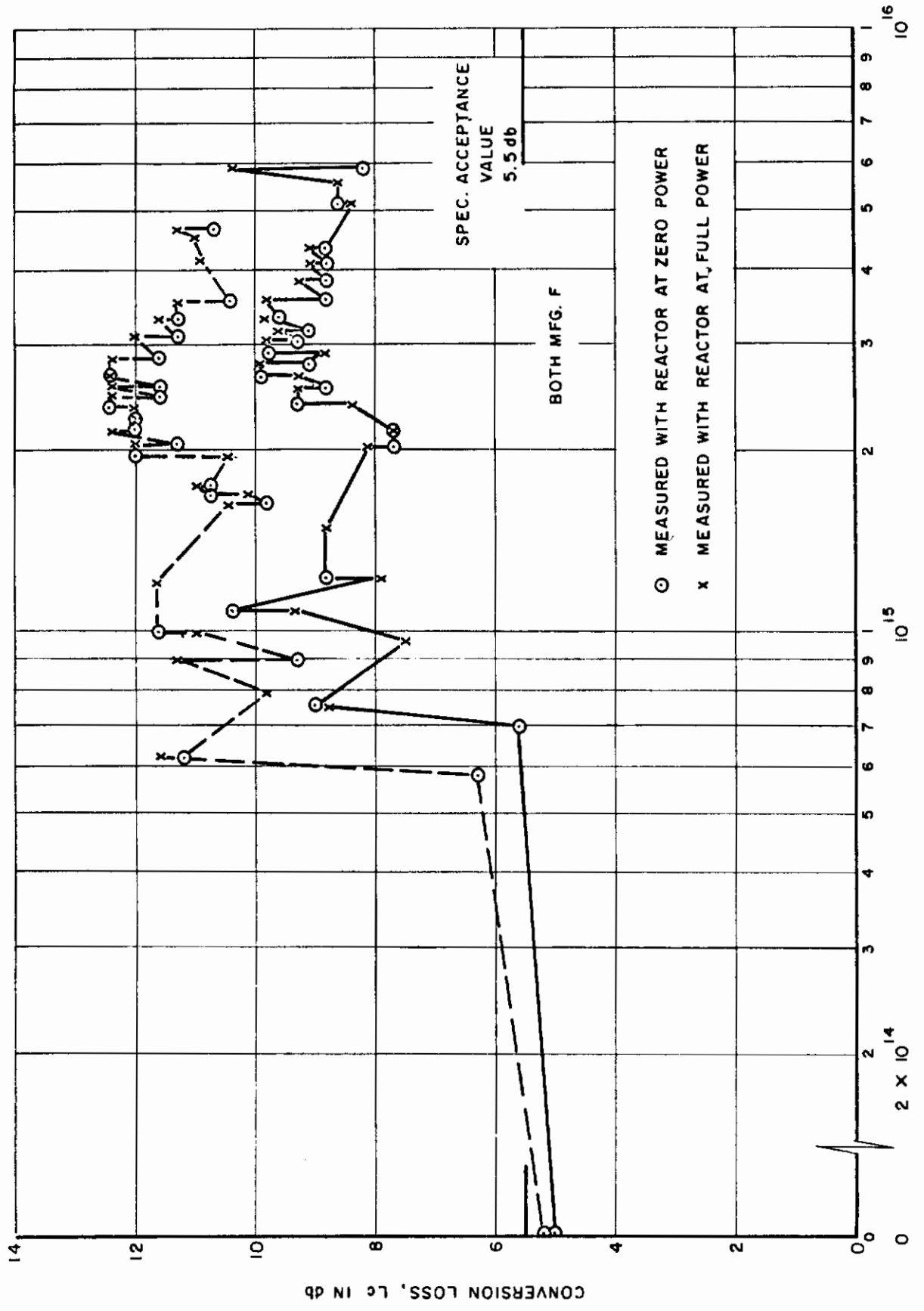

FIG. 17 CONVERSION LOSS — IN263 GERMANIUM DIODES (ENERGIZED WITH X-BAND POWER DURING IRRADIATION)

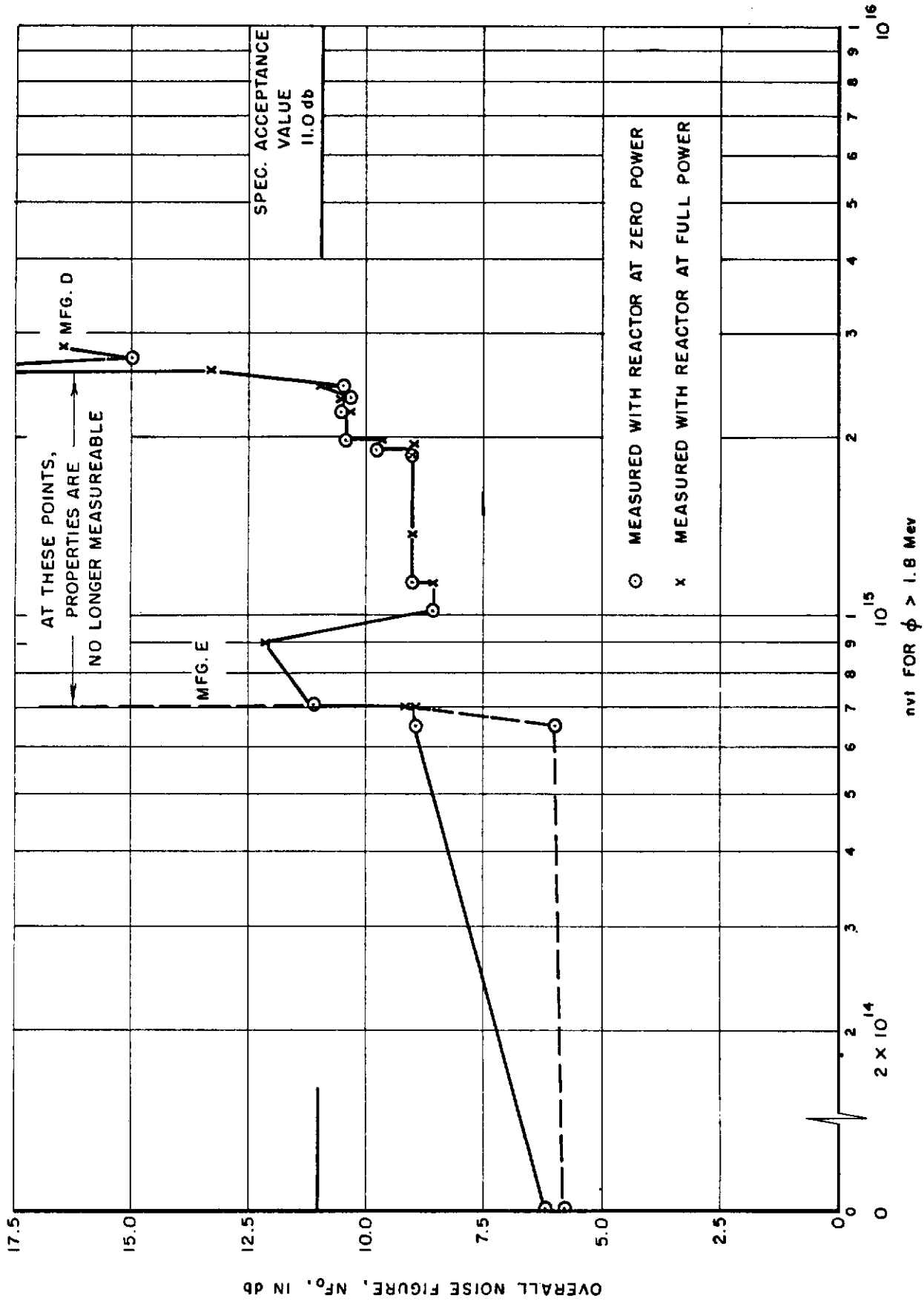

FIG. 18 OVERALL NOISE FIGURE — IN23B SILICON DIODES (ENERGIZED WITH X-BAND POWER DURING IRRADIATION)

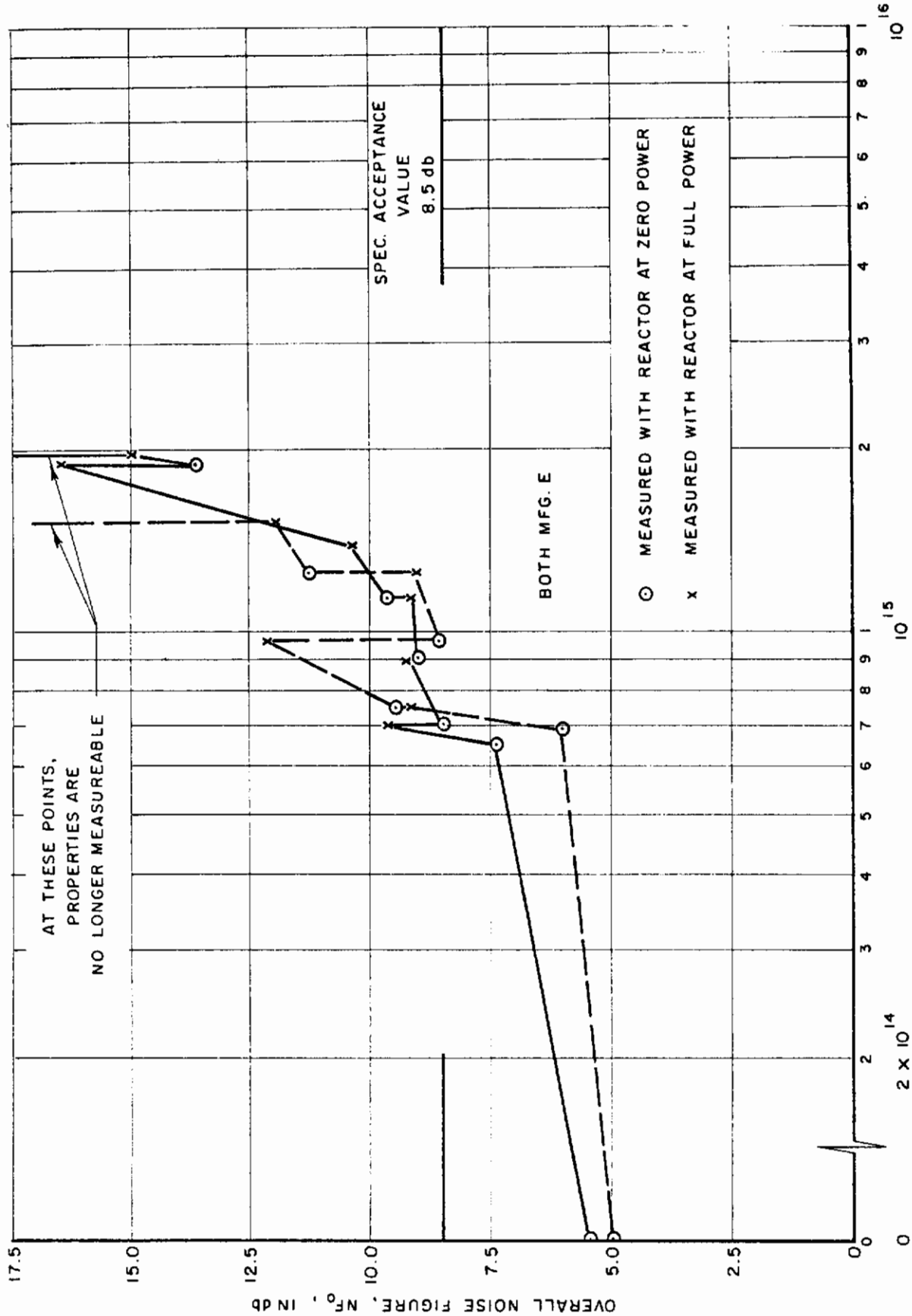

FIG. 19 OVERALL NOISE FIGURE — IN23WE SILICON DIODES (ENERGIZED WITH X-BAND POWER DURING IRRADIATION)

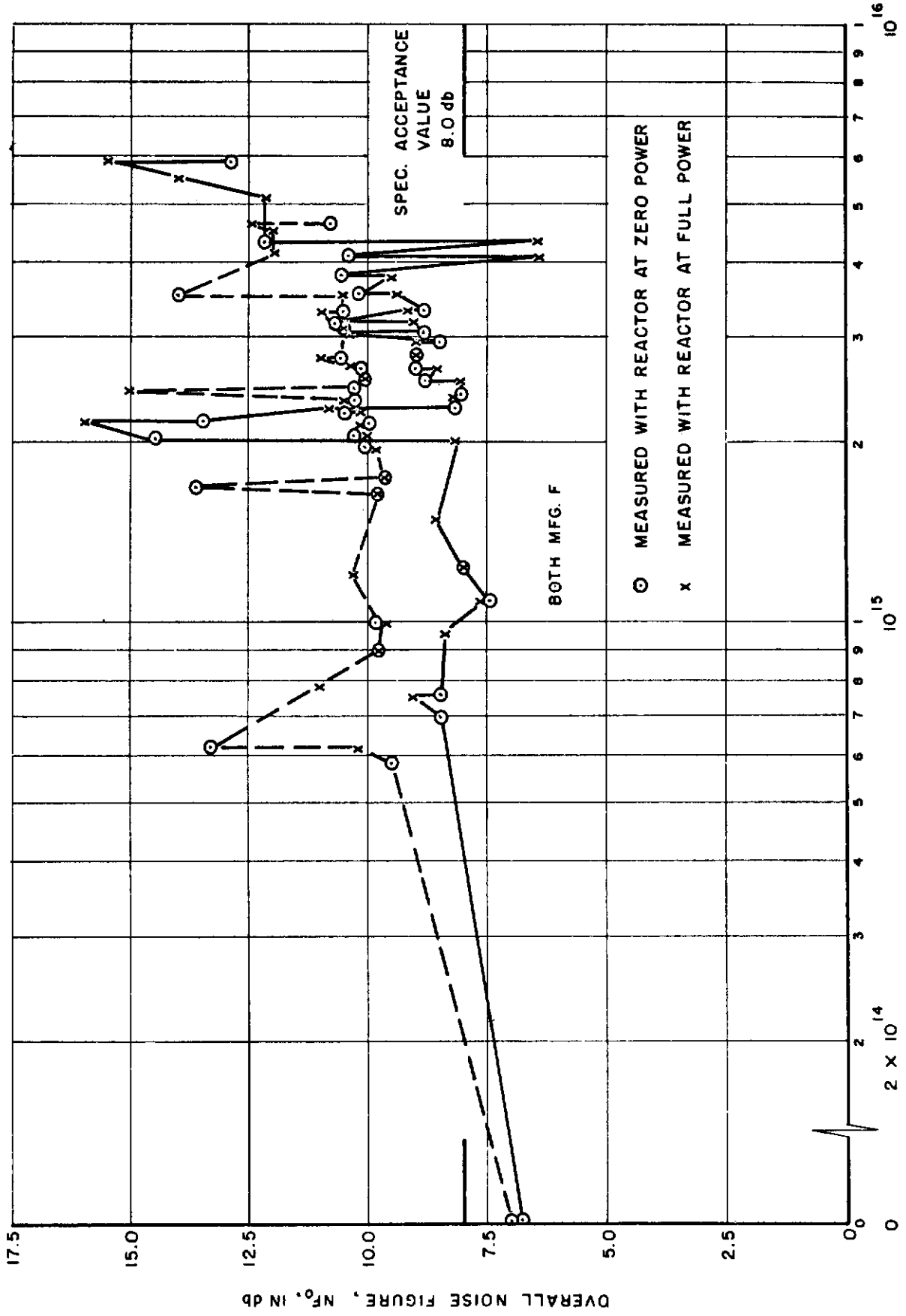

FIG. 20 NOISE FIGURE — IN263 GERMANIUM DIODES (ENERGIZED WITH X-BAND POWER DURING IRRADIATION)

static specimens, in that the 1N263 germanium diodes survived longer exposure than did the silicon diodes and did not fail catastrophically.

One of the 1N23B dynamic units failed quite rapidly, and one of the 1N23WE units also failed shortly thereafter. The 1N23WE unit suffered gradual degradation in its noise figure characteristic, but the 1N23B failed after the initial exposure. The two 1N263 units remained measurable throughout an exposure which would be in excess of an equivalent of 1000 hours' operation at a flux level of 10^{10} n/cm^2-sec even if "damaging flux" (see Appendix C) were not considered. A twenty-day anneal at room temperature produced only slight reductions in noise figure and conversion loss, and these values are still in excess of specification acceptance requirements. Nevertheless, these units show more promise for usefulness in a radiation atmosphere than others investigated.

IV CONCLUSIONS AND RECOMMENDATIONS

This investigation has again emphasized the fact that semiconductor devices cannot be selected for operation in nuclear environments solely on the basis of electrical characteristics. It is apparent that manufacturing methods and techniques are paramount in importance, and that uncontrolled items, such as the application of forming current for attaching the point contact to germanium, and the mechanical "tapping" to adjust the point contact to silicon, might well bear closer scrutiny.

None of the units investigated exhibited satisfactory performance following an exposure equivalent to 1000 hours at a flux level of 10^{10} neutrons/cm^2-sec. However, the germanium point-contact 1N263 diode did still exhibit measurable properties following this exposure. Damage in all instances was found to be quite permanent.

Several recommendations for possible improvement are apparent. With regard to point-contact devices in general, the geometrical precision might be increased through the use of surface barrier techniques. Further, the employment of advanced diffusion (Ref. 19), or micro-alloying techniques may be desirable.

It is possible that the smaller diameter point-contacts of the 10 kmc diodes added some measure of radiation tolerance. This is due to the reduction in minority carrier diffusion with smaller diameter contacts. Further reduction in contact diameters, would however, result in seriously decreased mechanical strength.

The heavy doping of the n-type germanium in commercially available diodes retards conversion of the material from n-type to p-type during radiation. This may be another reason for the better performance of the germanium mixer diodes since silicon does not exhibit this preferential conversion. It is therefore felt that p-type germanium should be investigated more thoroughly, since the minority carrier lifetime in this material is less affected by radiation. (Ref. 5) Some means have been found for increasing radiation tolerance. For example, reduction in base width by a factor of ten has increased radiation tolerance by 100. The diffused structure assists minority carrier transport giving markedly improved radiation behavior.

Varnish-coating the surface of a diffused pellet also resulted in improved performance during radiation exposure. These positive results should form a basis for implementation of the other aforementioned recommendations, with the assurance that more radiation-resistant units will be achievable.

V. REFERENCES

Books:

(1) Billington, D. S. and Crawford, J. H. Jr., Radiation Damage in Solids, Princeton University Press (1961)

(2) Fan, H. Y. and Lark-Horwitz, K., Fast Particle Irradiation of Germanium Semiconductors, Purdue University, Lafayette, Indiana

(3) Weinberg, A. M. and Wigner, E. P., The Physical Theory of Neutron Chain Reactors, (1938)

Periodicals:

(4) Behrens, W. V. and Shaull, J. M., "The Effect of Short Duration Neutron Radiation on Semiconductor Devices," Proceedings of the IRE, V. 46, pp. 601-605 (1958)

(5) Curtis, O. L. Jr., "Radiation Effects on Recombination in Germanium," Journal of Applied Physics, V. 30, No 8, pp. 1117-1322 (1959)

(6) Evans, J. E., "Fast Neutron Spectra from the Water Boiler," LA-1395 (1951)

(7) Howerton, R. J., "Tabulated Neutron Cross Sections," UCRL-5226 (May 1958)

(8) Hughes, D. S. and Harvey, S. A., "Neutron Cross Sections," BNL-325 (1955)

(9) Keister, G. L. and Stewart, H. V., "The Effect of Nuclear Radiation on Selected Semiconductor Devices," Proceedings of the IRE, V. 45, pp. 931-937 (1957)

(10) Leachman, R. B., P.I.C.G. 2 (1955)

(11) Messenger, G. C. and McCoy, C. T., "Theory and Operation of Crystal Diodes as Mixers," Proceedings of the IRE, V. 45, pp. 1269-1283 (1957)

(12) Primak, W. and Fuchs, L. H., "Fast Neutron Damaging in Nuclear Reactors. I. Radiation Damage Monitoring with the Electrical Conductivity of Graphite," Nuclear Science and Engineering, V. 2, No. 1, pp. 49-56 February, 1957)

(13) Primak, W., "Fast Neutron Damaging in Nuclear Reactors. II. The Radiation Damage Function of Graphite," Nuclear Science and Engineering, V. 2, pp. 117-125 (1957)

(14) Primak, W., "Fast Neutron Damaging in Nuclear Reactors. III. The Radiation Damage Dosage," Nuclear Science and Engineering, V. 2, pp. 320-333 (1957)

(15) Uhlir, A. Jr., "Two Terminal P-N Junction Devices for Frequency Conversion and Computation," Proceedings of the IRE, V. 44, pp. 1183-1191 (1956)

(16) Watt, B. E., Phys. Rev. 87 (1952)

V. REFERENCES (Continued)

Report:

(17) Burrus, W. R., "Standard Instrumentation Technique for Nuclear Environmental Testing," WADC TN 57-207 (May 1957)

Miscellaneous:

(18) Unpublished work by R. C. Barrall and W. N. McElroy. Additional information may be found in ARF Project Suggestion No. 61-140-AX, "Reappraisal of Requirements for Measuring and Reporting of Reactor Fast Flux Data" (April 12, 1961)

(19) Transitron Bulletin PB 65 - 1N919 Radiation-Resistant Silicon Diodes

(20) Private communications from Dr. W. Primak, Argonne National Laboratory, dated April 21, 1961

(21) Bibliography, Radiation Effects on Semiconductor Devices AD-254548

APPENDIX A

GENERAL PURPOSE DIODE INSTRUMENTATION

Design of the measurements circuitry was approached with two main objectives: reduction of the number of display photographs by obtaining one continuous display of both forward and reverse characteristics; and a means for operating all the diodes, with one lead of each diode being a common ground connection. This was desirable to reduce the number of leads entering the reactor port, with a consequent reduction of shielding and switching complexity.

Figure A-1 shows a simplified diagram of the circuit which was used for obtaining meter measurements of forward current, reverse current and forward voltage drop for the general purpose test diodes. Meters accurate to at least ±0.5 percent were used for all measurements. This applies to the following discussion of each of the measured quantities.

The forward voltage drop is defined as the drop across the diode during its conducting half cycle, averaged over the full cycle. With the correct value of a-c voltage applied, the load resistance, R_L is adjusted to give the proper value of forward diode current as indicated by the d-c ammeter, A_1. The reverse current of the test diode is also passed through this ammeter, but this current is so small with respect to the forward current that the accuracy of the forward current setting will not be affected.

When diodes D_1 and D_T are forward-biased, the forward voltage drop across D_T is indicated by the d-c voltmeter, whose impedance is high (5000 ohm/volt) with respect to the forward resistance of the test diode, D_T. When diodes D_1 and D_T are reverse-biased, the test diode is shunted by the d-c voltmeter, whose impedance is low with respect to the reverse resistance of the test diode. As a result, all of the voltage during reverse bias will be developed across D_1, except for a negligible quantity across D_T. Thus, the forward voltage drop will be averaged over the full cycle by the d-c voltmeter.

Again referring to Figure A-1, the forward voltage drop is measured when switch S_1 is in the closed position, as shown. To measure reverse current, the switch S_1 is moved to the left, removing the d-c voltmeter from the circuit, and inserting the diode D2 and microammeter A_2 across D_1 and A_1. The forward and reverse currents of the test diode are separated by diodes D_1 and D_2. When D_1 is forward-biased, D_2 will be reverse-biased, so that the forward current is prevented from flowing through the d-c microammeter A_2. This meter indicates the one-cycle average of the reverse current. When D_1 is reverse-biased, D_2 will be forward-biased, and the reverse current of the test diode will flow through the low impedance path of D_2 and the microammeter A_2. Because either D_1 or D_2 is always forward-biased, except near the zero voltage points of the a-c input waveforms, the voltage drop across the parallel combination can never be greater than the forward voltage drop of a conducting diode, assuming the ammeter voltage drops to be negligible.

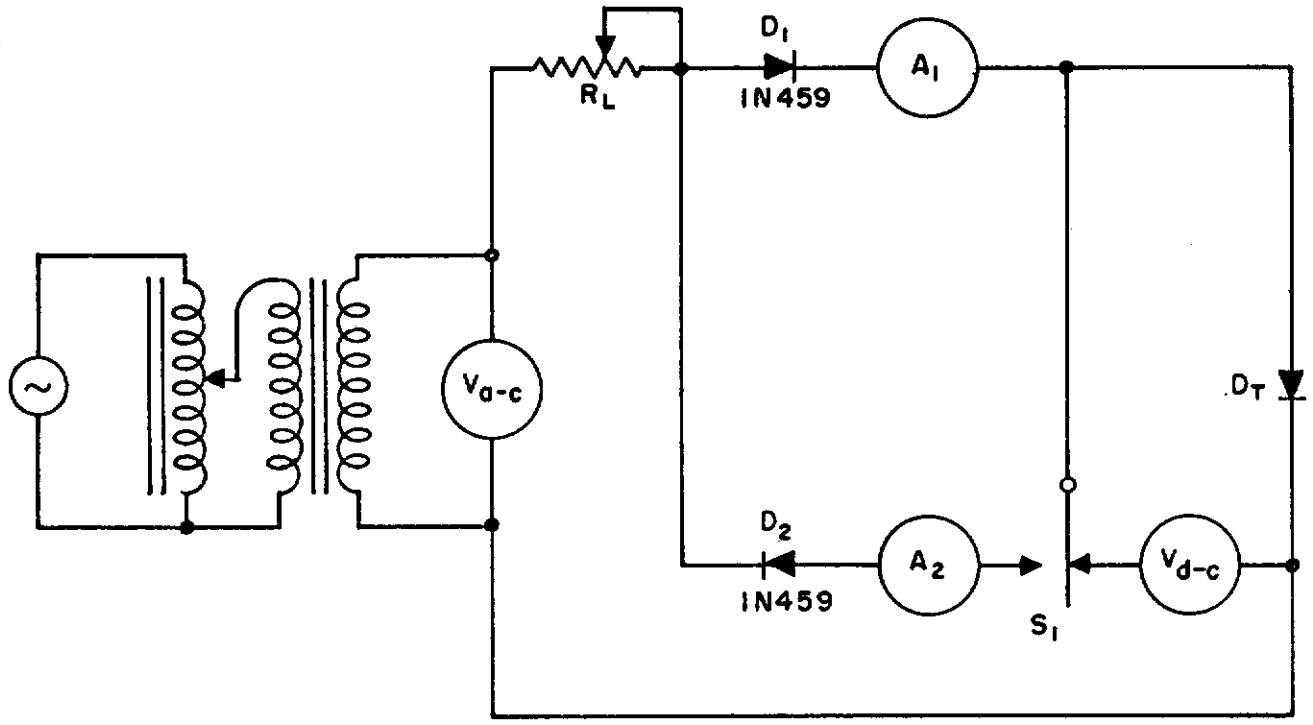

FIG. A-1 CIRCUIT FOR MEASURING DIODE CURRENTS AND VOLTAGES

The two types of general purpose test diodes under consideration are the 1N464 silicon junction diode and the 1N127 germanium point contact diode. The 1N464 has a rated maximum reverse current of 0.5 microamperes at its rated inverse voltage, while the reverse current of the 1N127 could be as high as 1.0 milliampere at its rated inverse voltage. D_1 and D_2 are both 1N459 silicon junction diodes whose maximum reverse current is 0.025 microampere at 175 volts inverse. Since leakage current for either D_1 or D_2 is established by the very low forward voltage drop of the other diode, errors introduced by leakage currents in the diodes are negligible with respect to test diode reverse current.

In the area very near the zero points of the a-c input voltage waveform, neither diode will have sufficient voltage impressed across it to bias the diode into forward conduction. It is therefore very difficult to predict the pattern of conduction through the two parallel branches. However, since neither diode is biased to conduction, it is known that the branch currents must be small, and since the reverse current measurement is averaged over a full cycle, the averaged effects of these currents during the small time period near zero are very small and can be neglected.

Figure A-2 shows the circuit established for obtaining a continuous display of forward and reverse characteristics simultaneously. The two 1N459 diodes separate forward and reverse currents of the test diode in the same manner as was discussed for diodes D_1 and D_2 in Figure A-1. The forward current of the test diode is measured by determining the voltage drop across an equivalent resistance of approximately 50 ohms. The reverse current is similarly measured across approximately 5000 ohms. Resistors R_1 and R_2 determine the voltage scale factors. Diode D_1 is selected to have a high reverse resistance with respect to R_1 and a low forward resistance with respect to R_2. Calibration of the dynamic display of the test diode is effected by photographing, to the same scale factors, the display of a diode of the same type which has not been subjected to radiation exposure. In this manner, any changes occurring as a result of radiation damage will be immediately obvious.

The circuit of Figure A-2 divides the scope face into four quadrants for display of forward and reverse characteristics. The location of the (0, 0) point is fixed by the selected values of resistance. As diode characteristics change, e.g., increase in reverse current, it is necessary to change relative gain settings of the horizontal and/or vertical controls to contain the trace within the full scope face. Because of the fixed distance relationships between forward and reverse regions, there is some limit to the ability to retain the same relative sensitivity between forward and reverse characteristics.

Circuit arrangments were also made to operate the dynamic diodes with load current uninterrupted once the full scale test had begun. This is accomplished by suitable switching to select one diode for the measurements circuit while all others remain on load.

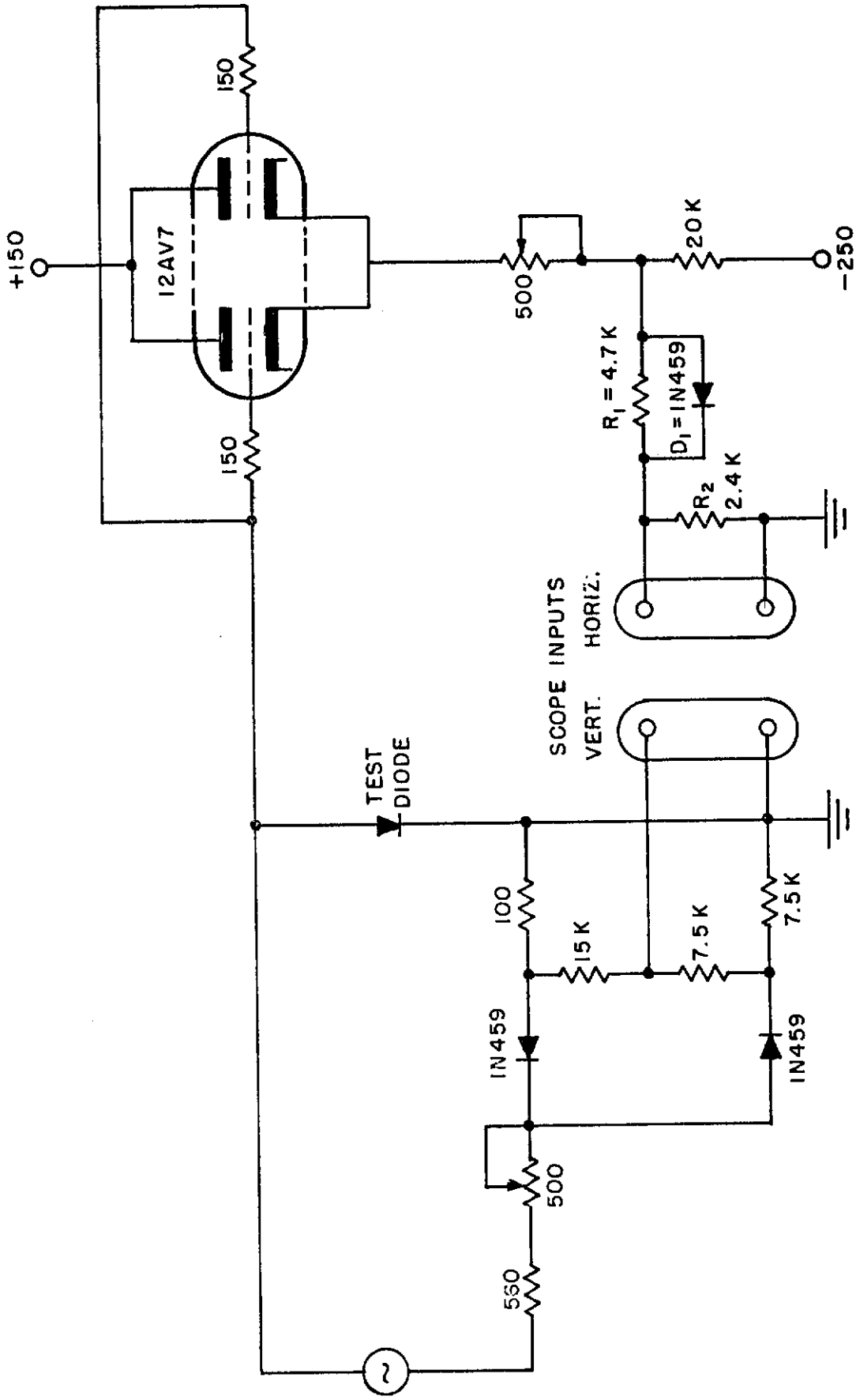

FIG. A-2 CIRCUIT FOR DYNAMIC DIODE DISPLAY CHARACTERISTICS

APPENDIX B

MICROWAVE INSTRUMENTATION AND SHIELDING REQUIREMENTS

I. MEASUREMENTS METHODS

The principal criteria of performance of a mixer diode are its capability as a converter and its noisiness. The factors by which this capability is assessed are the conversion loss, the noise temperature and the overall noise figure. These properties are defined as follows:

$$\text{Conversion Loss, } L_c = \frac{\text{available r-f signal power}}{\text{i-f signal power delivered by mixer}} \tag{3}$$

$$\text{Crystal noise temperature } t_c = \frac{\text{available noise power generated by crystal}}{\text{noise power available from an equivalent resistor at } 20^\circ\text{C}} \tag{4}$$

$$\text{Overall noise Figure, } NF_o = L_c(t_c + NF_{i\text{-}f} - 1)$$

$$\text{where } NF_{i\text{-}f} \text{ is the noise figure of the i-f amplifier} \tag{5}$$

Although there are many different methods of measuring the conversion loss and noise figure of microwave diodes, the use of the modulation method for measuring conversion loss and the Y-factor method for determining overall noise figure was judged more appropriate for this program.

The modulation method for measuring conversion loss is a relative method, and is referred to as Method B in MIL-E1D, paragraph 4.14.3.1. A slight amplitude modulation is placed on the local-oscillator signal and the mixer is connected to a load having an impedance, Z_m, at the modulation frequency, and a d-c resistance, R_L, specified for that diode. The amplitude of the modulation signal voltage across Z_m is measured, and that voltage is assumed to be inversely proportional to the square root of the conversion loss. Several reference diodes were checked to obtain reasonable standards, and all conversion loss calculations are based on the assumed conversion losses for those standards.

The Y factor is the ratio of the available noise output, N_o, of an i.f. amplifier fed by a crystal mixer, to the available noise power output, N_{os}, when the i.f. amplifier is fed from a standard (dummy) resistor, or

$$Y = \frac{N_o}{N_{os}} \tag{6}$$

The Y factor depends on the conductance and noise figure of the i.f. amplifier and the noise temperature of the mixer diode. The product $t_c L_c$ is the contribution to the overall noise factor, and is, hence, a direct contribution to the converter noise figure.

Thus, the Y-factor can be measured and t_c is obtainable from

$$t_c = NF_{i.f.}(Y-1) + 1 \quad (7)$$

where $NF_{i.f.}$ is the noise figure of the i-f amplifier

The overall noise figure NF_o is then related to these parameters by

$$NF_o = L_c(NF_{i.f.} + t_c - 1) \quad (8)$$

II. MICROWAVE INSTRUMENTATION

The block diagram of Figure B-1 illustrates the equipment which was designed and built to energize the X-Band diodes during reactor exposure. Each r.f.-powered diode in the reactor had its own 2K25 klystron supplying power to it during exposure. In this manner, it was possible to make individual adjustments of frequency and power level, as well as bias, on those diodes requiring it. The 2K25 klystron tube cannot be used as a source for noise figure measurements because of excessive noise and a relative frequency instability. However, the 2K25 can be used to good advantage as a continuously operating local oscillator for energizing the diodes during reactor exposure.

The block diagram shown in Figure B-2 is a separate, highly refined test system which was established to measure noise figure and conversion loss at X-Band frequencies. This system incorporates an X-13 klystron as the low noise, frequency stable source for supplying power to each diode as it is being measured while under radiation exposure.

Systems similar to that of Figure B-2 were established for measuring the diodes designed for "L" and "S-Band" frequencies. Since only the X-Band diodes were energized with r.f. continuously, they were the only diodes which could be measured in place in the reactor.

The static microwave diodes and those dynamics which were energized at 60 cps were monitored during exposure, using the simple d-c technique of the crystal test set. This technique measures the non-linearity of the diode voltage-current curve by measuring the incremental change in crystal current caused by an incremental change in forward voltage. The non-linearity is directly related to conversion loss and noise figure. This technique is incorporated in Airborne Instruments Laboratory test set Type 391. This test set is versatile enough to check biased crystals, and, as such, is suitable for these monitoring measurements.

Figure B-3 is a photograph of the entire instrumentation for the program, in place near Port I of the reactor. All of the leads and coaxial cables are brought out of the reactor through Port I. The general purpose test set labeled in Figure B-3 contains all of the measurements and switching circuitry for the static and dynamic general purpose

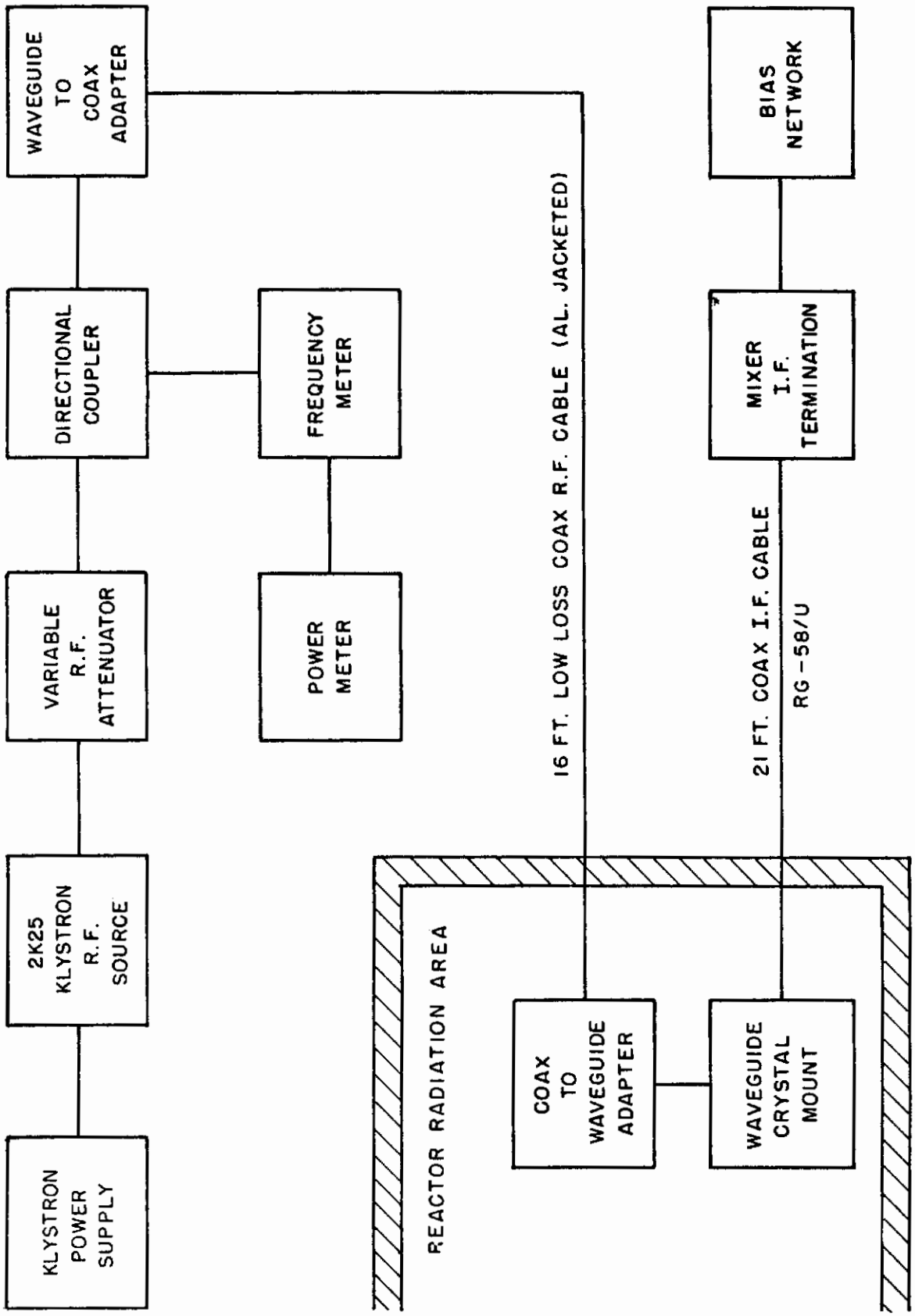

FIG. B-1 DIODE R.F. POWER SYSTEM

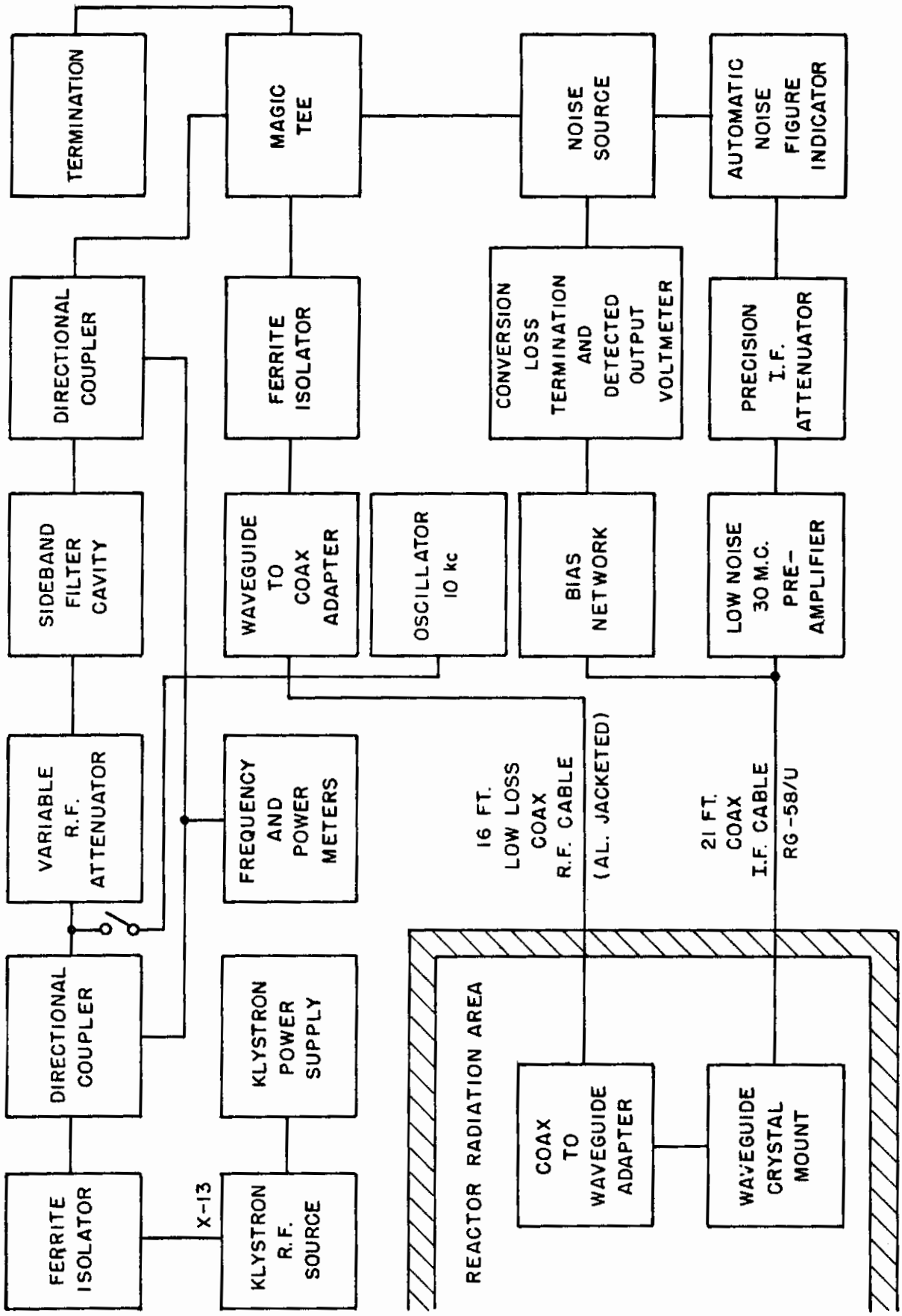

FIG. B-2 DIODE R.F. MEASUREMENTS SYSTEM

FIG. B-3 INSTRUMENTATION FOR DIODE MEASUREMENTS

diodes, as well as the static microwave diodes and the dynamic microwave diodes which were energized by 60 cps current. The adjacent relay rack contains the 2K25 Klystrons, mounts, and associated circuitry for adjusting frequency and output level. The X-Band test set, together with the Automatic Noise Figure Indicator, is shown on the movable table. Other equipment shown includes attenuators, power meters, and power supplies for the 2K25 klystrons and the X-Band test set.

III. SHIELDING AND PHYSICAL ARRANGEMENTS

The diodes, in their shielded enclosure, were located in the area indicated in Figure B-4. This was done by removing several graphite stringers from the thermal column area behind the bismuth shield and inserting the diode box in their place. The cabling was brought out into the void volume and connected to the port insert in Port I, which in turn connects to the external instrumentation.

Aluminum was used wherever possible in the construction of mechanical mounts for the diodes, and in support structures. Polystyrene and polyethylene were used as insulation in critical areas, and polyvinyl-chloride was used as the insulation for all hook-up wire that was exposed to radiation. PVC was selected for the hook-up wire because it is apparently the only readily available hook-up wire insulation having good resistance to radiation exposure.

Figure B-5 illustrates the manner in which cables and wire were brought out through the reactor port. The cylinder is an aluminum pipe with aluminum plates at one end to anchor the connectors mechanically. The pipe is filled with paraffin for radiation absorption, and is inserted directly into the port, with a short portion protruding slightly into the void space near the thermal column.

The general purpose diodes and those dynamic microwave diodes which were energized at low frequency power are mounted on a polystyrene sheet. This sheet is fastened to a mounting rack constructed of aluminum angle. The waveguide crystal holders are also mounted in this rack. The static microwave diodes are mounted on a similar polystyrene sheet which is fastened to a separate, easily removable drawer. The separate drawer facilitates removal of the static diode group for purposes of effecting external microwave measurements. Details of the mounting arrangements of the crystal holders are shown in Figure B-6. Figure B-7 shows details for the mounting of the remainder of the diodes.

The diodes, crystal holders, thermocouples and associated cabling are housed in a box constructed of Boral sheet. This material is a combination of aluminum and boron carbide, containing 35 percent boron carbide. Although this material is extremely difficult to machine, it was found necessary to use this for thermal neutron shielding, in place of cadmium, to reduce hazards of any required handling. The boral box, together with the diode rack assembly, (coaxial cables removed) is shown in Figure B-8.

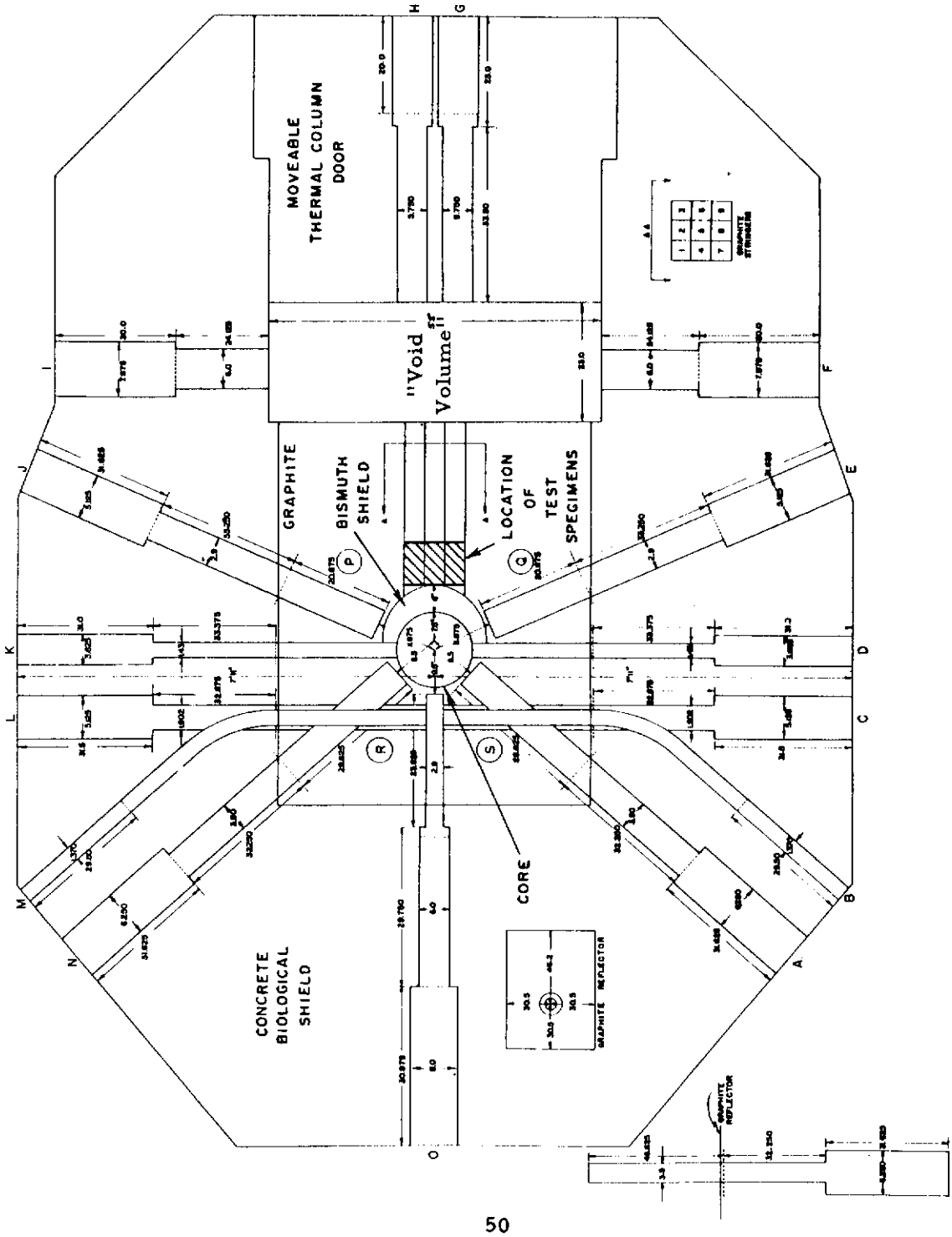

FIG. B-4 THE IRRADIATION AND EXPERIMENTAL FACILITIES OF ARMOUR RESEARCH REACTOR

FIG. B-5 REACTOR PORT CABLING INSERT

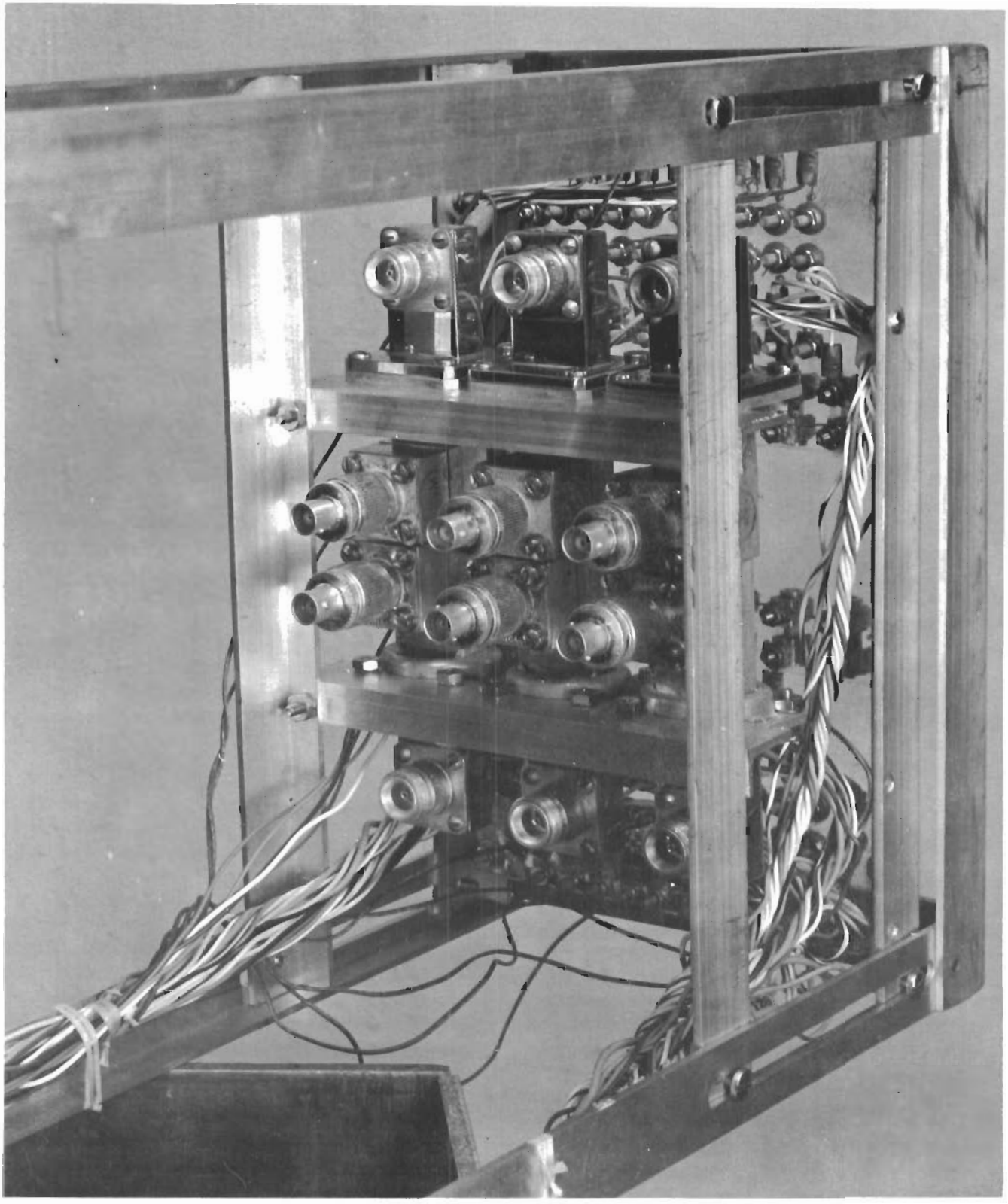

FIG. B-6 WAVEGUIDE DIODE HOLDER MOUNTING

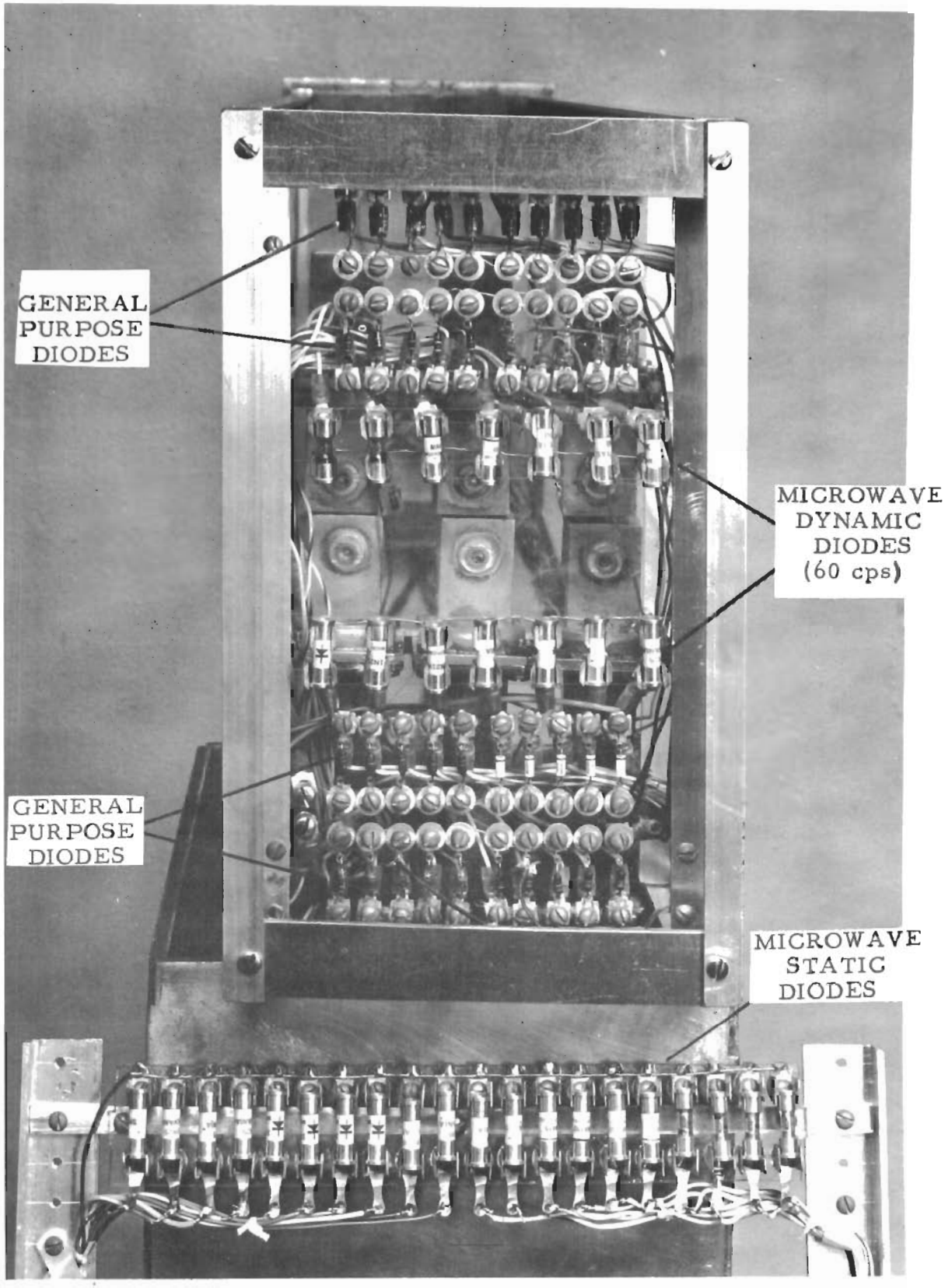

FIG. B-7 DIODE MOUNTING

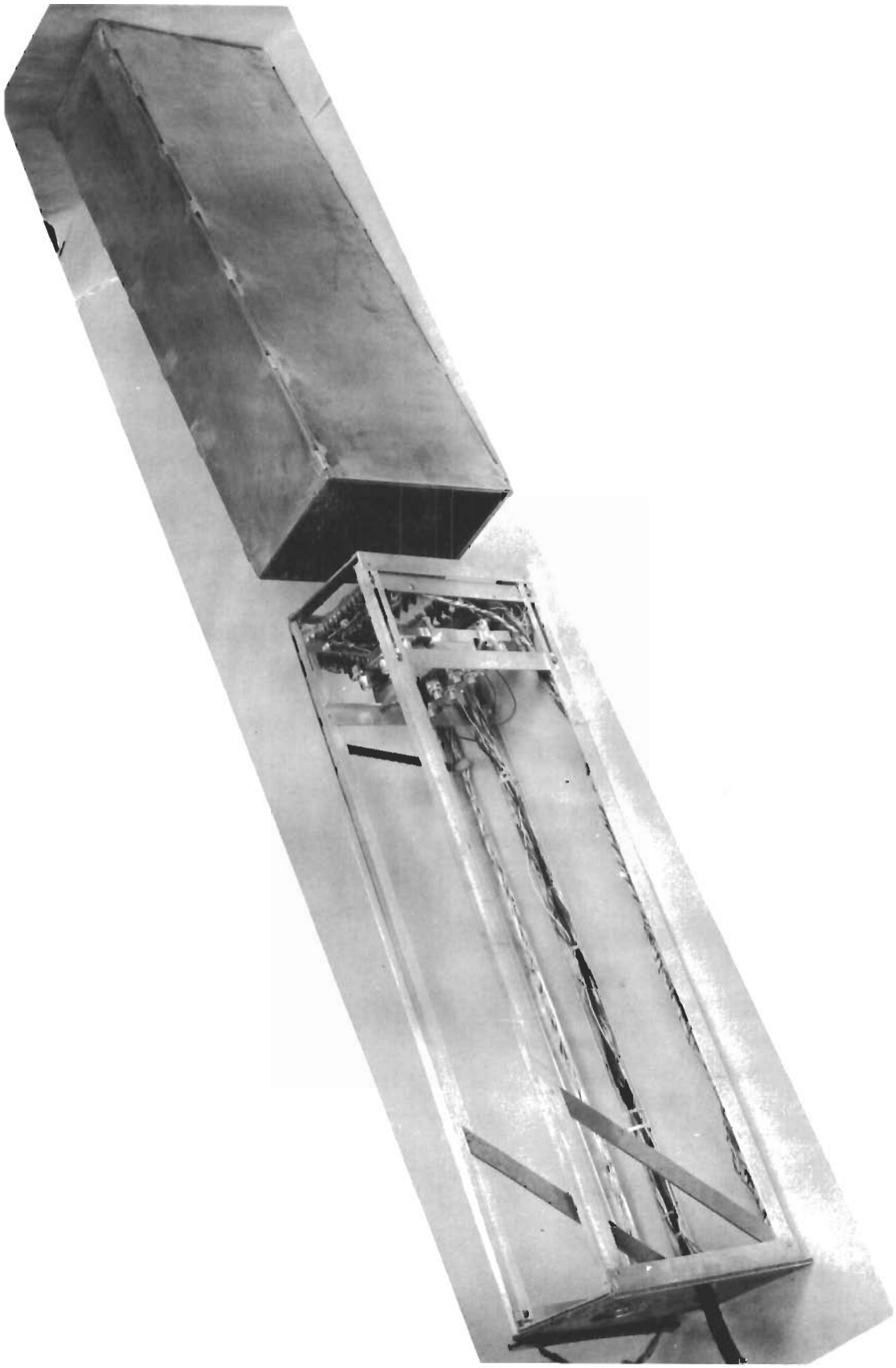

FIG. B-8 DIODE RACK ASSEMBLY WITH BORAL SHIELDING

IV. PRELIMINARY EXPERIMENTS

Prior to determining the final design of instrumentation, it was necessary to perform some preliminary experiments in the reactor. These experiments were designed to determine the suitability of the proposed techniques, as well as the degree of degradation to be expected from materials and components forming part of the associated circuitry.

Two 30 foot long RG-9A/U cables were inserted in the thermal column (Port I) of the reactor, where the neutron density (neutrons/cm^2-sec greater than 1.8 Mev) is approximately 10^{10}. A pair of standard connectors was assembled to the middle of one of the cables, and both cables were looped so that the connectors, as well as portions of the cable, were exposed to radiation levels consistent with those to which the diodes were to be exposed.

No changes were observed in the VSWR and insertion loss, nor was any other sign of deterioration, during two and one-half hours of reactor operation at 50 kw while measurements were being made with the reactor power on.

To determine the length of trouble-free life of the cables and connectors, two other cables were inserted in the central exposure port, Port K. One cable consisted of 40 feet of RG-9A/U polyethylene r.f. cable, and the other of 15 feet of RG-8A/U polyethylene r.f. cable and 15 feet of RG-58/U polyethylene i.f. cable. The former was looped through the high flux area. The latter was also looped so that the standard connectors which joined the r.f. and i.f. cable were exposed to the high flux area. X-Band (9.375 kmc) energy was fed in the RG-9A/U cable and a 30 mc signal in the RG-8A/U combination.

During approximately the first 10 minutes of operation, the RG-9A/U cable which was inserted in the central exposure port showed slight changes of VSWR and insertion loss, failing completely after about 30 minutes of continuous operation at 10^{12} nv. Visual examination of the cable showed that the insulation had cracked. This may be attributed to the softening of the dielectric under the 160° F temperature of the port (this temperature differs from that in the lower flux regions), and subsequent yielding of the dielectric until the inner and outer conductors of the coaxial cable had shorted.

In these tests it was necessary to have access to both ends of the cable. Because of the small diameter of the port, the resulting bend is, of necessity, quite sharp. It is believed that the failure of the RG-9A/U cable was due in large part to this bend, since it could have created a condition leading to failure.

In the same port, the RG-8A/U-RG-58/U cable combination was also inserted. However, the RG-8A/U cable went in unbent, terminated in a series of connectors (type N to BNC) at the end of which the thinner RG-58/U cable was connected and subsequently bent out. No visual damage took place in this combination. The 30 mc insertion loss was not changed appreciably during the two and one-half hour operation (corresponding to about 1000 hours of continuous operation at 10^{10} nv).

The observed radioactivity of these cables was about 400 roentgens per hour, measured at one foot distance. This level of radioactivity was quite high and dangerous for handling purposes. Since the brass used, which is part of the cables and connectors, contains zinc, which has a half life of many months, the transmission lines would not be able to be handled with bare hands for a long period after they were removed from the reactor, unless proper handling instruments were used.

The preliminary measurements showed that the reliability of some of the coaxial cables in radiation atmospheres is somewhat questionable, and that the induced activity represents a biological hazard. Because of these considerations, it was decided to use aluminum-jacketed, polyethylene-filled, low-loss (about 16 db/100 ft at X-Band) coaxial lines to bring in the r.f. power to the diode holder located in the radiation area. The i.f. power was brought out by means of an RG-58/U coaxial cable which was approximately one wavelength long at 30 mc, amplified, and then detected. The use of these cables gave trouble-free operation throughout the extent of the full-scale reactor program.

APPENDIX C

NEUTRON FLUX SPECTRA AND EXPOSURE MEASUREMENTS

I. The "Armour Research Foundation Method" for Measuring Reactor Fast Neutron Flux-Spectra (ref. 18)

A study of investigations made during the last few years has shown that there is still no definite agreement on one set of values of the fission spectrum-weighted effective cross-sections and threshold energies to be used for the different threshold detectors. Moreover, since most measurements are made on neutrons that do not have a fission spectrum energy distribution, the currently accepted values of effective cross-sections and energies cannot be expected to give correct values for the measured fast neutron flux-spectra. For these and other reasons, another method of making fast flux-spectra measurements is used and is currently being refined at the Armour Research Foundation.

The efforts aimed at improving the techniques applicable to the use and interpretation of resonance and threshold detectors have been supported separately by the Armour Research Foundation. These studies were prompted in part by the realization that an understanding of radiation damage must ultimately be based on precise experiments in facilities which have been carefully calibrated for neutron flux-spectra.

The ARF method is largely equivalent to methods and techniques in use by many others, in that a spectrum is initially assumed. After obtaining the neutron flux data from a number of detectors on the basis of the assumed spectrum, a revised estimate of the spectrum is prepared and new averaged values of cross-sections are assigned. The values of the flux above the different detector's neutron energy threshold are then recalculated, and the process repeated, until further efforts do not result in a significant change in these values of flux. The salient feature of this process is the specification of a given value of neutron flux as being present above the true value, rather than an effective energy threhold for the different detectors. It is in this prominent respect that the ARF method differs from other methods. The selection of the proper energy detection limits of the detector and of the averaged value of cross section is accomplished with the aid of the detector sensitivity function, $\sigma(E)\phi(E)$, where $\sigma(E)$ is the functional form for the energy dependent cross-section and $\phi(E)$ is the differential neutron flux in units of n/cm^2-Mev.

A plot of the $S^{32}(n, p)P^{32}$ sensitivity function is shown in Figure C-1 as an illustration. Note particularly that, within the limitations of the assumed form for $\phi(E)$, the area under this curve is the actual response of the detector per atom of target material. For the sulfur reaction, one obtains the lower energy detection limit of 1.8 Mev as the true effective threshold. Data obtained with this detector is then reported as neutron flux above 1.8 Mev, using a value of $\overline{\sigma}_i = 0.148$ barns. This procedure seems more meaningful than the current practice, which is to report the value of the neutron flux above an effective energy of 2.9 or 3.0 Mev, with a value of

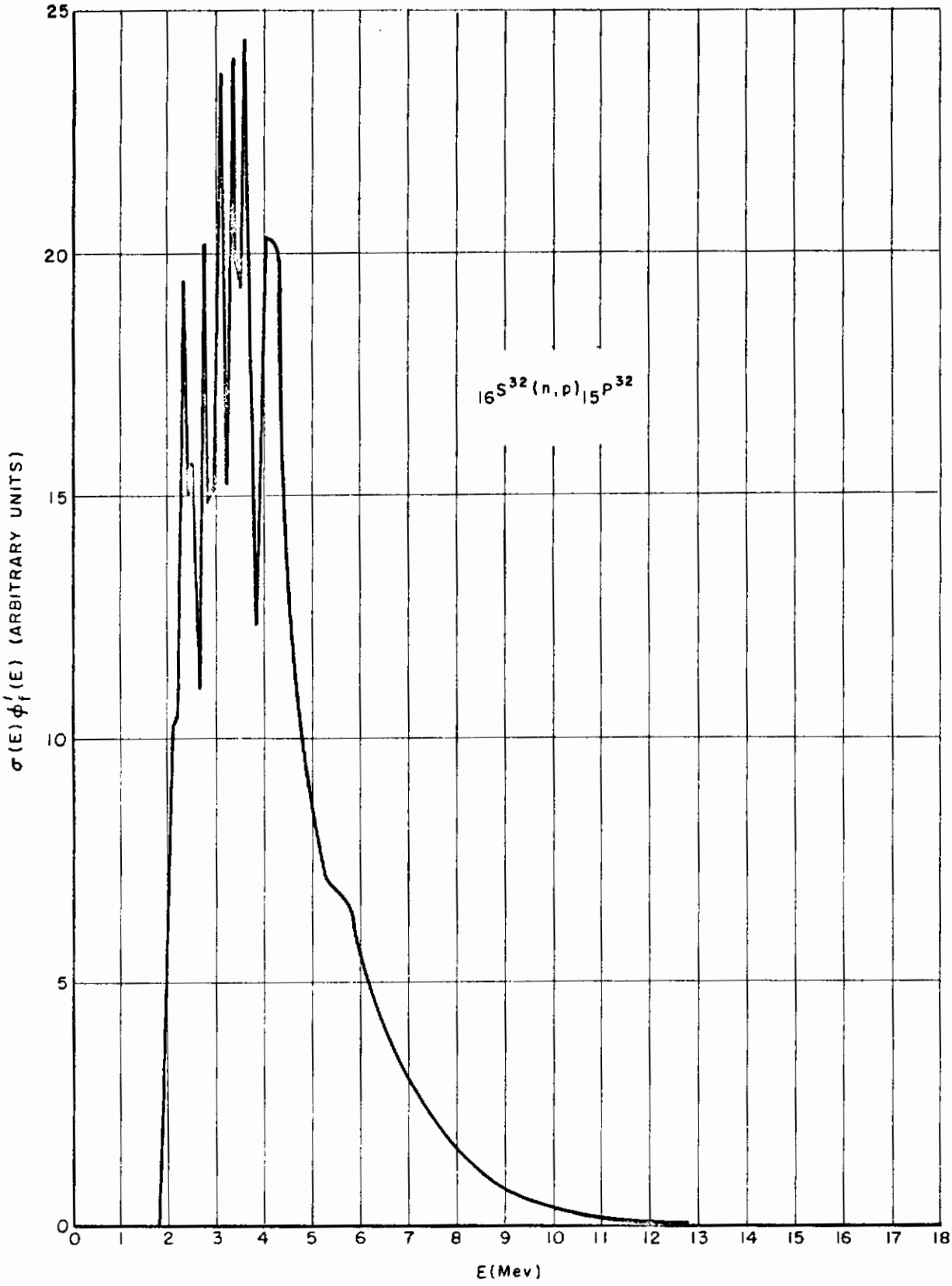

FIG. C-1 SENSITIVITY FUNCTION, SULPHUR REACTION

effective cross-section of 0.300 barns. A study of Figure C-1 makes it quite clear that about 1/4 of the measured activity of the sulfur detector is due to neutrons between 1.8 and 3.0 Mev.

With these comments as background, a more detailed description of the ARF Method of making flux-spectra measurements is now presented.

To determine the total fast flux ϕ_T, in some energy interval E_1 to E_2, the relationship

$$A_i = N_i \, \overline{\sigma}_i \phi_T (1 - e^{-\lambda t}) e^{-\lambda T} \tag{9}$$

where A_i is the measured activity per unit volume of foil i, N_i is the number of target nuclei per unit volume, λ is the decay constant, t is the irradiation time, and T is the decay time, may be used where $\overline{\sigma}_i$, the integrated averaged cross-section for activation over the energy interval, is given by

$$\overline{\sigma}_i = \int_{E_1}^{E_2} \sigma_i(E)\phi(E)dE \Big/ \int_{E_1}^{E_2} \phi(E)dE \tag{10}$$

and ϕ_T, the total flux in the energy interval, is given by

$$\phi_T = \int_{E_1}^{E_2} \phi(E)dE \tag{11}$$

where $\sigma_i(E)$ is the energy dependent cross section for activation and $\phi(E)$ is the flux distribution function (the differential neutron flux). Note that the limits E_1 and E_2 of integration need to be considered carefully if the resulting $\overline{\sigma}_i$ is to have a real physical meaning.

Now consider sulfur as a threshold detector. It is known that in many of the locations of higher flux in a reactor, the neutron spectrum above 1.6 Mev is similar to a fission spectrum. As such, one can take published values of $\sigma_i(E)$ for the sulfur n-p reaction in the energy range above 1.6 Mev, and can initially assume a fission spectrum for the form of $\phi(E)$ and numerically integrate equation (10) to obtain $\overline{\sigma}_i$. The resulting value of $\overline{\sigma}_i$ and the measured or known values of the other parameters then can be used in equation (9) to obtain ϕ_T for the fast flux above the "true measurable effective threshold energy E_1 and below E_2" in any reactor.

In relation to detection limits, a "Sensitivity Curve" is prepared (see Figure C-1) and values of $\sigma_i(E)\phi(E)$ are plotted against energy in order to find that 1.8 Mev is about the correct value for the "true measurable effective threshold energy" for sulfur. The prime on $\phi(E)$ is used to indicate a fission spectrum. Therefore, at least in the case of sulfur, it is natural to use a lower limit of integration for E_1 of 1.8 Mev. The upper limit of integration E_2 is obviously more difficult to choose, and some researchers have set it equal to ∞ as a matter of convenience; however, this should not be done arbitrarily--the shape of the sensitivity curve should be used to determine both E_1 and E_2.

If a number of different threshold detectors are taken which would cover the energy range below and above 1.8 Mev, the same thing can be done with these detectors as was done with sulfur in obtaining values of $\overline{\sigma}_i$ and determining their detection sensitivity curves, $\sigma_i(E)\phi(E)$ as a function of E. These detectors can then be used to determine the total fast flux above their "true measurable effective threshold energy E_1 and below E_2." Now obviously, the fact that the actual neutron spectrum may be greatly different than a fission spectrum means that the initial value of the flux above the "true measurable effective threshold energy E_1 and below E_2," which is obtained by using a value of $\overline{\sigma}_i$ (that is based on a fission or some other suitable spectrum), may be significantly in error. Therefore, one uses the initial results obtained through use of the different detectors and assumed values of $\overline{\sigma}_i$ to plot a spectral distribution curve. Since, in general, this initially determined form of the spectral distribution will be incorrect, this determined form must be used to calculate new values of the $\overline{\sigma}_i$'s, to obtain new values for the fast flux for an improved form of the spectral distribution. This process can be repeated as many times as needed, and this "method of iteration" should lead to a determination of the actual spectrum in the reactor. Obviously, the success of this method is dependent on having an adequate number of threshold detectors.

The ARF method of approach has a greater fundamental simplicity and correctness than the present "effective threshold method." In addition, this method gives a more meaningful value to the effective threshold energy and should be used for those theshold detectors that have tabulated cross-section data, as reported in such references as (8) and (18).

In order to calculate initial values of $\overline{\sigma}_i$, it was necessary to select a tentative spectrum. For purposes of calculation, the flux distribution was assumed to be a fission flux distribution function, $\phi'(E)$. Measurements of the emitted neutron spectrum from Los Alamos Water Boiler Reactor (ref. 6.) (similar to the ARR), using nuclear emulsion techniques, indicate that this is a valid approximation (the thermal neutrons were removed by cadmium for these measurements.)

There are many models of $\phi'(E)$ which are in good agreement with each other and with experimental data. For the purpose of this calculation, $\phi'(E)$ is taken from Weinberg (ref. 3) who cites Leachman (ref. 10) and Watt (ref. 16). Leachman (ref. 10) shows that when U^{235} fission is induced by 3 Mev neutrons, $\phi'(E)$ is only slightly different from $\phi'(E)$ when thermal neutrons are used to induce fission. One may conclude that $\phi'(E)$ is not a

strong function of the energy of the neutron inducing fission.

From Weinberg's formula, we have

$$\phi'(E) = 1.55 \left[\frac{0.775E}{\pi}\right]^{1/2} e^{-0.775E} \qquad (12)$$

Values of $\sigma_i(E)$ for the sulfur n-p reaction above the measured threshold energy, E_1 of about 1.8 Mev, were taken from BNL-325 (ref. 8) and UCRL-5226 (ref 7), and equation (10) was numerically integrated in 0.01 Mev intervals to obtain $\overline{\sigma}_i$. It was assumed that $\sigma_i(E)$ changes linearly from 0.0225 barns at 5.4 Mev to 0.0100 barns at 4.0 Mev. The value of $\overline{\sigma}_i$ obtained was

$$\left[(1.8 \text{ Mev} < E < 12 \text{ Mev}) \quad {}_{16}S^{32}(n, p){}_{15}P^{32}\right] \overline{\sigma}_i = 0.148 \text{ barns} \qquad (13)$$

By using equation (9), the calculated value of $\overline{\sigma}_i$, and beta counting to determine A_i, values of the total fast flux ϕ_T above 1.8 Mev have been obtained in the various exposure facilities.

In general, most test specimens are located in such a position that there is some moderator or scattering material between the fuel region and specimen. In addition, neutrons may be reflected to the specimen from nearby materials. If this physical arrangement causes a significant spectral perturbation, as is usually the case, one needs to have several threshold detectors, and must use a process of iteration wherein the value of $\overline{\sigma}_i$ is finally adjusted to the actual spectral distribution.

With reference to Figure B-4 and the indicated location of the test specimens, preliminary measurements were made in a one cubic foot cadmium box; the value of $\phi_T(E > 1.8 \text{ Mev})$ was found to vary over the one foot cube volume by a factor of about 3 from a position next to the bismuth to a point one foot away. The maximum measured value of $\phi_T(E > 1.8 \text{ Mev})$ in this thermal column area was approximately 1.3×10^{10} n/cm^2-sec. Similar measurements showed that the maximum values of $\phi_T(> 1.8 \text{ Mev})$ in Ports N and D were approximately 1.2×10^{11} and approximately 8.4×10^{11} n/cm^2-sec, respectively.

Subsequent to these preliminary measurements, more detailed measurements were made in the two areas of greatest concern. These two areas are the thermal column where the diodes were placed for the full-scale reactor runs, and the central exposure ports (Ports D and K) where preliminary experiments on the diodes were conductef for shorter periods of time at higher fast flux levels. Values of the fast neutron flux, $\phi_T(E > 1.8$ Mev), in the thermal column are listed in Table C-1 for the positions shown in Figure C-2.

Figure C-3 and Figure C-4 represent the most recent determinations of neutron flux in the central exposure ports, Ports D and K. Data has also been obtained showing the thermal flux in Port K at 95 inches from the reactor face (center of the core) to be 1.0×10^{12} n/cm^2-sec at 50 kilowatts. The cadmium ratio at this location is 3.3.

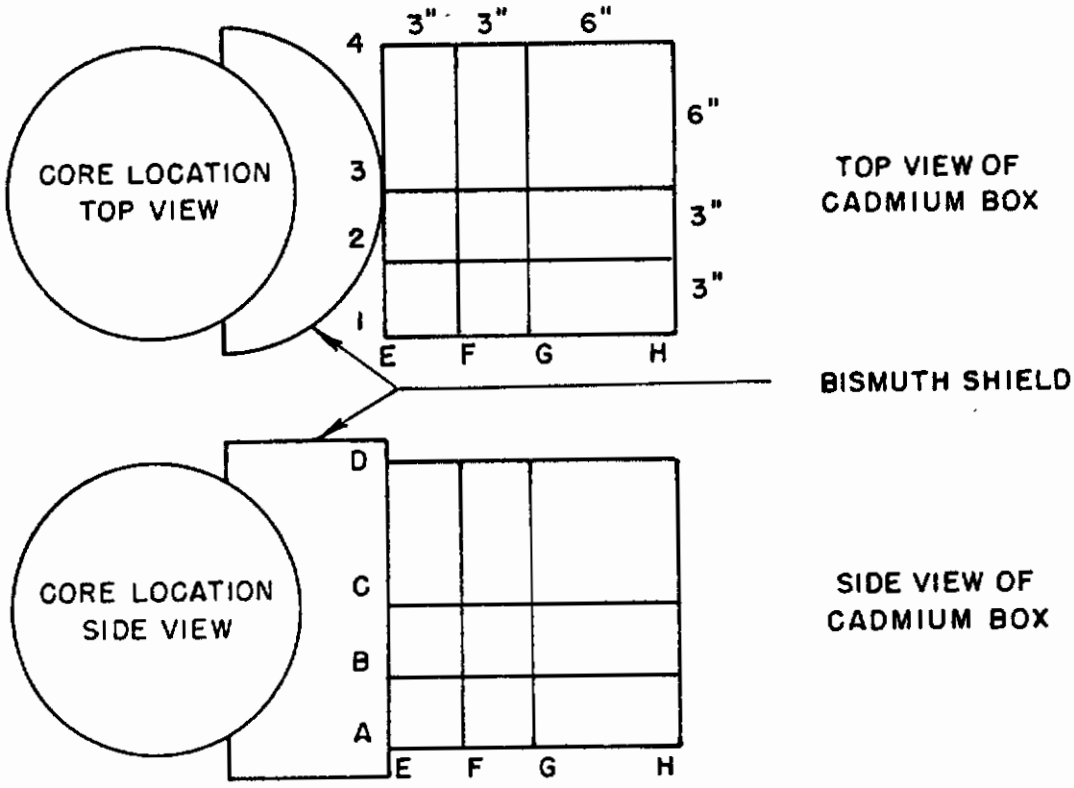

FIG. C-2 FAST FLUX IN THERMAL COLUMN

TABLE C-I Tabulated Values of 10^9 n/cm^2-sec $>$ 1.8 Mev

Position	1	2	3	4
AE	9.25		10.3	9.94
F	7.57		7.53	7.22
G	5.66		5.62	5.29
H	3.40		3.93	3.16
BE	11.4		12.8	11.7
F	8.13		8.79	8.42
G	6.07		6.56	5.90
H	3.15		4.48	3.58
CE	12.4	13.0	13.2	12.1
F	8.46		9.32	8.56
G	6.34		6.44	6.37
H	3.88		4.60	3.81
DE	9.66		9.90	9.34
F	7.38		7.39	7.69
G	6.13		5.14	5.79
H	3.42		3.41	3.26

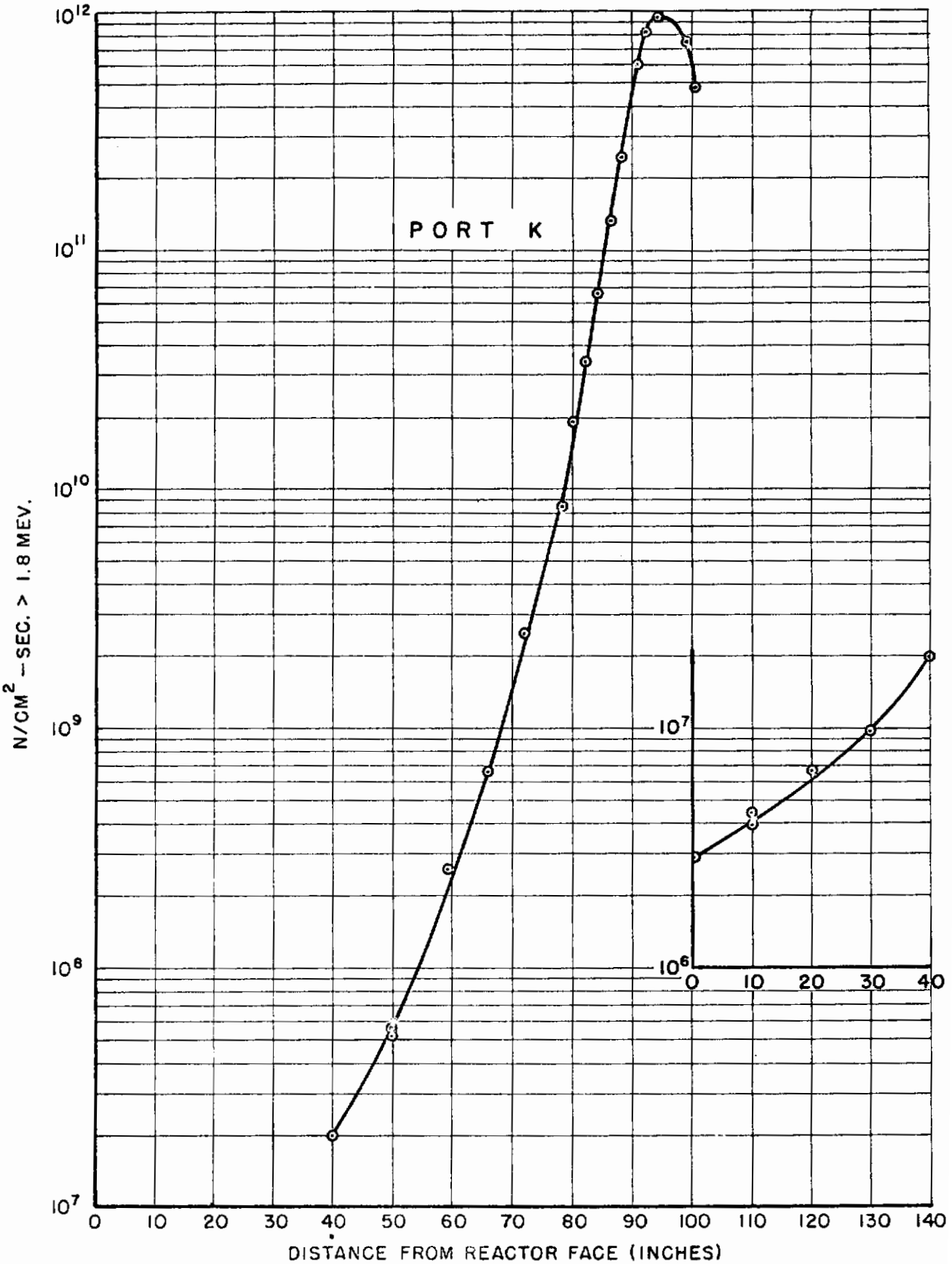

FIG. C-3 FAST NEUTRON FLUX MEASUREMENTS (ENTIRE PORT K)

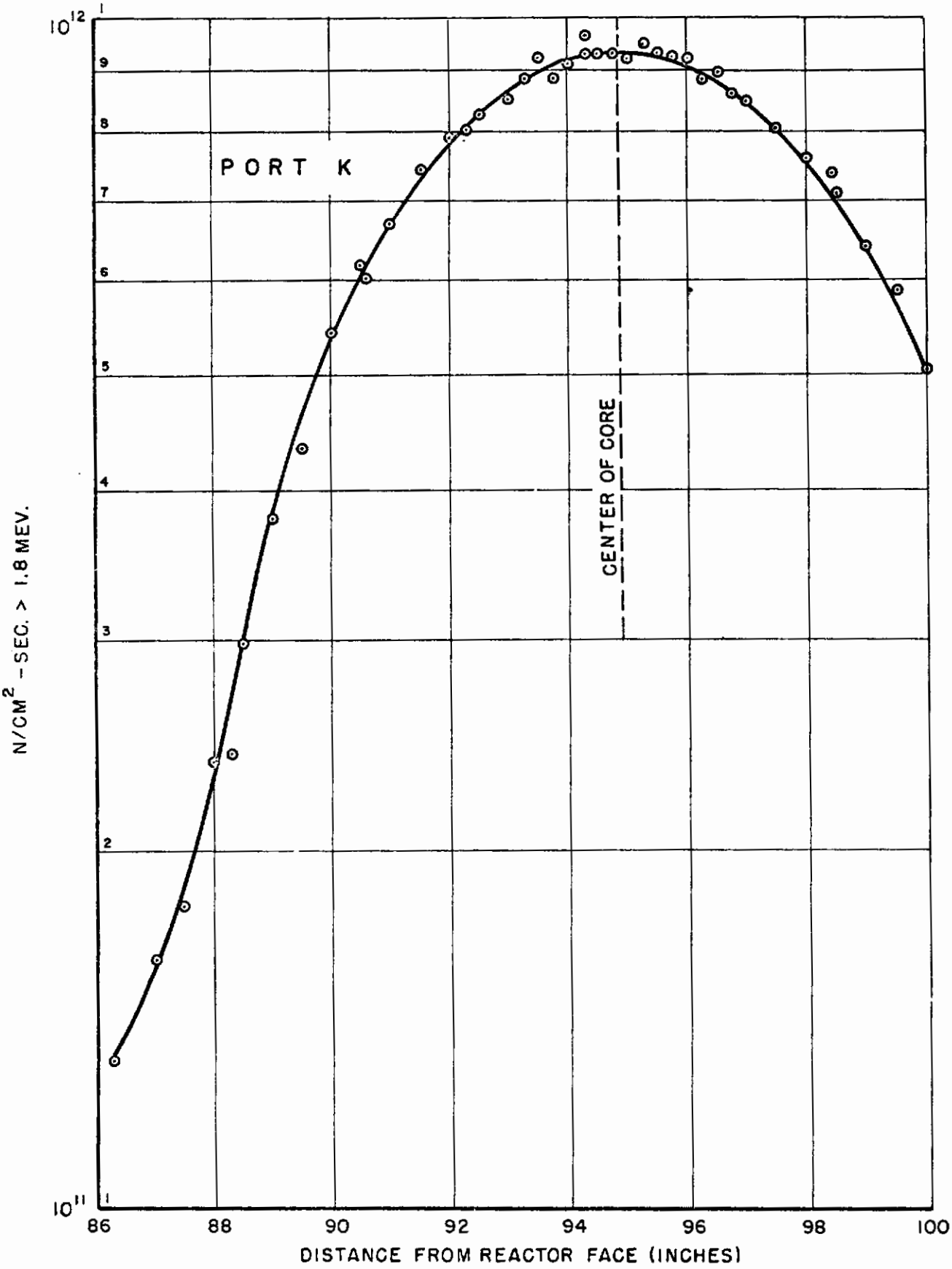

FIG. C-4 FAST NEUTRON FLUX MEASUREMENTS (CENTRAL AREA—PORT K)

Cobalt-aluminum foils supplied by Oak Ridge were irradiated in the thermal column and in Port K. The foils were sent to Oak Ridge for analysis. These foils were returned and used as standards in subsequent work.

Factors for determining the time-integrated fast flux, nvt, were obtained. By irradiating cadmium-covered cobalt, the fast flux integrated over time may be obtained as follows:

$$\text{Port K(95" from face)} nvt\left(\frac{n}{cm^2} > 1.8 \text{ Mev}\right) = 0.97 \times 10^{12} \frac{\text{n-g}}{cm^2\text{-dps}} \times \frac{\text{dps}}{\text{g}}$$

$$\text{Thermal column (3CF position)} nvt\left(\frac{n}{cm^2} > 1.8 \text{ Mev}\right) = 1.0 \times 10^{11} \frac{\text{n-g}}{cm^2\text{-dps}} \times \frac{\text{dps}}{\text{g}}$$

shere $\frac{\text{dps}}{\text{g}}$ is the Co-60 activity per gram mass of (0.15% Co), Co-Al foil.

Note that these factors are dependent upon the ratio of fast flux to epithermal flux, and should not be applied to other locations.

The basic instrumentation, counting equipment and a special seven-inch-thick lead shield designed to hold a two-inch scintillation well crystal, was set up for the gamma counting of the cobalt foils (small wires approximately 0.25 inch long, composed of pure aluminum and 0.50% cobalt).

The initial portion of the first reactor run with the diodes in place was scheduled to permit shutdown and removal of some cobalt wires and sulfur pellets after an appropriate exposure. The data obtained was a series of sulfur-cobalt intercalibrations, which were subsequently used in calculating nvt.

Other detectors were used in the same manner as the sulfur. The energy detection limits and cross-section were evaluated as described for the ${}_{16}S^{32}(n, p){}_{15}P^{32}$ reaction. The values used are summarized as Table C-2. These values are the numerically integrated values from equation (10), based on an assumed fission distribution. The question of the optimum energy limits deserves a great deal more study.

Figures C-5 and C-6 present the fast neutron spectra as determined in the boral box in the thermal column and in the center core region. The dotted curves represent a fission spectrum normalized to the sulfur points. Figure C-7 presents differential flux data in the center core region. The resonance detector data are intended primarily as guide points for the extrapolation of the lower energy fast flux. The literature on resonance detectors is very misleading, in that a considerable number of investigators have reported data in which the detector has a very slight portion of its sensitivity at the resonance energy, or has other factors which make interpretation difficult. This problem is currently under investigation by several groups at ARF.

Table C-2

THRESHOLD DETECTORS, AVERAGED CROSS SECTIONS, AND ENERGY DETECTION LIMITS

Reaction	True Effective Threshold (Mev)	True Effective Upper Limit (Mev)	Averaged Cross-section (barns)
$_{49}In^{115}(n, n')_{49}In^{115m}$	0.36	7.4	0.093
$_{16}S^{32}(n, p)_{15}P^{32}$	1.8	12.	0.148
$_{16}S^{34}(n, \alpha)_{14}Si^{31}$	4.0	14.	0.025
$_{13}Al^{27}(n, \alpha)_{11}Na^{24}$	6.15	14.	0.064

Flux Measurements

The analysis of sulfur pellets and cobalt wires (used for calibration) which were removed from the diodes after a few hours of irradiation during the full scale reactor run, as well as the analysis of the cobalt wires removed from the diodes that failed, will now be considered. In addition to diode locations, Figure C-8 also shows locations of sulfur pellets and cobalt wires in the boral box. The position of a sulfur pellet (attached to a diode) is indicated by a small circle, and that of a cobalt wire by an X. The large circles with numbers in them next to the diode location indicate the sample number of the corresponding sulfur-cobalt sample used for calibration.

Table C-3 is a complete tabulation of the measured and corrected counts per minute of each cobalt sample and the corresponding conversion factor from the measured cobalt activity per gram of sample to the fast flux above 1.8 Mev (as measured with the sulfur sample at the same location). Table C-4 contains similar data on the sulfur pellets, and these data were used with the data in Table C-3 on dps/gm (disintegrations per second per gram of cobalt-aluminum alloy - 0.5% Co and 99.5% Al) to obtain the conversion factors given in Table C-3.

Table C-5 contains data on the total nvt (n/cm^2) above 1.8 Mev received by the general purpose diodes up until the time of removal of cobalt wires attached to each diode. The data which is labeled as "removed 1-4-61" is for all of the diodes, except five of the dynamic silicon junction diodes.

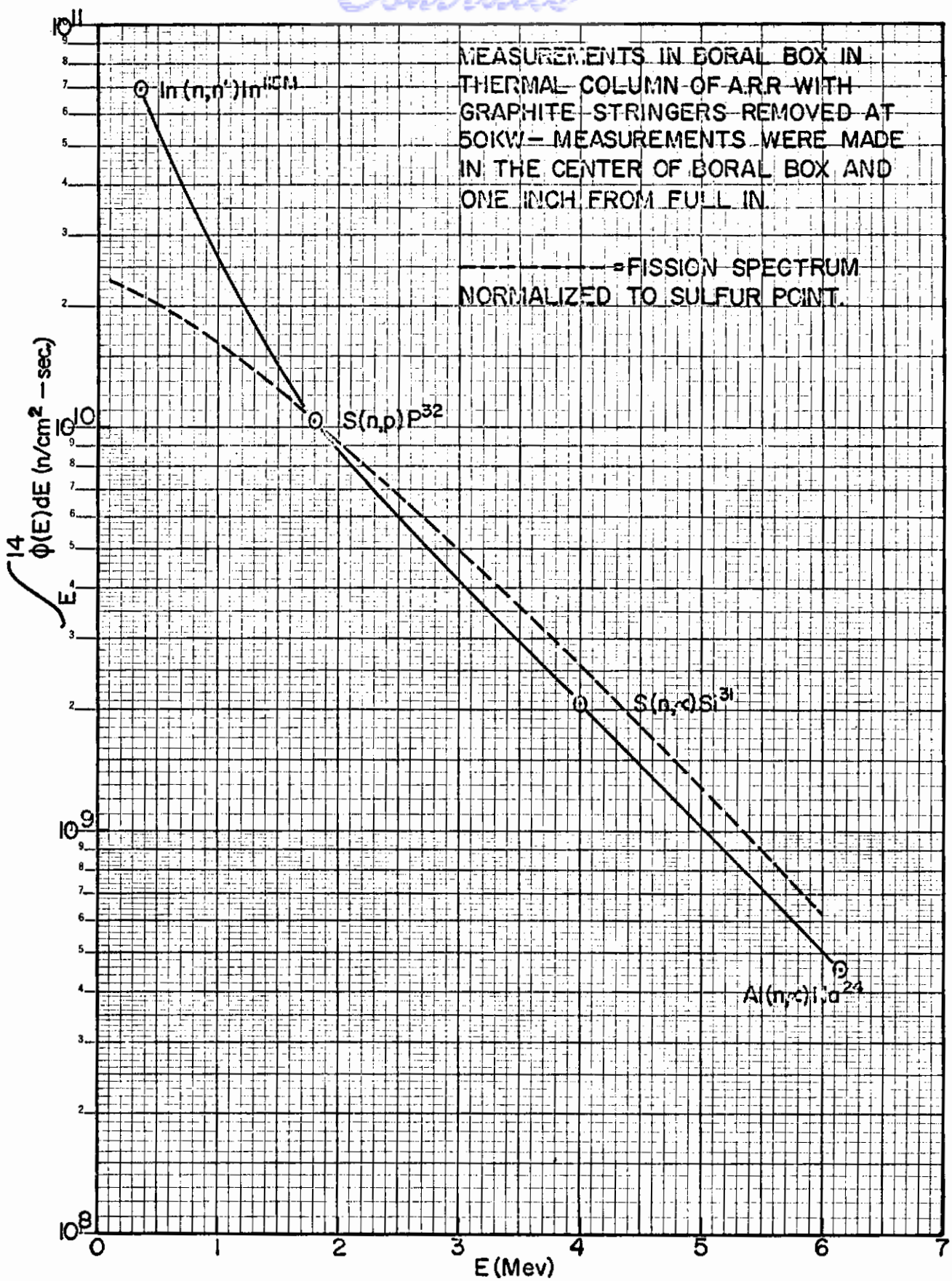

FIG. C-5 FAST NEUTRON SPECTRA — THERMAL COLUMN

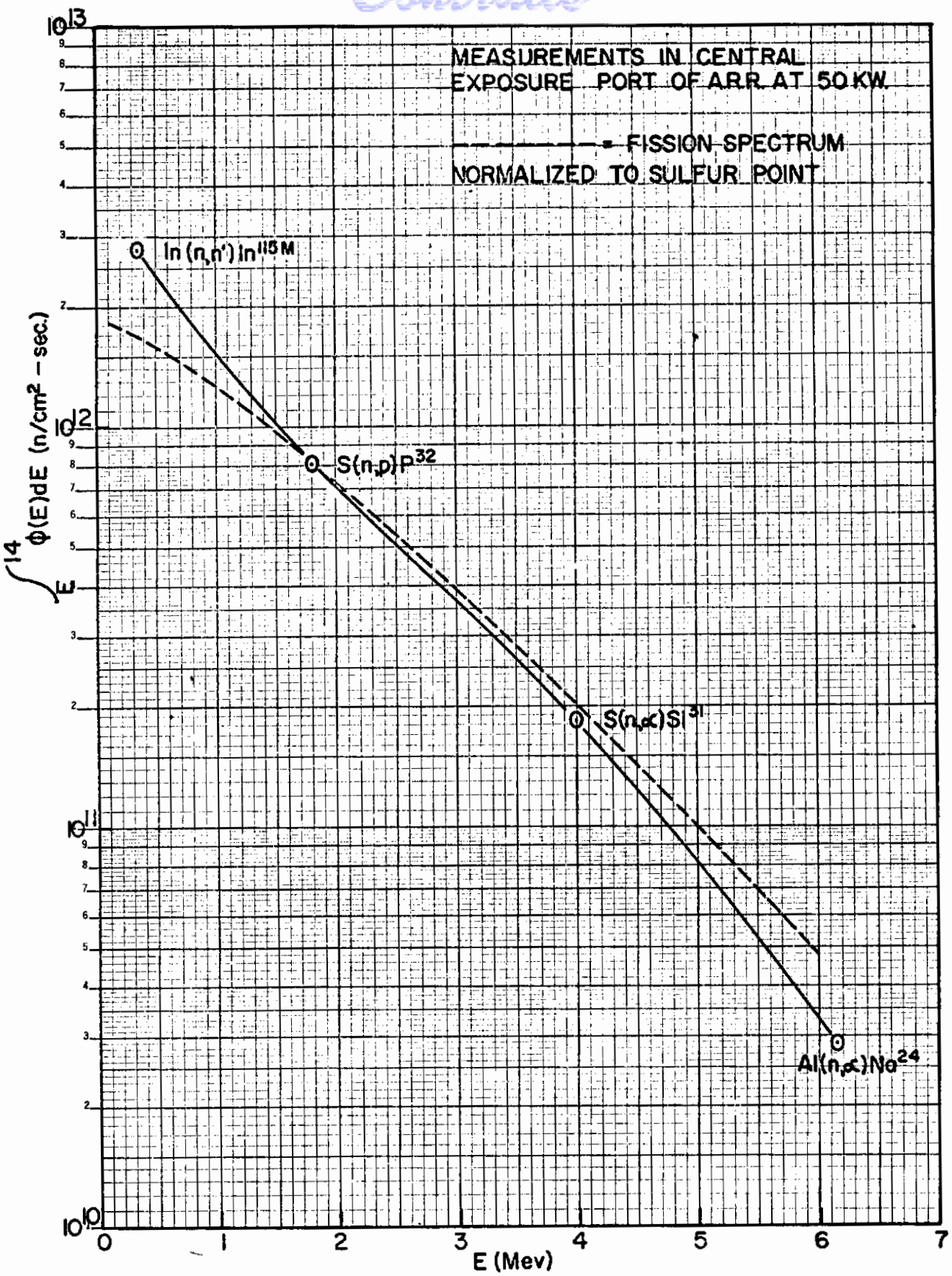

FIG. C-6 FAST NEUTRON SPECTRA – CENTRAL EXPOSURE PORT

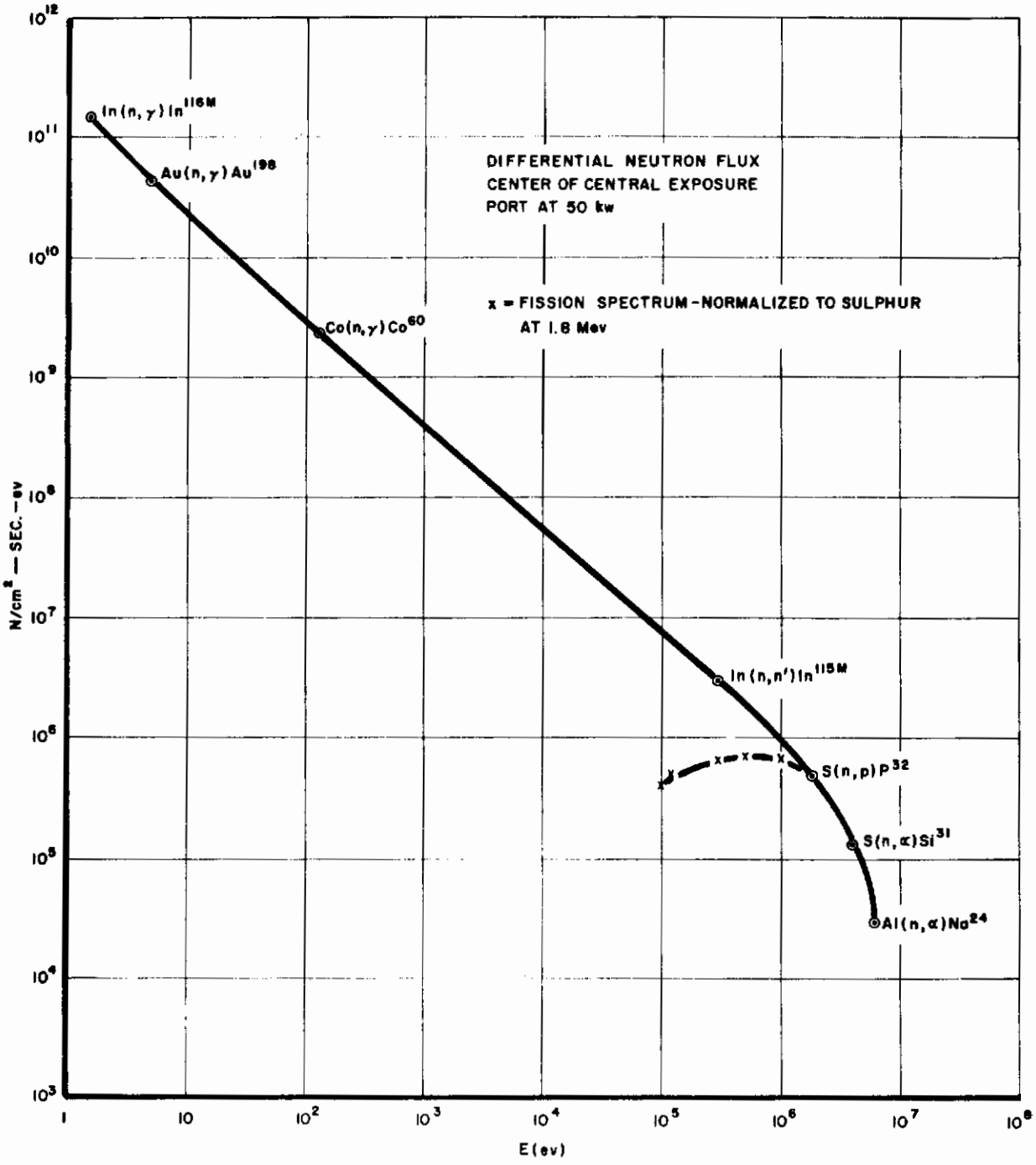

FIG. C-7 DIFFERENTIAL NEUTRON FLUX — CENTRAL EXPOSURE PORT

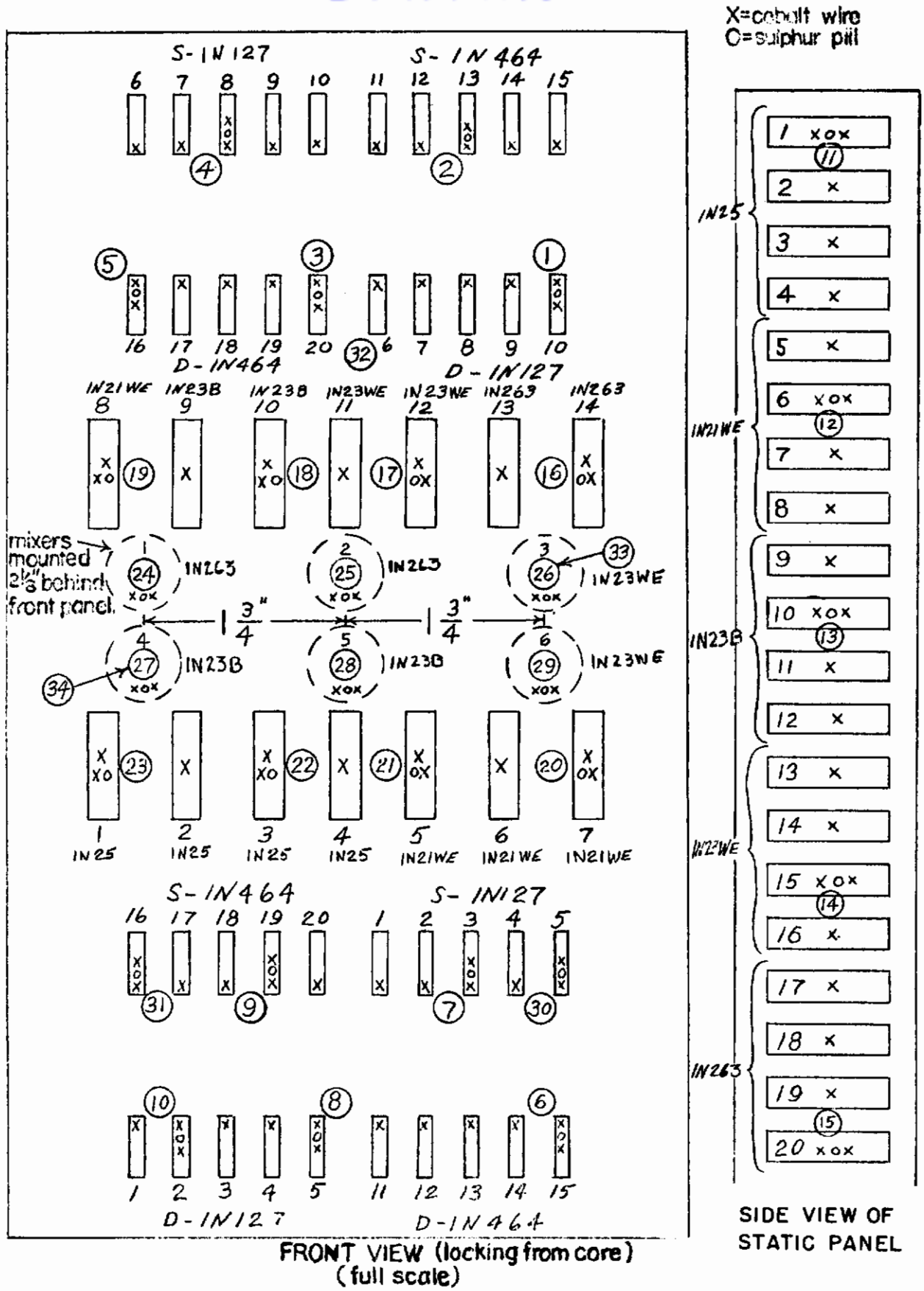

FIG. C-8 LOCATIONS OF DIODES, SULPHUR PELLETS AND COBALT WIRES

Table C-3

All Samples Irradiated 12-28-60 — Except Pos. (6) Irradiated on 12-28-60 to 1-4-61

Sample Position	Total Counts	Gross CPM	BKG Corrected CPM	Cobalt Activity $\frac{dps}{g}$ (cpm x 3.29)	Conversion Factor $\frac{n/cm^2}{dps/g}$ (x 10^{10})	Remarks
		COUNTED 1-17-61				
1	12619	1261.9	1074	3533	3.82	
2	13055	1305.5	1118	3678	3.43	
3	13077	1307.7	1120	3685	3.15	
4	12560	1256	1069	3517	3.58	
5	13070	1307	1120	3685	3.55	
6	325437	32543.7	32356	106451		Irradiated 12-28-60 to 1-4-61
7	15352	1535.2	1348	4435	3.36	
8	15363	1536.3	1349	4438	3.09	
9	15144	1514.4	1327	4366	3.32	
10	14856	1485.6	1298	4270	3.07	
		COUNTED 1-18-61				
11	14152	1415.2	1236	4066	3.05	
12	14060	1406	1227	4037	3.54	
13	14685	1468.5	1289	4241	3.61	
14	14270	1427	1248	4106	3.58	
		COUNTED 1-23-61				
15	12209	1220.9	1029	3385	3.81	
16	12127	1212.7	1021	3359	4.38	
17	13045	1304.5	1113	3662	4.26	
18	13101	1310.1	1119	3682	3.99	
19	12421	1242.1	1051	3458	4.05	
20	12569	1256.9	1065	3504	4.51	
21	12994	1299.4	1108	3645	4.20	
22	12837	1283.7	1092	3593	4.06	
23	12874	1287.4	1096	3606	3.99	
24	11134	1113.4	922	3033	3.10	

Table C-3 (Contd.)

Sample Position	Total Counts	COUNTED 1-26-61 Gross CPM	BKG Corrected CPM	Cobalt Activity $\frac{dps}{g}$ (cpm x 3.29)	Conversion Factor $\frac{n/cm^2}{dps/g}$ ($\times 10^{10}$)	Remarks
25	11284	1128.4	937	3083	3.50	
26	11256	1125.6	934	3073	3.55	
		COUNTED	1-27-61			
27	11380	1138	960	3158	3.39	
28	11522	1152.2	974	3204	3.43	
29	11354	1135.4	957	3149	3.40	
30	34174	3417.4	3239	10656		Irradiated 12-28-60 to 1-4-61
32	12206	1220.6	1042	3428	4.00	
33	10434	1043.4	865	2846	3.97	Irradiated
34	10454	1045.4	867	2852	3.75	1-4-61
		COUNTED	2-3-61			
31	34429	3442.9	3261	10729		Irradiated 12-28-60 to 1-4-61

Table C-4

CALIBRATION FACTORS

Sample Position	Total Counts	Gross CPM	$t_r + Bkg^*$ Corrected CPM	$e^{-\lambda t}$ corr. CPM	$\frac{CPM}{mg}$	$\phi_T > 1.8$ Mev n/cm^2-sec	nvt > 1.8 Mev neutrons/cm^2
1	160849	32169	39800	58250	1660	9.27×10^{9}	1.35×10^{14}
2	143889	28778	34750	50800	1554	8.67×10^{9}	1.26×10^{14}
3	131281	26256	31150	45600	1432	7.99×10^{9}	1.16×10^{14}
4	145887	29177	35300	51600	1543	8.61×10^{9}	1.26×10^{14}
5	142713	28543	34400	50400	1608	8.97×10^{9}	1.31×10^{14}
6	154802	30960	37950	55500	1646	9.18×10^{9}	1.34×10^{14}
7	156792	31358	38600	56500	1828	1.02×10^{10}	1.49×10^{14}
8	153620	30724	37550	54950	1691	9.43×10^{9}	1.37×10^{14}
9	147109	29422	35600	52100	1778	9.92×10^{9}	1.45×10^{14}
10	156989	31398	38650	56550	1615	9.01×10^{9}	1.31×10^{14}
11	132770	26554	31550	46150	1528	8.52×10^{9}	1.24×10^{14}
12	157376	31475	38750	56650	1750	9.77×10^{9}	1.43×10^{14}
13	170179	34036	42650	62450	1892	1.05×10^{10}	1.53×10^{14}
14	152455	30491	37200	54450	1808	1.01×10^{10}	1.47×10^{14}
15	153208	30642	37450	54750	1583	8.84×10^{9}	1.29×10^{14}
16	168556	33711	42050	61550	1809	1.01×10^{10}	1.47×10^{14}
17	175338	35068	44000	64950	1915	1.07×10^{10}	1.56×10^{14}
18	159177	31835	39250	57400	1803	1.01×10^{10}	1.47×10^{14}
19	169938	33988	42550	62300	1725	9.62×10^{9}	1.40×10^{14}
20	181994	36399	46400	67900	1933	1.08×10^{10}	1.58×10^{14}
21	168120	33624	41950	61400	1888	1.05×10^{10}	1.53×10^{14}
22	168370	33674	42100	61600	1792	1.00×10^{10}	1.46×10^{14}
23	162241	32449	40250	58900	1768	9.87×10^{9}	1.44×10^{14}
24	112582	22516	25950	37950	1151	6.43×10^{9}	0.94×10^{14}
25	136828	27366	32700	47800	1321	7.37×10^{9}	1.08×10^{14}
26	101926	20385	23150	33850	1343	7.49×10^{9}	1.09×10^{14}
27	114706	22941	26550	38850	1313	7.33×10^{9}	1.07×10^{14}
28	119782	23956	27950	40900	1349	7.52×10^{9}	1.10×10^{14}
29	133803	26761	31750	46450	1311	7.32×10^{9}	1.07×10^{14}
30	182876	36575	46600	68250	1777	9.91×10^{9}	1.45×10^{14}
31	163930	32786	40800	59750	1683	9.39×10^{9}	1.37×10^{14}

NOTE: The effective irradiation time at 50 KW = 4.05 hours.
These irradiations were made before paraffin was added to diode rack.

* Resolving time plus background correction.

Table C-5

FIRST REACTOR RUN DATA

		COUNTED 1-27-61			Cobalt Activity	Conversion Factor*	Nvt
Diode No.	Diode Type**	Total Counts	Gross CMP	Corrected CMP	$\frac{dps}{g}$	$\frac{n/cm^2}{dps/g_{10}}$ ($\times 10^{10}$)	n/cm^2 >1.8 Mev ($\times 10^{14}$)
1	SIN127	33952	3395.2	3208	10554	3.36	3.55
2	SIN127	34022	3402.2	3217	10584	3.36	3.56
3	"	33835	3383.5	3198	10521	"	3.54
4	"	33764	3376.4	3191	10498	"	3.53
5	"	33776	3377.6	3192	10502	"	3.53
6	SIN127	31229	3122.9	2944	9686	3.58	3.47
7	"	31777	3177.7	2999	9867	"	3.53
8	"	32057	3205.7	3027	9959	"	3.57
9	"	31850	3185	3007	9893	"	3.54
10	"	32091	3209.1	3031	9972	"	3.57
11	SIN464	32310	3231	3053	10044	3.43	3.45
12	"	32640	3264	3086	10153	"	3.48
13	"	32407	3240.7	3062	10074	"	3.46
14	"	32204	3220.4	3042	10008	"	3.43
15	"	32033	3203.3	3025	9952	"	3.41
16	SIN464	33580	3358	3171	10433	3.32	3.46
17	"	34111	3411.1	3224	10607	"	3.52
18	"	33112	3311.2	3124	10278	"	3.41
19	"	34478	3447.8	3261	10729	"	3.56
20	"	34050	3405	3218	10587	"	3.51

* From Table C-3.

** "S" prefix denotes static diode, not energized during irradiation.

Table C-5 (Cont'd)

FIRST REACTOR RUN DATA

		COUNTED 1-31-61			Cobalt Activity	Conversion Factor	Nvt	
Diode No.	Diode Type**	Total Counts	Gross CMP	Corrected CMP	dps/g	n/cm^2 dps/g ($\times 10^{10}$)	n/cm^2 > 1.8 Mev ($\times 10^{14}$)	Remarks
1	DIN127	33357	3335.7	3150	10364	3.07	3.18	Removed
2	"	33940	3394	3209	10558	"	3.24	1-4-61
3	"	33354	3335.4	3150	10364	"	3.18	
4	"	33088	3308.8	3123	10275	"	3.15	
5	"	33279	3327.9	3142	10337	3.09	3.19	
6	DIN127	32397	3239.7	3061	10071	3.43	3.17	
7	"	33317	3331.7	3153	10373	3.43	3.27	
8	"	33209	3320.9	3133	10308	3.82	3.94	
9	"	32597	3259.7	3072	10107	"	3.86	
10	"	33284	3328.4	3141	10334	"	3.95	
11	DIN464	80186	8018.6	7833	25771	3.09	7.96	
12	"	80056	8005.6	7820	25728	"	7.95	Removed
13	"	80992	8099.2	7914	26037	"	8.05	1-11-61
14	"	81370	8137	7952	26162	"	8.08	
15	"	81379	8137.9	7952	26162	"	8.08	
16	DIN464	32360	3236	3058	10061	3.55	3.57	
17	"	32963	3296.3	3118	10258	"	3.64	Removed
18	"	33467	3346.7	3168	10423	"	3.70	1-4-61
19	"	32620	3262	3084	10146	3.15	3.20	
20	"	32896	3289.6	3111	10235	"	3.22	
1	MIN263	12014	6007	5674	18667	3.10	5.79	
2	"	12807	6403.5	6070	19970	3.50	6.99	
3	MIN23WE	12638	6319	5986	19694	3.55	6.99	
4	"	12191	6095.5	5762	18957	3.39	6.43	
5	"	12771	6385.5	6052	19911	3.43	6.83	
6	MIN23WE	12426	6213	5880	19345	3.40	6.58	

** "D" prefix denotes dynamic diode energized with 60 cps current
"M" prefix denotes diode energized with X-Band power

Table C-5 (Cont'd)

FIRST REACTOR RUN DATA

		COUNTED 1-31-61			Cobalt Activity	Conversion Factor	Nvt	
Diode No.	Diode Type	Total Counts	Gross CMP	Corrected CMP	$\frac{dps}{g}$	$\frac{n/cm^2}{dps/g_{10}}$ ($\times 10^{10}$)	n/cm^2 > 1.8 Mev ($\times 10^{14}$)	Remarks
2	SIN25	13343	6671.5	6338	20852	3.05	6.36	
3	"	13504	6752	6419	21118	3.05	6.44	
4	"	13692	6846	6515	21428	3.05	6.54	
5	SIN21WE	13686	6843	6510	21418	3.54	7.58	Irradiated
6	"	13595	6797.5	6464	21266	3.54	7.53	12-28-60
7	"	13724	6862	6529	21480	3.54	7.60	to
8	"	13401	6700.5	6368	20951	3.54	7.42	1-11-61
9	SIN23B	13980	6990	6657	21902	3.61	7.91	
10	"	13781	6890.5	6558	21576	3.61	7.79	
11	"	13439	6719.5	6386	21010	3.61	7.58	
12	"	13834	6917	6584	21661	3.61	7.82	
13	SIN23WE	13771	6885.5	6552	21556	3.58	7.72	
14	"	13913	6956.5	6624	21793	3.58	7.80	
15	"	13027	6513.5	6180	20332	3.58	7.28	
16	"	13770	6885	6552	21556	3.58	7.72	
17	SIN263	12914	6457	6124	20148	3.81	7.68	
18	"	12874	6437	6104	20082	3.81	7.65	
19	"	12558	6279	5946	19562	3.81	7.45	
20	"	12740	6370	6037	19862	3.81	7.57	
2	DIN25	14700	7350	7017	23086	3.99	9.21	
3	"	14948	7474	7141	23493	4.03	9.47	
4	"	14609	7304.5	6972	22938	4.20	9.63	
5	DIN21WE	14558	7279	6946	22852	4.02	9.19	
6	"	14455	7227.5	6894	22681	4.51	10.23	
7	"	14424	7212	6879	22632	4.51	10.21	
8	DIN21WE	14408	7204	6871	22606	4.05	9.16	
10	DIN23B	14596	7298	6965	22915	3.99	9.14	
11	DIN23WE	14599	7299.5	6966	22918	4.14	9.49	
12	DIN23WE	14601	7300.5	6968	22925	4.26	9.77	
13	DIN263	13438	6919	6386	21010	4.38	9.20	
14	DIN263	12918	6459	6126	20154	4.38	8.83	

All except these five had failed at this point. These five dynamic silicon junction diodes were given an additional exposure, as indicated by the data labeled "removed 1-11-61." However, these too were failed after this exposure.

Table C-6 summarizes cobalt wire data obtained during the second irradiation period. The data are again reported as $n/cm^2 > 1.8$ Mev. Figure C-5 may be used to obtain the integrated flux above other energies, if desired. For example, to obtain the integrated flux greater than 0.5 Mev, one multiplies the integrated flux greater than 1.8 Mev by 5.3.

Additional data on the "damaging fast flux" in the low Mev region (over a range of two decades such as 0.01 to 1 Mev) have been obtained in the central exposure port of the ARR. The experimental work was performed by Dr. Primak of Argonne National Laboratory and staff members of ARF, and was sponsored jointly by ARF and Argonne (ref. 20). The results obtained from this work should be considered as provisional data, and are presented because they provide additional data that are relevant.

The measurements by Dr. Primak of the "damaging fast flux" in the central exposure port gave a value of approximately $3.8 \times 10^{12} n/cm^2$-sec. This value was obtained by measuring the change in resistivity of graphite samples placed in the port, and compares favorably with the value of $2.8 \times 10^{12} n/cm^2$-sec for the total fast flux above 0.36 Mev, as measured by the $In(n, n')In^{115m}$ reaction. Dr. Primak has published a number of papers on his work (references 12, 13, and 14), and the literature should be consulted for more details about his method and as to the exact meaning of the terminology "damaging flux."

If $3.8 \times 10^{12} n/cm^2$-sec is used for the value of the total damaging flux and $2.8 \times 10^{12} n/cm^2$-sec for the total value of the flux above 0.36 Mev, the ratio, 1.36, of these two values of flux gives the factor by which the measured fast flux above 0.36 Mev must be multiplied to obtain the value of the total damaging fast flux in the central exposure port. If this analogy is carried over to the measurements of the fast flux in the thermal column, the minimum value of the "fast damaging flux" in the location where most of the diodes were irradiated is 1.36 times the value as measured with the $In(n, n')In^{115m}$ detector. This gives a minimum value for the "fast damaging flux" in the thermal column of $(1.36) \times (6.9 \times 10^{10} n/cm^2\text{-sec}) = 9.4 \times 10^{10} n/cm^2$-sec.* With reference to Figures C-5 and C-6, there is a significant difference in the lower Mev region in the spectral form between the central exposure port and the thermal column. From the curves, it is apparent that there are more lower-than high-energy neutrons in the thermal column. Because of this, it may be said with reasonable confidence that the value of $9.4 \times 10^{10} n/cm^2$-sec is a minimum value for the "damaging flux" in the thermal column region.

* See Figure C-5 for location.

Table C-6

SECOND REACTOR RUN DATA

Diode No.	Diode Type	Total Counts	Gross CPM	Net CPM	$\frac{dps}{g}$	n/cm^2 dps/g ($\times 10^{10}$)	n/cm^2 >1.8 Mev ($\times 10^{15}$)	Remarks
1	IN23B	382858	7657	7473	24603	3.05	0.750	Failed 6-5-61 Removed
2	IN23B	123578	2472	2293	7544	3.05	0.230	" 5-18-61 on date
12	IN23B	115911	2318	2139	7037	3.60	0.253	" " of failure
M-1	IN263	409385	40939	40776	132318	3.10	4.10	Removed 7-7-61
M-2	IN263	460567	46057	45894	148926	3.50	5.21	" " Crystal
M-3	IN23WE	431189	43119	42956	139392	3.97	5.53	" " holders
M-4	IN23WE	408449	40845	40672	131981	3.75	4.95	" " continued
M-5	IN23B	446899	44690	44527	144490	3.43	4.96	" " from 1st
M-6	IN23B	429938	42994	42831	138987	3.40	4.73	" " run
3	IN23WE	144892	14490	14327	46491	3.52	1.64	These values are all aver-
4	IN23WE	"	"	"	"	"	"	ages for removable rack
5	IN263	"	"	"	"	"	"	Removed 7-7-61 Continued
6	IN263	"	"	"	"	"	"	" " from 1st run
9	IN23B	"	"	"	"	"	"	These values are all aver-
10	IN23B	"	"	"	"	"	"	ages fro removable rack
11	IN23B	"	"	"	"	"	"	Removed 7-7-61
13	IN23WE	"	"	"	"	"	"	" "
14	IN23WE	"	"	"	"	"	"	" "
15	IN23WE	"	"	"	"	"	"	" "
16	IN23WE	"	"	"	"	"	"	" "
17	IN263	"	"	"	"	"	"	" " Continued
18	IN263	"	"	"	"	"	"	" " from 1st
19	IN263	"	"	"	"	"	"	" " run
20	IN263	"	"	"	"	"	"	" "

The above, as well as previous considerations, should emphasize the difficulty of trying to correlate radiation damage effects in two different positions in the same reactor, or in different reactors if measurements are not made by a method such as Dr. Primak's or are not made of the fast flux spectral distribution in the lower Mev energy region. Measurements with sulfur alone, the normal procedure followed by many researchers, would have given no indication that there was a significant spectral difference between the normally assumed fission spectrum and the actual spectrum (and in turn the "damaging flux") in the two locations in the ARR; see Figures C-5 and C-6. This in turn could lead to serious unexplained discrepancies between the results of a radiation damage study on the same materials in two different locations in the same or in different reactors. With these final statements concluding the discussion of fast flux measurements, consideration will now be given to gamma level measurements.

Drawings were obtained for the carbon ionization chamber referenced in WADC TN 57-207 (ref. 17). However, it was apparent that this unit would be too large (2 inches O. D.) to be used in the central exposure facility (which is a maximum of 1. 4 inches O. D.), or in certain areas of the Boral box that contained the diodes. It was therefore necessary to build a smaller and somewhat different type of carbon ionization chamber, in order to make an empirical comparison of the chemical dosimetry and other ionization chamber data with that of the carbon ionization chamber.

Measurements made in the thermal column with the carbon ionization chamber indicate that the maximum value of the gamma level is about 0.2×10^6 rad/hour. A comparison of the carbon ionization chamber results with those obtained using an aluminum walled ion chamber and $FeSO_4$ dosimetry as a function of distance in the boral box is presented in Figure C-9. Measurements with $FeSO_4$ dosimetry indicate that the maximum value of the combined gamma and fast neutron dose rate is about 0.45×10^6 rad/hour.

The carbon ionization chamber has also been used to measure the maximum gamma dose rate in the central exposure port (D and K), where preliminary tests were made on some of the different diodes. The measurements indicate that the gamma dose rate is about 2×10^7 rad/hour. Ferrous sulfate dosimetry was used as a comparison, and a value of a total deposited dose rate of about 4×10^7 rad/hour was obtained. The measured value of approximately 4×10^7 rad/hour with the $FeSO_4$ dosimetry includes the effect of fast neutrons. In the absence of a proper "G" value for fast neutrons, all ferrous sulfate dosimetry was based on a "G" value of 15.6.

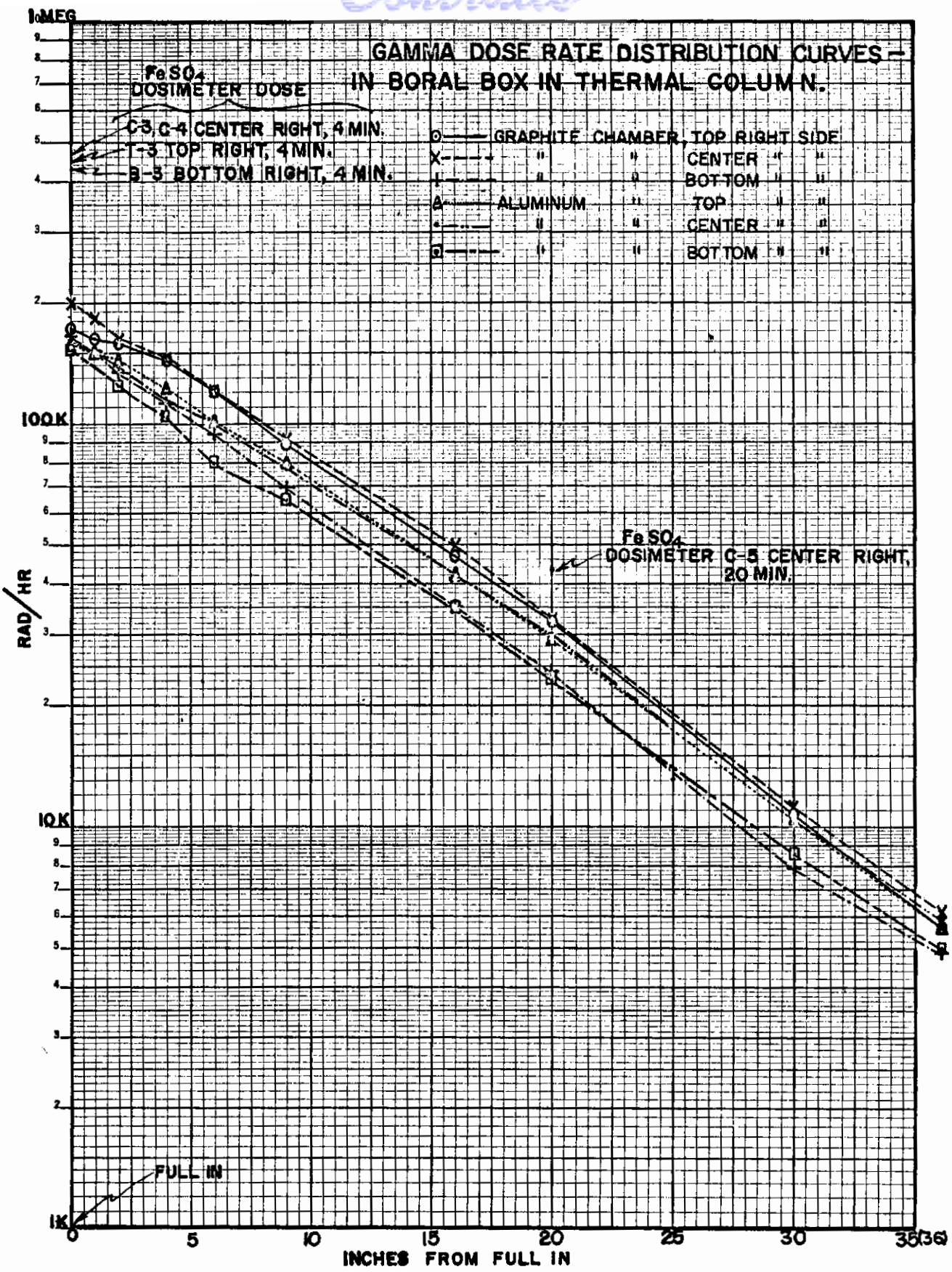

FIG. C-9 GAMMA DOSE RATE DISTRIBUTION — THERMAL COLUMN